Joint Transportation Research Program

JTRP

Final Report

MOMENT-ROTATION RELATIONSHIPS FOR UNIFIED AUTOSTRESS DESIGNS OF CONTINUOUS-SPAN BRIDGE BEAMS AND GIRDERS

Donald W. White
Julio A. Ramirez
Karl E. Barth

November 17, 1997

Indiana
Department
of Transportation

Purdue
University

Final Report

MOMENT-ROTATION RELATIONSHIPS FOR UNIFIED AUTOSTRESS DESIGN OF CONTINUOUS-SPAN BRIDGE BEAMS AND GIRDERS

Donald W. White
Julio A. Ramirez
Karl E. Barth
Purdue University

The contents of this report reflect the views of the authors, who are responsible for the facts and accuracy of the data presented herein. The contents do not necessarily reflect the official views or policies of the Indiana Department of Transportation or the Federal Highway Administration at the time of publication. This report does not constitute a standard, specification, or regulation.

1. Report No. FHWA/IN/JTRP-97/8	2. Government Accession No.	3. Recipient's Catalog No.
4. Title and Subtitle Moment-Rotation Relationships for Unified Autostress Design of Continuous-Span Bridge Beams and Girders		5. Report Date July 28, 1997
		6. Performing Organization Code
7. Author(s) Donald W. White, Julio A. Ramirez, and Karl E. Barth		8. Performing Organization Report No. FHWA/IN/JTRP-97/8
9. Performing Organization Name and Address Joint Transportation Research Program 1284 Civil Engineering Building Purdue University West Lafayette, Indiana 47907-1284		10. Work Unit No.
		11. Contract or Grant No. HPR-2093
12. Sponsoring Agency Name and Address Indiana Department of Transportation State Office Building 100 North Senate Avenue Indianapolis, IN 46204		13. Type of Report and Period Covered Final Report
		14. Sponsoring Agency Code

15. Supplementary Notes

Prepared in cooperation with the Indiana Department of Transportation and Federal Highway Administration.

16. Abstract

This report summarizes the development and trial application of simplified moment-rotation relationships for inelastic design of continuous-span beam and girder bridges. The research described within involves the execution of a reasonably comprehensive set of finite element parametric studies to fill in knowledge gaps in the available experimental data pertaining to the hogging moment-plastic rotation behavior of steel and composite steel-concrete bridge girders. Based on these studies, relationships have been developed for the moment-plastic rotation behavior at the pier sections in these types of bridges. The moment-rotation model is validated against available experimental data, several focused new experimental tests, and current American specification strength formulas. This study concludes with a detailed trial inelastic design of a three-span continuous plate-girder bridge using suggested new inelastic design procedures. The characteristics of the calculations and the resulting proportions are compared to those of an elastic design of the same bridge by current AASHTO LRFD procedures. The elastic design is a modified version of a three-span continuous plate-girder bridge example recently published by the American Iron and Steel Institute for a Highway Structure Design Handbook.

17. Key Words autostress design, finite element modeling, inelastic design, inelastic redistribution, load and resistance factor design, moment-rotation characteristics, moment capacity, noncompact cross-sections, plate girders, rotation capacity, steel bridges.		18. Distribution Statement No restrictions. This document is available to the public through the National Technical Information Service, Springfield, VA 22161	
19. Security Classif. (of this report) Unclassified	20. Security Classif. (of this page) Unclassified	21. No. of Pages 138	22. Price

Form DOT F 1700.7 (8-69)

ACKNOWLEDGMENTS

MOMENT-ROTATION RELATIONSHIPS FOR UNIFIED AUTOSTRESS DESIGN OF CONTINUOUS-SPAN BRIDGE BEAMS AND GIRDERS

Implementation Suggestions

This report summarizes the development and trial application of simplified moment-rotation (M-θ_p) relationships for inelastic design of continuous-span steel beam and girder bridges. It complements a parallel National Science Foundation study by Schilling et al. (1996) on the inelastic design of steel girder bridges. It is recommended that the M-θ_p equations developed in this research should be incorporated into the inelastic design provisions developed in (Schilling 1997) and (Schilling et al. 1996). This requires little change to the proposed provisions other than the replacement of effective plastic moment (M_{pe}) equations in these provisions by the M-θ_p model developed in this work.

The proposed M-θ_p model is illustrated in Fig. 1. As shown by this figure, the behavior can be divided into three regions: (1) a linear pre-peak curve from zero plastic rotation at $M = 0.7M_n$ to a θ_p of *0.005* at M_n (where M_n is the nominal flexural capacity), (2) a plateau at the nominal resistance M_n from $\theta_p = 0.005$ to a value denoted by the parameter θ_{RL} (where θ_{RL} can be as small as *0.005*, in which case the girder unloads immediately upon reaching its peak moment capacity), and (3) a quadratic unloading curve given by the equation shown in the figure.

The linear pre-peak curve is the same as the pre-peak curve specified for Unified Autostress design of compact I shapes in the AASHTO LRFD Specifications (1994). This curve is a reasonable approximate fit to experimental test data as well as finite element solutions in which the residual stresses due to welding and flame cutting are based on girder dimensions representative of laboratory tests. In the report, the authors note that this curve is likely to over-predict the pre-peak plastic rotations in actual bridge girders of larger dimensions.

The authors suggest the following equation for the nominal moment capacity,

$$\frac{M_n}{M_p} = 1 + \frac{3.6}{\sqrt{\frac{2D_{cp}}{t_w}}} + \frac{1}{10a_{rp}} - 0.4\frac{M_p}{M_y} \le 1 \tag{1}$$

and the equation

$$\theta_{RL} = 0.128 - 0.0119\frac{b_{fc}}{2t_{fc}} - 0.0216\frac{D}{b_{fc}} + 0.002\frac{b_{fc}}{2t_{fc}}\frac{D}{b_{fc}} \qquad (2)$$

for the extent of the "plateau" in the $M\text{-}\theta_p$ behavior shown in Fig. 5. The parameter a_{rp} is defined as

$$a_{rp} = \frac{2D_{cp}t_w}{b_{fc}t_{fc}} \qquad (3)$$

and M_y is the yield moment of the pier cross-section, taken as the sum of the moments due to the factored loads at the applicable limit state, applied separately to the steel, long-term composite, and short-term composite sections to cause first yield in either steel flange (see article A6.2 of (AASHTO 1994)). For a slab that is not post-tensioned within the negative moment regions, such as in the trial inelastic design, the long- and short-term composite sections are both taken as the steel member plus the reinforcing steel within the AASHTO effective width of the slab. That is, the slab is assumed to be fully cracked for the composite loadings in calculating M_y at the pier sections.

Equations (1), (2) and the equations in Fig. 1 are a fit to a suite of finite element studies in which transverse stiffeners are placed such that the applied shear is less than $0.6V_n$ in the web, and cross frames are spaced at the following inelastic limit defined in the AASHTO Specifications (1994):

$$\frac{L_b}{r_y} \leq \left[0.124 - 0.0759\frac{M_{min}}{M_{max}}\right]\left(\frac{E}{F_{yc}}\right) \qquad (4)$$

The authors recommend that r_y in this equation should be based on the compression flange plus one-half the total depth of the web about the minor axis of the cross-section. This produces the same value as the r_y of the full cross-section for symmetrical all-steel sections, and it is simple to apply for unsymmetrical and composite girders. The suggested $M\text{-}\theta_p$ model is applicable for members that satisfy these limits plus the

restrictions $\frac{2D_{cp}}{t_w} \leq 6.77\sqrt{\frac{E}{F_{yc}}}$, $\frac{b_{fc}}{2t_{fc}} \leq 0.4\sqrt{\frac{E}{F_{yc}}}$, $\frac{D}{b_{fc}} \leq 4.25$, and $\frac{D_{cp}}{D} \leq 0.75$. The limit

on $\dfrac{2D_{cp}}{t_w}$ is the same as the limit in the AASHTO LRFD Specifications (1994) for girders without longitudinal stiffeners. The last four limits are based on the ranges of design parameters encompassed by the available finite element and experimental tests, and it can be argued that they are reasonable practical limits for economical designs. The limit on $\dfrac{b_{fc}}{2t_{fc}}$ is slightly more liberal than the current AASHTO LRFD definition of a compact compression flange.

Equations (1), (2) and the equations in Fig. 5 are based on $F_{yc} = 345$ MPa. They may be applied for other yield strengths by determining equivalent values for the slenderness of the web and flange plates of $\left(\dfrac{2D_{cp}}{t_w}\right)_{eq} = \dfrac{2D_{cp}}{t_w}\sqrt{\dfrac{F_{yc}}{50}\dfrac{29\,000}{E}}$ and

$\left(\dfrac{b_{fc}}{2t_{fc}}\right)_{eq} = \dfrac{b_{fc}}{2t_{fc}}\sqrt{\dfrac{F_{yc}}{50}\dfrac{29\,000}{E}}$. These conversions are used in the report to account for yield stresses in experimental tests that are different than the nominal values of $F_{yc} = 345$ MPa (50 ksi), and they are based on limited finite element studies with $F_y = 480$ MPa (70 ksi). On-going studies of girders fabricated from high-performance steels with $F_y \geq 480$ MPa may lead to refinements in the suggested M-θ_p model accounting for variations in F_y and other material parameters.

Usage of the above explicit M-θ_p relationships avoids the conservatism introduced by the M_{pe} equations in (Schilling 1997) and (Schilling et al. 1996), which are based on an upper-bound of the expected pier plastic rotations anticipated over a wide range of designs. The use of the direct M-θ_p equations in the design procedures proposed by Schilling (1997) and Schilling et al. (1996) requires minor additional effort on the part of the engineer, since the calculations can be easily implemented in existing ordinary spreadsheet or mathematical manipulation software. Also, the explicitly M-θ_p relationships should be more useful for potential future three-dimensional bridge analysis software that can account for the inelastic redistribution of excess elastic moments from interior pier sections.

For the design procedures based on (Schilling 1997), (Schilling et al. 1996) and this work to be available for design use, they will first need to be accepted by AASHTO as changes to the existing inelastic design provisions of the AASHTO LRFD Specifications (1994).
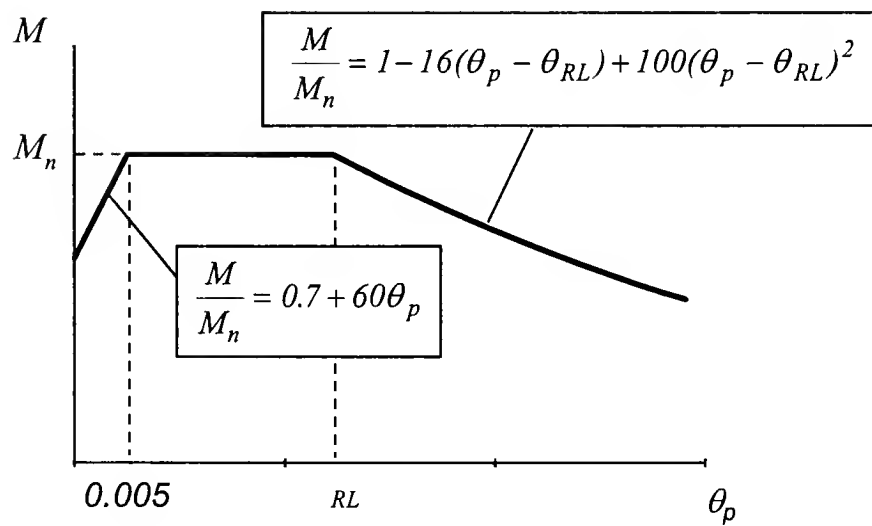
Figure 1. Moment-plastic rotation model.

TABLE OF CONTENTS

LIST OF TABLES

LIST OF FIGURES

CHAPTER 1

INTRODUCTION

In 1986, AASHTO adopted the *Guide Specifications for Alternate Load Factor Design (ALFD) Procedures for Steel Beam Bridges Using Compact Sections*. These specifications are based on "autostress" methodologies (Haaijer et al. 1983), which account for the ability of continuous-span steel and composite steel-concrete bridges to adjust automatically for the effects of local yielding over interior supports caused by overloads. Several cases have been cited in the literature where significant design economy has been achieved with these procedures (Schilling 1986; Wasserman and Holloran 1993). More recently, the traditional autostress approaches, which utilize a mechanism analysis, have been extended to a more general "unified autostress" analysis approach (Schilling 1993) and incorporated into the *AASHTO LRFD Bridge Design Specifications* (AASHTO 1994) under the section "Inelastic Analysis Procedures." Related techniques for inelastic analysis and rating of steel bridges have been developed in research by Dishongh and Galambos (1992) (titled "residual deformation analysis") and by others. The unified autostress and residual deformation types of analysis involve the explicit use of moment-inelastic rotation curves for checking strength and permanent deflection limits. Schilling et al. (1996) have recently recommended improvements to the AASHTO inelastic LRFD provisions that account for the general performance of both compact and noncompact section members. These recommended inelastic design procedures are summarized in (Schilling 1997).

By using the above procedures to take advantage of the inherent inelastic redistribution capabilities of continuous-span bridge beams and girders, designers can generally limit section transitions to field splice locations, or they can justify the economical use of prismatic members along the entire length of a bridge. In the design of new bridge structures, such practices reduce fabrication costs. Furthermore, these methodologies have tremendous potential for rating of existing structures, since they account more realistically for the true strength of straight beam and plate-girder bridges.

According to the American Institute of Steel Construction, these bridge types constitute 80 to 85 percent of the steel bridge market (Grubb 1993).

Although the above approaches are in general terms applicable to both compact and noncompact sections, the AASHTO inelastic design rules (1994) address only compact-section beams, i.e., beams that have a compression flange slenderness ($b_{fc}/2t_{fc}$) not exceeding *9.2* and a web slenderness ($2D_{cp}/t_w$) not exceeding *91* for Grade 50 steels (i.e., $F_y = 50\ ksi$ or *345 MPa*). Furthermore, the new recommendations by Schilling (1997) and Schilling, et al. (1996) are based only on a limited set of experimental tests. Research studies (Croce 1970; Grubb and Carskaddan 1981; Schilling 1985, 1988; Schilling and Morcos 1988; Tansil 1991; FHWA 1992; White and Dutta 1993; White 1994) have shown that members with noncompact webs ($2D_{cp}/t_w$ between *91* and *163* for Grade 50 steels) and compact or ultracompact flanges ($b_{fc}/2t_{fc}$ less than *9.2* or *7.0* respectively for $F_y = 350\ MPa$ (*50 ksi*)) can exhibit a reliable capacity for inelastic redistribution of moments from their interior pier sections. However, the behavior of sections with noncompact webs has not been quantified over a sufficient range of parameters such that the inelastic procedures can be extended to cover these cases (AASHTO 1994).

Further analytical parametric studies and specifically focused experimental tests are needed to fill in the knowledge gaps in the behavior of I girders with noncompact webs. This new information and the data from previous studies then need to be collected and analyzed together as one data set to develop comprehensive moment-rotation (M-θ_p) relationships for potential AASHTO LRFD use. By developing comprehensive M-θ_p curves applicable to both compact and noncompact sections, the benefits of inelastic design and rating methods can be realized on a much broader scale in steel bridge design practice.

1.1 Project Objectives

This study investigates the performance of composite and non-composite steel bridge beams and plate girders over interior pier supports. A more complete understanding of the factors that influence the inelastic moment-rotation characteristics within these regions of continuous-span bridge members is necessary for the benefits of autostress-

type methods to be realized fully in practice. The ultimate goal of this research is to develop simple comprehensive moment-rotation relationships for use in AASHTO autostress-type design procedures, and to illustrate by a detailed design study the application of these relationships within the specific context of the procedures recommended by Schilling (1997) and Schilling et al. (1996). This research encompasses bridge beams and girders with compact and noncompact webs, and with compact and ultra-compact flanges. The studies are focused predominantly on Grade 50 steels, since these steels are the most used in current bridge design practice. Other important variables considered include: (i) laterally-unsupported length, (ii) transverse stiffener spacing, (iii) moment gradient or moment to shear ratio (which is closely related to the total span-length to depth ratio L/D), (iv) the girder aspect ratio D/b_{fc}, and (v) the depth of the web in compression.

1.2 Work Plan

The above objectives have been pursued within the following work plan:

a. Information from prior experimental and analytical studies has been reviewed, collected and compiled into a uniform data set, to facilitate access to and comprehensive evaluation of the existing knowledge.

b. The existing data has been extended through a wide range of refined finite element parametric studies, to fill in the major knowledge gaps.

c. A focused set of experimental studies has been conducted to provide confirmation of several key attributes predicted based on analytical studies not available from existing experimental test data.

d. Comprehensive moment-rotation relations have been developed that are suitable for direct use in the new inelastic procedures that have been proposed by Schilling (1997) and Schilling et al. (1996) for incorporation into the AASHTO LRFD Specification.

e. The moment-rotation equations developed in this research have been verified against the existing and new experimental data, and have been compared to the strength equations in current design standards.

f. A detailed inelastic design of a three-span continuous plate-girder bridge has been developed, and the results of this design are compared to an elastic design of the same bridge by AASHTO LRFD (1994) procedures, published in (AISI 1995).

1.3 Organization

The main body of the report is subdivided into three chapters. Chapter 2 summarizes the implementation and execution of a reasonably comprehensive set of finite element parametric studies to fill in knowledge gaps in the available experimental data pertaining to the hogging moment-plastic rotation behavior of steel and composite steel-concrete bridge girders. This constitutes predominantly items (b) and (d) of the work plan. This chapter highlights key requirements for proper finite element modeling of the behavior, outlines the design of the finite element parametric studies, and presents the important "numerical test" results. Based on the finite element predictions, simple moment-rotation relationships are developed for use in design and rating of bridge structures.

Chapter 3 reviews the available experimental and finite element test data pertaining to the negative moment-plastic rotation behavior of continuous-span steel I-girders with compact or ultra-compact flanges. Current American specification formulas for the pier-section strength of these types of members and the moment-plastic rotation model developed by the authors are examined against the experimental and finite element test results. Several weaknesses in current specification provisions are observed. The new M-θ_p model avoids these weaknesses and provides a lower-bound approximation of the complete moment-plastic rotation response at the pier section. This chapter addresses items (a), (c) and (e) of the work plan.

Chapter 4 discusses the calculations and presents the results of a detailed trial inelastic design of a three-span continuous plate-girder bridge using suggested new inelastic design procedures – item (f) of the work plan. The characteristics of the calculations and the resulting design are compared to those of an elastic design of the same bridge by current AASHTO LRFD procedures. Various advantages, limitations and implications of the recommended procedures are observed based on this study.

The results of the study and recommendations for implementation are summarized in Chapter 5.

CHAPTER 2

FINITE ELEMENT EVALUATION OF PIER MOMENT-ROTATION CHARACTERISTICS IN CONTINUOUS-SPAN STEEL I-GIRDERS

This chapter summarizes the implementation, execution, and application of a reasonably comprehensive set of finite element parametric studies to fill in knowledge gaps in the experimental data on the hogging moment-plastic rotation behavior of steel and composite steel-concrete bridge girders. This is part of the larger overall effort by the authors with the objective of extending inelastic procedures to the design and rating of bridge plate girders with noncompact webs. The overall effort includes further experimental testing (Barth 1996), comparison with and verification against prior and new experimental data and current specification provisions (Chapter 3), and assessment of design procedures (Chapter 4). This chapter highlights key requirements for proper finite element modeling of the behavior, outlines the design of the finite element parametric studies, summarizes the analysis results, and presents moment-plastic rotation equations developed for use in design and rating of bridge structures.

2.1 Fundamental Behavior and Analysis Approach

The physical characteristics that can influence the pier moment-rotation behavior of noncompact composite or non-composite plate girders include:

1. Initial geometric imperfections such as out-of-flatness, bowing, tilting, and lack of alignment of the web and flange plates, as well as the overall initial sweep and twisting of the girder cross-section along the length.

2. Residual stresses due to flame cutting and welding.

3. Spread of plasticity, including strain-hardening and multi-dimensional plasticity effects.

4. Cross-section distortion.

5. Interaction of various local and overall modes of instability, that is, local flexural, shear and distortional buckling of the web panels, local buckling of the flange plates, and lateral buckling of the girder between brace points.

A shell finite element approach and J2 theory are chosen in this work as being both necessary and sufficient for modeling of the above behavior. Incremental-iterative solution procedures are applied to capture the combined geometric and material nonlinear effects on the pre- and post-peak (i.e., load shedding) response of isolated component specimens representing the hogging-moment region of prototype bridge I girders.

Only all-steel component specimens are considered in the parametric studies. This is justified by the fact that the nonlinearity caused by tension cracking of the bridge deck within the hogging-moment region of a composite girder is not associated with any plastic rotation in itself (Carskaddan 1991). As illustrated in Fig. 2.1 from (Carskaddan 1980), when a composite beam specimen is tested in three-point negative bending, the elastic unloading slope is reduced as the maximum applied moment at the simulated pier section is increased. This reduced elastic stiffness is due to cracking of the concrete deck. A slight increase in the elastic stiffness can be observed due to closure of cracks as the specimen is returned to zero load. For all practical purposes, the plastic (i.e., permanent) rotation θ_p comes solely from yielding in the steel.

The inelastic stability behavior of the steel section in a composite girder can be captured sufficiently by an all-steel test in which the size of the tension flange is increased to simulate the forces contributed by the reinforcing steel within the effective width of the concrete deck. In such a test, the change in the elastic unloading stiffness with increasing inelastic deformations is generally negligible. The nonlinear cracking behavior of the concrete deck is most appropriately addressed in conjunction with the consideration of time-dependent effects (e.g., creep and shrinkage), within the assumed elastic stiffness used for analysis of the bridge. All-steel tests may be used to develop the M-θ_p relationships for inelastic design. The validity of the above logic has been shown to be reasonable by comparison of similar composite and all-steel experimental tests (Carskaddan 1980), and it is further investigated in Chapter 3 and (White and Dutta 1993). As in the routine design of composite bridge girders, it is assumed that adequate shear connectors are provided such that the effects of slip between the steel girder and the concrete deck are negligible.

2.2 Test Configurations and Parameters

A generic configuration for the finite element "numerical tests" performed in this research is shown in Fig. 2.2. Specific characteristics and attributes modeled in all these studies are as follows:

- All the tests involve three-point bending to simulate the behavior within the hogging-moment region of composite or noncomposite continuous-span I girders. The dead weight of the test girders is neglected.

- The "numerical specimens" generally have multiple unbraced segments on each side of the peak moment location (i.e., the simulated pier section). This characteristic is significant because the noncritical segments (represented by L_{b2} in the figure) generally provide some end warping and lateral bending restraint to the critical unsupported segment of length L_{b1}. Although Fig. 2.2 shows only two unsupported segments on each side of the maximum moment location, a larger number of segments is specified in many of the tests. The total number of unsupported segments depends in general on the relationship between the lateral bracing requirements and the moment to shear (M/V) or span to depth (L/D) ratios of the prototype girders. In most of the tests, the simulated inflection point falls outside of the critical segment adjacent to the pier. However, the simulated inflection point is located within the critical unbraced length in three of the tests. All the studies include at least two unsupported segments on each side of the maximum moment location. The total length of the test girders is greater than or equal to $2L_{hog}$ in all the cases, where L_{hog} is the length of the simulated hogging moment region on each side of the pier. The rules for setting L_{b1} are presented later in this chapter. The "noncritical" unsupported lengths are in all the cases specified as

$$L_{b2} = 1.76r_t\sqrt{\frac{E}{F_{yc}}} \qquad (2.1)$$

but not less than L_{b1}. Equation (2.1) is the AASHTO LRFD (1994) bracing rule which ensures that a given unsupported length can develop the yield moment M_y in uniform bending prior to lateral-torsional buckling.

- A yield strength of *350 MPa (50 ksi)* is assumed in all the studies.

- The geometric imperfections are modeled based on AWS tolerances (AWS 1995).

- Residual stresses due to welding and flame cutting are modeled as per equations specified in (ECCS 1976).

Detailed information on modeling of the constitutive behavior, geometric imperfections, and initial residual stresses is presented later in this chapter.

Variables considered in the parametric studies are:

- The lateral unsupported length within the critical unbraced segment, or more specifically, the lateral slenderness of the girder as represented by the nondimensional parameter L_{b1}/r_y.

- The transverse stiffener spacing adjacent to the pier, represented by the aspect ratio of the associated web panels, $d_{o.in}/D$ (see Fig. 2.2).

- The moment gradient or moment to shear ratio (M/V), addressed by varying the total span length to depth ratio of the prototype girder (L/D), and assuming that the length of the hogging-moment region is $L_{hog} = 0.2L$ (see Fig. 2.2).

- The effective web slenderness ($2D_{cp}/t_w$), where D_{cp} is the depth of the web in compression associated with the plastic moment capacity of the section.

- The slenderness of the compression flange ($b_{fc}/2t_{fc}$).

- The girder section aspect ratio, that is, the ratio of the total web depth to the width of the compression flange (D/b_{fc}).

- The depth of the web in compression relative to the total web depth (D_{cp}/D).

The significance of each of these variables, and the specific values considered within the parametric studies, are summarized in the following subsections.

Lateral slenderness ratio L_{b1}/r_y

Two different equations for L_{b1}/r_y are considered: one based on the current AASHTO lateral bracing requirements for use of the Q formula (AASHTO 1994), developed in large part from the research by Bansal (1971), and a similar but more restrictive lateral bracing rule developed in early plastic design research by White (1956) and by Kusuda et al. (1960), and summarized in the ASCE-WRC Plastic Design Guide and Commentary (ASCE 1971). The current AASHTO formula can be written in the form

$$\frac{L_{b1}}{r_y} \leq \left[0.124 - 0.0759\frac{M_{min}}{M_{max}}\right]\left(\frac{E}{F_{yc}}\right) \tag{2.2a}$$

which is applicable for all values of M_{min}/M_{max}, whereas the requirement from (ASCE 1971) is

$$\frac{L_{b1}}{r_y} \leq \left[2.11 - 1.41\frac{M_{min}}{M_{max}}\right]\sqrt{\frac{E}{F_{yc}}} \tag{2.2b}$$

with the exception that the right-hand side of this equation is not required to be less than

$$\frac{L_{b1}}{r_y} = 0.0481\frac{E}{F_{yc}} \tag{2.2c}$$

In Eqs. (2.2a) and (2.2b), M_{max} is the maximum negative bending moment at the pier section, and M_{min} is the bending moment at the opposite end of the critical unsupported length. The ratio M_{min}/M_{max} is negative when these moments cause reverse curvature.

Only compact I shapes were considered in the original research by Bansal (1971), and by White (1956) and Kusuda et al. (1960), upon which the above lateral bracing rules are based. Equation (2.2a) ensures that continuous-span members of compact section can develop a *system deformation capacity* of at least three, defined by Bansal (1971) as

$$R_{sys} = \frac{\Delta_F}{\Delta_H} - 1 \tag{2.3}$$

The term Δ_F is the midspan deflection at the time when his continuous-span test girders have unloaded in post-collapse to *95* percent of their maximum load capacity, and Δ_H is the midspan deflection when the plastic moment is reached at the same point in the beam (the maximum positive bending moment is located at the midspan in all of Bansal's tests). Equation (2.2b) was developed in part from a simple analytical buckling model in which the beam is assumed to be partially elastic and partially strain hardened. Based on comparisons to experimental tests, Eqs. (2.2b) and (2.2c) appear to ensure a rotation capacity of approximately

$$R_{max} = \frac{\theta_{max}}{\theta_e} = 10 \tag{2.4}$$

for statically-determinate beams composed of I sections having plastic design proportions (ASCE 1971). In the above equation, θ_{max} is the maximum relative rotation that the test beams sustain between their ends before instability occurs due to lateral and/or local buckling, and θ_e is the corresponding theoretical rotation at which the plastic moment capacity is reached based on the elastic beam stiffness.

In the AASHTO Specifications (1994), usage of Eq. (2.2a) has been extended to I girders with noncompact webs. There is only limited experimental evidence to justify the use of Eq. (2.2a) for these cases and/or for members with $D_{cp}/D > 0.5$. In many of the tests that have been conducted

to date, the spacing of the lateral braces is significantly less than that required by the AASHTO limits (Eq. (2.2a)). Figure 2.3 shows the results of a preliminary finite element study by the authors, in which a symmetric girder tested in three-point bending by (Schilling and Morcos 1988), with $b_{fc}/2t_{fc} = 6.47$ and $D/t_w = 80.7$ (i.e., having an ultracompact flange and a compact web), is lengthened such that $L_{b1}/r_y = L_{hog}/r_y$ (see Fig. 2.2) is equal to the AASHTO limit (Eq. (2.2a)). As a result of increasing the length of the girder from that of the experimental test, the maximum shear is reduced to the extent that an unstiffened web is sufficient. Therefore, the only stiffeners provided in this numerical test are the bearing stiffeners at the load and reaction points. As in the experimental test (Schilling and Morcos 1988), the modified girder is not extended beyond the simulated inflection points (i.e., $L_{b2} = 0$).

Figure 2.3 compares the moment-rotation results obtained for this girder to the behavior of the same girder when additional braces are provided at one, two, and three additional equally-spaced locations on each side of the pier section, and when continuous lateral support is provided to the compression flange. It can be seen that the response of the girder depends significantly on the lateral brace spacing, and that for lateral bracing based on Eq. (2.2a), the girder is not able to reach the plastic moment capacity M_p. These results are discussed in more detail in Barth (1996). Equation (2.2a) was selected for the parametric studies to further test the current AASHTO bracing limits. Equation (2.2b) was selected somewhat arbitrarily, but generally would cut the maximum permitted cross-frame spacing adjacent to the piers approximately in half. It should be noted that M_{min}/M_{max} is generally larger when the cross-frames are located by Eq. (2.2b) rather than by Eq. (2.2a).

Transverse stiffener spacing adjacent to the pier, $d_{o.in}/D$

Schilling and Morcos (1988) conducted a series of component tests on noncompact web girders in which an additional stiffener was welded at $D/2$ on each side of the peak moment location. These stiffeners appeared to help restrain local buckling within the "plastic hinging" region of the girder. The three girders tested by Schilling and Morcos exhibited better moment-plastic rotation characteristics relative to earlier tests conducted by Schilling (1985, 1988). However, this improved behavior was due in part to the use of stockier ultracompact flanges and stockier webs in the second series of tests. Also, the maximum shears in the second set of tests

were reduced to values less than approximately *60* percent of the computed web shear capacities (thus, avoiding potential interactions between the flexural and shear strengths).

Huang (1994) performed finite element studies of noncompact web girders with various stiffener spacings near the pier section, using shell finite element procedures similar to those applied in this research. He refers to these plates as "inelastic restraint stiffeners." His results suggest that *D/3* may be an "optimum" spacing of the inelastic restraint stiffeners, if two stiffeners are used on each side of the pier section.

White (1994) conducted a suite of finite element studies in which several parameters of the Schilling (1985, 1988) and Schilling and Morcos (1988) tests were varied to ascertain their significance. In one set of his studies, the Schilling (1985, 1988) and Schilling and Morcos (1988) girders were analyzed with and without transverse stiffeners at *D/2* from the peak moment location. The usage of an inelastic restraint stiffener had a significant effect on the moment-rotation response in two of the component tests, but had very little influence on the behavior of the other specimens. The specific causes of this behavior could not be determined from these studies. However, it appeared that the influence of the stiffeners may be greatest for intermediate web slendernesses and for cases in which the compression flange is small compared to the area of the web in compression. Also, the improvements in the moment-rotation characteristics by the use of additional transverse stiffeners appeared to be due largely to restraint of twisting of the compression flange about the longitudinal axis of the girder relative to the web plate, and restraint of distortional buckling of the girder, rather than their influence on shear buckling distortions within the web.

Based on the above research, it was decided to consider two cases for further parametric study: two inelastic restraint stiffeners on each side of the pier, spaced at *D/3*, and no additional inelastic restraint stiffeners. In all the studies, "ordinary" one-sided transverse stiffeners were placed such that the nominal shear capacity of the "numerical tests," including web post-buckling strength where applicable, is greater than or equal to *1/0.6 = 1.67* of the applied shear corresponding to development of the plastic moment at the pier section. This decision is derived from the current AASHTO LRFD provisions (1994), which for noncompact webs designed based on shear post-buckling strength, specify an interaction between flexural and shear strengths when the applied concomitant shear exceeds *60* percent of the design shear strength of the web panel, $\phi_v V_n$. Based

on preliminary discussions with the advisory groups for this research, it was decided to design the numerical test specimens such that moment-shear strength interaction would not need to be considered in checking the girders by the AASHTO LRFD provisions. Minimum bearing and intermediate stiffener sizes that satisfy the AASHTO LRFD (1994) provisions are used in all the current studies with one exception -- if the required size of the transverse stiffeners is larger than that of the bearing stiffeners, the same size plate is used for both types of stiffeners. The stiffener widths vary from *0.25* to *0.37* of the flange width for girders with $D/b_{fc} = 3$, and from *0.36* to *0.56* of the flange width for girders with $D/b_{fc} = 4.25$.

In current practice, it appears that many fabricators would prefer to eliminate as many transverse stiffeners as possible to reduce costs. It is expected that the above $V \leq 0.6\phi_v V_n$ restriction could be applied only within the critical unbraced segment adjacent to the pier without having any significant effect on the $M\text{-}\theta_p$ behavior of the girders. However, intermediate transverse stiffeners generally help stiffen the web against distortional buckling in addition to providing web shear post-buckling strength, particularly for high D/t_w values. Therefore, reducing the number of transverse stiffeners within the critical unsupported length from that required by the above rule would require further study. Nevertheless, the authors have observed that for girders with $D/b_{fc} = 4.25$ and $L/D = 30$, the cross-frame connection plates alone are usually sufficient to satisfy this requirement for the range of web slenderness considered in this work ($2D_{cp}/t_w \leq 163$). In other words, if the aspect ratio (D/b_{fc}) and the span-to-depth ratio (L/D) of a girder are specified close to the upper limits considered in this study, transverse stiffeners are generally not needed to satisfy the $V \leq 0.6\phi_v V_n$ requirement for the shear concomitant with the maximum moment loading conditions.

Moment gradient and span-to-depth ratio L/D

Numerous research studies have demonstrated some sensitivity of the $M\text{-}\theta_p$ response of I sections to moment gradient, e.g. (Lay and Galambos 1967; Grubb and Carskaddan 1979; Kemp 1986; Kuhlmann 1989; White 1994). Since the moment gradient is equal to the transverse shear force in the member, some interaction between the shear and flexural strengths might be expected if the moment gradient exceeds a certain value. To avoid these possible interaction effects in the design of the test girders, the applied shear force corresponding to the theoretical plastic moment

at the pier section is limited to a maximum of *60* percent of the nominal shear strength in this work, as noted above.

If moment-shear strength interaction is avoided, then it is expected that smaller moment gradients will be more detrimental to the M-θ_p behavior. This is due to the fact that the inelastic length of the compression flange adjacent to the pier is larger for smaller moment gradients. The influence of moment gradient on the lateral-torsional buckling behavior is captured to some extent by the M_{min}/M_{max} term within the lateral bracing requirements of Eqs. (2.2a) and (2.2b). Accordingly, the lateral braces are placed exactly at the positions specified by these equations in the numerical tests performed in this work. However, the moment gradient generally affects more than just the lateral-torsional buckling behavior -- the inelastic length of the compression flange also has a significant effect on the local buckling response. For compact section beams, Kemp (1986) and Kuhlmann (1989) conclude that L_{hog}/b_{fc} is a significant parameter, whereas Grubb and Carskaddan (1979) have concluded that L_{hog}/D_{cp} is important. In this work, it was decided that the prototype bridge girder span to depth ratio *(L/D)* would be the best parameter to vary to investigate the effect of the moment gradient. This is because L/D possibly has the greatest physical meaning of the above ratios to the bridge designer, and also because variations in L_{hog}/b_{fc} and L_{hog}/D_{cp} are handled implicitly due to the parametric variations in D/b_{fc} and D_{cp}/D in these studies. Two values of L/D representative of relatively deep and relatively shallow bridge girders were selected: *L/D = 20* and *30*. To transform the resulting bridges back to hogging-moment component tests, it is assumed that L_{hog} = *0.2 L*. In addition to accounting for moment gradient effects, this variation in L/D provides data for assessment of the potential significance of changes in the ratio of the moment and shear *(M / V)* at the pier section, associated with the "actual" loadings on continuous-span bridge girders.

Cross-section based variables

Each of the variables discussed above involves dimensions along the *length* of the bridge girder. The other variables considered in the parametric studies involve only attributes of the girder cross-section. These variables are discussed together in this subsection. After careful consideration of all the possible parametric studies, the authors decided to lower-bound the effect of each of the above "length-related" variables in the development of design M-θ_p relations. This decision was based in part on the fact that initial parametric studies showed these variables to be

generally of lesser significance compared to the cross-section attributes for practical girder proportions. However, of equal importance is the fact that the inclusion of lateral brace spacing, transverse stiffener spacing, and moment gradient effects would significantly complicate the simplified M-θ_p expressions needed for design and rating procedures.

Of the cross-section based variables, the web and flange slenderness parameters ($2D_{cp}/t_w$ and $b_{fc}/2t_{fc}$) are of course expected to influence significantly the strength and inelastic rotation capacity. The web slenderness is varied from maximum limit stated in the 1986 Alternate Load Factor Design Specification of *86* for Grade 50 steels to the maximum slenderness permitted without the use of longitudinal stiffeners, $2D_{cp}/t_w = 163$ for Grade 50 steels in the AASHTO LRFD provisions (1994). Also, an intermediate web slenderness between these two limits of $2D_{cp}/t_w = 125$ is considered. These $2D_{cp}/t_w$ values are the same as the target values tested by Schilling and Morcos (1988). It should be noted that the web compactness limit in the AASHTO LRFD Specifications (1994), $2D_{cp}/t_w = 91$ for Grade 50 steel, is based largely on the experimental studies by Croce (1970). Croce tested eight different symmetric, all-steel, continuous-span girders fabricated from A36 steel plates, and found that the a plastic mechanism was developed even for the girder with the largest D/t_w that he tested ($D/t_w = 123$). Croce recommended extending conventional plastic design procedures to webs up to $D/t_w = 125$ (for A36 steel) as long as the applied shear stress is less than the elastic/inelastic buckling stress of the web plate, assuming simply-supported edge boundary conditions.

Flange slenderness values $b_{fc}/2t_{fc}$ based on the current AASHTO (1994) compactness limit of *9.2* and based on the limit of *7.0* for conventional plastic design (for Grade 50 steels) are considered in this work. The compactness limit of *9.2* comes largely from the experimental research reported by Lukey and Adams (1969). The Lukey and Adams test data indicates that adequately braced simply-supported beams of symmetric I sections, with $D/t_w \leq 52$ (for $F_y = 350$ *MPa*) and an effective flange slenderness equal to the above compactness limit, are capable of providing a rotation capacity

$$R_{ult} = \frac{\theta_{ult}}{\theta_e} - 1 \tag{2.5}$$

of at least three, where θ_{ult} is defined as the maximum total rotation at which the resisting moment falls below M_p on the descending portion of the moment-rotation curve. Schilling and Morcos

(1988) were the first to introduce the term "ultracompact" for Grade 50 flanges with $b_{fc}/2t_{fc} \leq$ *7.0*. This limit has been derived and/or specified by numerous researchers as a value for which conventional steel I sections can sustain substantial inelastic rotations prior to the onset of flange local buckling (Haaijer 1957; Lay 1965; Climenhaga and Johnson 1972b; Kuhlmann 1989). Available experimental test data suggests that an R_{ult} greater than about *10* can be achieved in three-point bending tests of simply-supported beams when this limit and a web compactness limit of approximately $2D_{cp}/t_w = 60$ are satisfied (ASCE 1971; Climenhaga and Johnson 1972b; Kuhlmann 1989). However, there is wide scatter in the test results, and in some cases, R_{ult} is as low as *5* for these same flange and web proportions (Kuhlmann 1989). This is possibly due in part to variability of the strain-hardening properties, but also, it is likely caused by the complex dependencies of R_{ult} on a wide number of test variables. For sections with larger web slenderness values, the rotation capacity, as measured by the traditional definitions such as Eqs. (2.4) or (2.5), is substantially reduced. However, the prior test data indicates that the moment capacity (ignoring strengths larger than M_p) is relatively independent of the flange slenderness for values of $b_{fc}/2t_{fc}$ less than the flange compactness limit (i.e., *9.2* for Grade 50 steels). This is reflected by the fact that the flexural strength specified by the Q formula in the present AASHTO LRFD Specifications (1994) is independent of the flange slenderness for sections satisfying the flange compactness limit.

Of the two remaining cross-section variables listed at the beginning of this section, the influence of D_{cp}/D on the moment-rotation behavior is well documented in the literature (Climenhaga and Johnson 1972b; Grubb and Carskaddan 1979; Schilling 1985, 1988). However, its precise influence on the M-θ_p characteristics is not well understood. Based on discussions with various researchers and practicing engineers in the advisory groups for this research, it was decided that engineers would often attempt to proportion the pier cross-sections such that approximately one-half the depth of the web would be placed in compression (based on a cracked plastic section analysis). Nevertheless, it was decided that in some cases, D_{cp}/D may need to be as large as *0.75* in practical designs. Therefore, values of D_{cp}/D equal to *0.5*, *0.625*, and *0.75* were selected for this research program, with the majority of the studies focused on $D_{cp}/D = 0.5$.

Finally, it was determined that the aspect ratio of the cross-section, D/b_{fc}, could have a significant influence on the girder M-θ_p behavior. Figure 2.4 illustrates the importance of this

parameter. Basically, for constant D/t_w, $b_{fc}/2t_{fc}$, and D_{cp}/D, increasing D/b_{fc} significantly changes the ratio of the area of the web in compression to the area of the compression flange. The traditional AASHTO formula for the flexural strength of plate girders specified in the LRFD Specifications (1994) contains a "load-shedding" factor R_b, which accounts for the reduced effectiveness of noncompact webs in resisting flexural compression due to local web buckling. This factor is influenced significantly by the parameter

$$a_r = \frac{2D_c t_w}{b_{fc}t_{fc}} \tag{2.6}$$

i.e., the ratio of two times the area of the web in compression for the hypothetical elastic section to the area of the compression flange. Figure 2.4 shows the relationship between a similar parameter, a_{rp}, (based on the plastic web depth in compression, D_{cp}, rather than the elastic depth D_c) and the variables considered in this work. For the ranges of the parameters considered in this work, a_{rp} varies from 0.78 to 4.5. More fundamentally, for larger a_{rp} (generated by a larger compressive web to flange area, or by use of a larger D/b_{fc}), the inelastic stability of the compression flange is more apt to be disturbed by the local buckling behavior of a noncompact web. Also, for larger a_{rp}, the number of intermediate transverse stiffeners required for the web to have adequate shear resistance is reduced (i.e., the required spacing of the transverse stiffeners is larger). The use of fewer transverse stiffeners makes the sections more susceptible to web distortional buckling effects. In this work, D/b_{fc} is treated as the independent variable in establishing a matrix of numerical tests, since the range of this parameter is simple to quantify. The parameter a_{rp} is derived from the independent variables D_{cp}/D, $b_{fc}/2t_{fc}$, D/t_w, and D/b_{fc} as shown in Fig. 2.4.

Summary

If all the tests in a matrix composed of the variables outlined above were conducted, a total of 288 analyses would need to be considered. However, many of these tests may be ruled out by first executing a subset of these studies to ascertain that certain variables have lesser influence than others. For the variables that appear to have a smaller influence on the behavior, only the tests necessary to be able to estimate a lower-bound $M\text{-}\theta_p$ response are retained. Tables 2.1 through 2.3 summarize the "numerical tests" that have been conducted, the sequencing of these tests, and the decision process in eliminating the need to consider certain combinations of the test variables. The majority of the finite element studies were conducted using symmetric girders with $b_{fc}/2t_{fc} =$

9.2. These tests, which are all given the designation "Cn" (C stands for compact flange and n represents the number assigned to each test), are shown in Table 2.1. These studies allowed the authors to ascertain the acceptability of using the current AASHTO lateral bracing rule (Eq. (2.2a)), stiffeners spaced only at $V/V_n = 0.6$, and $L/D = 30$ to establish lower-bound M-θ_p curves for these "length-related" variables. Table 2.2 shows the sequence of tests performed on girders with ultracompact flanges. These tests are given the designation "UCn," where UC stands for an ultracompact flange and n again represents the test number. The first three of these tests were actually conducted before the lower-bound bracing and inelastic restraint stiffener spacing limits were set. These tests serve to demonstrate close to upper-bound moment-rotation characteristics for the three different $2D_{cp}/t_w$ values that have been studied. Finally, Table 2.3 summarizes the unsymmetric girder tests considered in this work. For economical plate girder designs, it is expected that the web often will be close to the maximum $2D_{cp}/t_w$ permitted for transversely-stiffened girders when D_{cp}/D is significantly larger than *0.5*. Therefore, only values of $2D_{cp}/t_w$ = *163* were considered for the unsymmetric girder studies. The resulting D/t_w values are *130* for $D_{cp}/D = 0.625$ and *109* for $D_{cp}/D = 0.75$. The reader is referred to (Barth 1996) for a detailed presentation of each of the test girder designs.

It should be noted that the most economical plate girder designs will often involve a high $2D_{cp}/t_w$ to minimize the amount of web material. Also, D/b_{fc} is usually larger for plate girders than for rolled beam sections for increased efficiency in strong-axis flexure (rolled beam sections tend to have maximum D/b_{fc} values only slightly larger than three). Furthermore, the flanges will often tend to be close to the compactness limit of $b_{fc}/2t_{fc}$ = *9.2* (for Grade 50 steel), to maximize the L_b/r_y of the girder for a given amount of flange material. This increases the distance that the cross-frames can be spaced apart, and thus may reduce the total number of required cross-frames. There is a practical limit to the extent that D/b_{fc} can be increased before the cross-frame spacing required by Eqs. (2.2a) or (2.2b) becomes prohibitively small. The authors have estimated this extent to be in the neighborhood of D/b_{fc} = *4.25*.

2.3 Representation of Physical Attributes for Analysis

Finite Element Mesh and Nodal Constraints

Figure 2.5 shows a typical deformed finite element mesh and the nodal displacement constraints applied in all the finite element models. Ten elements through the depth of the web, eight elements across the width of the compression flange, and four elements across the width of the tension flange are used in all the studies. It should be noted that this mesh is shown in an inverted position relative to the hogging-moment region of the prototype girder, i.e., the top flange is placed in compression. The STARS finite element program and a displacement-based nine-node Lagrangian shell element (White and Abel 1990; Dutta 1992) are used for all the studies conducted in this work. The transverse stiffeners, outlined by dashed lines in the figure, are modeled using a compatible three-node Lagrangian eccentric beam element (Dutta and White 1992). The reference axis for these beam elements is located at the centerline of the web; eccentric one-sided stiffeners are modeled by integrating only over the cross-section of the physical one-sided stiffeners. The transverse stiffeners are assumed to remain elastic.

All the "numerical tests" are modeled using an assumed symmetry about a vertical axis through the web at the peak-moment location, which is on the right-hand end of the finite element mesh shown in the figure. The symmetry constraints and boundary conditions at this location are detailed in the figure. Only the bearing stiffener on one side of the web is modeled at the symmetry location. Also, the web nodes are all restrained against lateral and longitudinal movement at this location, and are prevented from twisting about the longitudinal axis of the girder and about the horizontal Z axis. However, they are free to move vertically and to rotate about the vertical Y axis. The flange nodes are all slaved to the web node at the web-flange juncture. This constraint effectively enforces the kinematic assumption that plane sections remain plane in each of the separate flanges at the pier section. However, the warping (i.e., cross-bending) of the flanges, associated with lateral-torsional and/or local buckling of the compression flange is not restrained.

It is important to recognize that the final failure mode in experimental tests often involves severe inelastic local and overall buckling on one side of the midspan, with predominant elastic unloading on the opposite side of the load point. The above constraints and boundary conditions at the pier section ignore any warping or lateral bending restraint that might be provided by the

elastically unloading side of the test specimen. In effect, the deformations on one side of the pier are assumed to be an identical reflection of those on the other side. In preliminary studies by the authors and detailed in (Barth 1996), the results of a full-length model of a component test, but with initial geometric imperfections specified only on one side of the peak-moment location, were compared to a model based on the above symmetry assumption. The two models produced results that are practically identical. It is believed that the total plastic rotation experienced in the vicinity of the pier for a given test is approximately the same regardless of the extent that each of the sides experience plastic loading or elastic unloading (which can be sensitive to slight differences between the two sides of the specimen).

The web nodes are restrained in the lateral direction at both the top and bottom of the web at each of the brace locations. Also, the node at the bottom flange-web juncture is restrained in the vertical direction at the simulated inflection point location of the tests.

Stress-Strain Characteristics

A single-surface plasticity model based on J2 theory is employed to represent the material response. The through-thickness normal stress within the plates is assumed to be zero, but otherwise the interaction between the transverse and longitudinal normal stresses and the membrane and transverse shear stresses within the cross-section plates are all included within the constitutive model. Kinematic hardening of the yield surface is assumed, producing the multi-linear (elastic-yield plateau-strain hardening) effective stress-strain response shown in Fig. 2.6. In addition to the elastic modulus E and the yield stress F_y, the strain-hardening modulus and the strain-hardening strain (ε_{st} and E_{st}) are of key importance to the inelastic moment-rotation behavior. Alpsten (1972) provides possibly the most comprehensive compilation of test data for assessment of these parameters. The values of ε_{st} and E_{st} shown in the figure are averages reported by Alpsten for twelve tension tests on A572 - Grade 50 material of medium thickness (*19* mm). Alpsten reports a distinct relationship between the plate thickness and the strain-hardening properties in that E_{st} increases and ε_{st} decreases with increasing thickness. He gives averages of E_{st} = *3200* MPa (*470* ksi) and ε_{st} = *0.019* for *13* mm plates, and E_{st} = *5700* MPa (*830* ksi) and ε_{st} = *0.006* for *38* mm material. These variations are greater than the differences between averages of different types of steel. For low-carbon material taken from the interior of thick steel plates,

Alpsten states that the material typically exhibits a gradual yielding transition from the elastic response into strain-hardening, without any definite yield plateau. Based on a large database of collected test data, he also observes that the values for E_{st} are generally about *25* to *50* percent higher in compression than in tension for steels ranging from F_y = *230* MPa (*33* ksi) to *450* MPa (*65* ksi). However, the only compression test data for Grade 50 steels cited by Alpsten is for A441 material, for which E_{st} is reported as *5600* MPa (*810* ksi) in compression versus *4500* MPa (*650* ksi) in tension. No distinction between ε_{st} in tension versus compression is reported. The values of ε_{st} and E_{st} specified in Fig. 2.6 are felt to reasonable "average" values for Grade 50 flange and web material in bridge plate girders. Given the variability of the data for the strain-hardening properties, the authors decided to assume the same stress-strain behavior in tension and compression in the studies presented here.

The shell finite element model employed in this work is based on the assumption of large displacements and large rotations, but small strains. The "cap" on the stress-strain curve at the ultimate tensile stress F_u is simply an approximate device to limit the extent of the strain hardening for tensile or compressive strains larger than about *0.03*. It should be noted that total effective strains larger than this magnitude tend to be developed only within local buckles of the flange and web plates well into the descending branch of the associated M-θ_p curves.

Residual Stresses

The ECCS Manual on Stability of Steel Structures (ECCS 1976) provides possibly the most comprehensive summary of simplified equations for estimating residual stresses. These equations reflect the two primary causes of longitudinal residual stress in welded I girders: flame cutting of the plates and longitudinal welding between the flanges and the web. The residual stresses are essentially equal to the yield stress of the material in tension within a small width at the heat affected zones, and a smaller near-constant self-equilibrating stress in compression is generated within the other regions of the plates. The ECCS Manual (1976) provides equations for estimating the widths that are effectively stressed at F_y in tension. For a plate that is flame-cut along a longitudinal edge, this width is

$$c_f = \frac{1100\sqrt{t}}{F_y} \quad (mm) \tag{2.7a}$$

adjacent to each flame cut edge, where t is the thickness of the plate in mm and F_y is the tensile yield stress in MPa. Also, assuming a continuous single-pass weld between the web and the flanges, the resulting width stressed at the tensile yield strength on each side of the centerline of the weld in the flanges, and on each of the top and bottom edges of the web plate is effectively

$$c_w = \frac{12000pA_w}{F_y \Sigma t} \quad (mm) \tag{2.7b}$$

where p is a process efficiency factor, equal to 0.90 for submerged arc welding, A_w is the cross-sectional area of the added weld metal in mm^2, and Σt is the sum of the plate thicknesses meeting at the weld in mm. The effect of welding along a previously flame-cut edge does not result in the algebraic addition of the tension block widths c_f and c_w since the weld heat tends to relieve the tension stresses caused by the cutting. The final tension block width c_{fw} at each of the web edges (assuming that both edges of the web plate are flame cut) is estimated as (ECCS 1976)

$$c_{fw} = \left(c_f^4 + c_w^4\right)^{0.25} \tag{2.7c}$$

If it is assumed that the web is fillet welded on each side to the flange plates, (ECCS 1976) suggests the following equation for the final tension block width in the flange plates on each side of the centerline of the web-flange juncture:

$$c_2 = c_w + 0.5t_w, \quad \text{for } t_w \le 2c_w \tag{2.7d}$$

Given the widths c_f and c_2 stressed at F_y at the edges and interior of the flange plates, and the widths c_{fw} stressed at F_y at the edges of the web plate, and neglecting the reduction in the residual stresses at the flange tips due to the compressive residual stresses generated by the welding, the smaller compressive residual stresses within the majority of the plate areas can be calculated based on equilibrium of the longitudinal residual stresses in each of the plates.

If the above equations are followed faithfully, one result is that the predicted residual stresses are highly dependent upon the size of the cross-section. The residual stresses will tend to be somewhat higher in typical experimental test specimens compared to the corresponding stresses computed for larger prototype bridge girders. Based on typical test specimen dimensions from (Schilling and Morcos 1988) and (Barth 1996), approximate "average" values of c_f/b_f from $1/20$ to $1/15$ and c_2/b_f from $1/16$ to $1/8$ may be estimated for the flange plates. For the web plates, c_{fw}/D may be estimated as approximately $1/60$ to $1/30$ for $D/t_w = 163$, $1/45$ to $1/22$ for $D/t_w = $

125, and *1/30* to *1/15* for $D/t_w = 86$. The resulting uniform compressive residual stresses generated in the bulk of the flange plates ranges from about *0.3* to *0.6F$_y$*. In the web plates, the compressive residual stresses are approximately *0.03* to *0.07F$_y$* for $D/t_w = 163$, *0.05* to *0.10F$_y$* for $D/t_w =125$, and *0.07* to *0.15F$_y$* for $D/t_w = 86$. For a given welding process, the most influential parameter in the above estimates is the area of the fillet welds between the web and the flanges. For the typical test specimen dimensions, small variations in the process and/or size of these welds can have a significant effect on the extent of c_w and c_{fw}, and the magnitude of the compressive residual stresses. Fortunately, preliminary studies conducted in the research by (White 1994) and (Barth 1996) indicate that the predominant effect of the residual stresses, for the types of girders studied in this work, is simply an early yielding and gradual softening of the pre-peak moment-rotation curves. The effect on the maximum moment capacity and on the post-peak inelastic rotations appears to be small.

Figure 2.7 illustrates the self-equilibrating Gauss point residual stresses specified for all the parametric studies conducted in this work. A 2x2 Gauss integration rule is employed within each shell element. Therefore, there are sixteen integration points across the width of the compression flange, eight across the width of the tension flange, and twenty through the depth of the web. Because of the coarser mesh across the width of the tension flange, it is important to "lump" the high residual tension stresses at one set of Gauss points, rather than specifying a set of smaller tensile Gauss point stresses that equilibrate the compressive stresses of *-0.5F$_y$*. Otherwise, the effects of the large tensile residual stresses are not as well approximated. The authors have found that this has a significant effect on the prediction of pre-peak inelastic rotations measured in experimental tests. In the web plates, a quadratic transition is assumed to occur from F_y in tension at the web-flange juncture to a constant compressive residual stress within the shell elements at the top and bottom of the web plate, rather than specifying a variable width tension block. This is acceptable since the 2x2 rule in the shell elements is capable of integrating up to a cubic variation in residual stresses exactly. Also, the compressive web residual stresses shown in the figure are significantly larger than the estimated maximum values discussed above for $D/t_w = 86$. The compressive residual stress of *-0.227F$_y$* for compact web plates is representative of the compressive web residual stress of *-0.25F$_y$* suggested for modeling of welded I sections in (ECCS 1984). The f_{rc} /F_y values shown in Fig. 2.7 are specified as *80* percent of the elastic buckling stress of the web plate, assuming uniform longitudinal compression and simply supported edges.

As a final note, it should be pointed out that the residual stresses shown in Fig. 2.7 are actually in equilibrium only within perfectly flat plates. Furthermore, these stresses must be zero at the free ends of the test specimens for satisfaction of equilibrium. Therefore, in the finite element solutions conducted in this work, zero load is applied in the first step of the analysis, and the residual stresses are allowed to equilibrate. This causes some small changes in the modeled residual stress patterns.

Initial Geometric Imperfections

Three types of geometric imperfections are specified in the analysis models: an out-of-flatness of the web, a tilt of the compression flange, and a lateral sweep of the compression flange. These imperfections are illustrated in Fig. 2.8. The specified initial out-of-flatness of the web is similar in magnitude to the maximum values permitted by the AWS Code (1995), which range from $d/67$ for panels of interior girders with one-sided stiffeners (where d is the least panel dimension) to $D/150$ for unstiffened girders (measured using a straight edge whose length is no less than d). In this work, the initial web out-of-flatness is specified as:

if $d_o < D$, then $\delta_{ow} = d_o /100$; otherwise $\delta_{ow} = D/100$.

The maximum tilt of the flanges, δ_{of}, permitted by the AWS Code is $1/100$ of the total flange width or $1/4 in.$, whichever is greater. The initial tilt of the compression flange is specified in this work by the relation:

if $b_{fc} < 0.3d_o$, then $\delta_{of} = b_f/150$; otherwise $\delta_{of} = 0.3d_o /150 = d_o /500$.

For long panels (i.e., $b_{fc} < 0.3d_o$), these values tend to be slightly less than that permitted by the AWS code; however, for short panels, they may be significantly less than the AWS tolerances. The authors believe that it is unlikely that the flanges would be distorted to the extent permitted by AWS code within a short panel length. The out-of-flatness of the web plate is assumed to be sinusoidal in the X and Y directions within each web panel (see Fig. 2.8), and the compression flange tilt is assumed to vary as a sinusoidal twist about the longitudinal X axis of the girder, with a linear variation of this imperfection in the Z direction. The web and flange imperfections are assumed to alternate in sequence from panel to panel (i.e., δ_{ow} and δ_{of} are either both positive, as illustrated in the figure, or both negative within any given panel).

The AWS Code (1995) limits the variation in straightness of welded beams or girders, where there is no specified camber or sweep, to $L/960$ (where L is defined as the total length). In this work, a sinusoidal sweep of the compression flange with an amplitude of $\delta_{oL} = L_b /1500$ is assumed along the length of the girder such that the lateral sweep at any location X, measured from the peak-moment location, is given by

$$\delta_L = \delta_{oL} \sin\left(\frac{N\pi X}{L_b}\right) \tag{2.8}$$

The initial geometric imperfections are increased slightly during the first increment of the analysis due to the equilibration of the residual stresses (see the discussion in the previous subsection). The specified initial imperfections are set such that the maximum imperfections at the end of this analysis step are still slightly less than the maximum AWS tolerances (1995).

2.4 Summary of Analysis Results

Figures 2.9 through 2.14 summarize the moment-plastic rotation results from all the parametric studies. In each of these figures, the normalized moment M/M_p is plotted versus the plastic rotation in radians. Only the portion of the curves for $M/M_p > 0.5$ is shown to increase the resolution of the plots. There are many comparisons that can be made between the various curves. Each of the figures focuses on illustrating the effects of several sets of parameters, and are discussed separately in the following subsections. All the results from the parametric studies except tests C22, C23, C24, and UC10 are shown in the collective plots. The results from tests C22, C23 and C24 did not differ significantly from tests C7, C8 and C9 respectively, and the results from test UC10 did not differ significantly from those for test UC5. All the plots in Figs. 2.9 through 2.13 show curves from the symmetric girder tests for each of the values of D/t_w studied (86, 125, and 163). In each of these figures, the thick solid curves correspond to $D/t_w = 86$, the thin solid curves correspond to $D/t_w = 125$, and the dashed curves are for $D/t_w = 163$. All the plots in Fig. 2.14 show curves for the different D_{cp}/D values studied (0.5, 0.625, and 0.75) in the unsymmetric and comparable symmetric girder tests. In this figure, the thick solid curves are for $D_{cp}/D = 0.5$, the thin solid curves are for $D_{cp}/D = 0.625$, and the dashed curves are for $D_{cp}/D = 0.75$.

Effect of L_{b1}/r_y and Stiffener Spacing (Figs. 2.9 and 2.10)

Figures 2.9 and 2.10 illustrate the effect of varying L_{b1}/r_y and $d_{o.in}/D$. In Fig. 2.9, the black curves correspond to test girders in which L_{b1}/r_y is set at the ASCE limit (Eq. (2.2b)) and two inelastic restraint stiffeners are spaced at $D/3$ on each side of the pier section. The light-grey curves are for L_{b1}/r_y set at the AASHTO limit (Eq.(2.2a)) and with transverse stiffeners placed only such that the maximum applied shear is less than $0.6V_n$ using the AASHTO shear strength equations. The plot on the left of Fig. 2.9 is for girders with compact flanges, whereas the plot on the right is from the tests with ultracompact flanges. The span-to-depth ratio and the cross-section aspect ratio are held constant at $L/D = 30$ and $D/b_{fc} = 3$ in this figure.

The following trends can be observed from the plots in Fig. 2.9:

- For both compact and ultracompact flange girders, the load-shedding behavior is somewhat less abrupt for smaller L_{b1}/r_y and $d_{o.in}/D$ values (compare the black curves to the light-grey curves in each of the plots).

- The moment capacity for test UC4, which is based on the AASHTO and $0.6V_n$ rules for the brace and stiffener spacings and has a $D/t_w = 163$, is five percent less than that of the comparable girder, UC1, which has a $D/t_w = 163$ but is based on the more restrictive brace and stiffener spacing rules. However, the variations in L_{b1}/r_y and $d_{o.in}$ have a negligible influence on the maximum moment capacity for the ultracompact-flange girders with $D/t_w = 86$ and 125, and for all the compact-flange girders (again, compare the black curves to the light-grey curves in each of the plots).

- The moment capacity and ductility of test UC1 is slightly better than that for UC2, even though the web is more slender for UC1. This trend appears to result from the fact that the transverse stiffeners were more closely spaced in UC1 than in UC2 ($d_{o.el}/D = 0.83$ versus 1.67).

- By comparing the curves in the plot on the left to those in the plot on the right, it is evident that the moment-rotation behavior is significantly more ductile for the girders having ultracompact flanges. Test UC3, which has ultracompact flanges, two inelastic restraint stiffeners spaced at $D/3$ on each side of the pier section, and L_{b1} based on the more stringent ASCE rule (Eq. (2.2b)), produces the most ductile moment-rotation behavior of all the specimens studied in this work.

The lateral brace and stiffener spacings are varied together in the comparisons of Fig. 2.9; therefore, it is not possible to discern the separate effects of these variables from this figure. Figure 2.10 provides some help in assessing the isolated effect of changing the stiffener spacing adjacent to the pier. In this figure, the black curves correspond to the use of two inelastic restraint stiffeners at $D/3$ on each side of the pier, whereas the light-grey curves are for transverse stiffeners placed solely based on the $0.6V_n$ rule. The plot on the left in Fig. 2.10 is for girders with an aspect ratio of $D/b_{fc} = 3$, whereas the plot on the right corresponds to $D/b_{fc} = 4.25$. All the curves in Fig. 2.10 are for constant $L/D = 30$, compact flanges, and L_{b1}/r_y based on the current AASHTO bracing requirements (Eq. (2.2a)).

The following behavior is evident from Fig. 2.10:

- For all the cases with $D/t_w = 125$ and 163, the use of the more closely spaced stiffeners has essentially zero effect on the moment capacity (compare the black curves to the light-grey curves in each of the plots).

- For $D/t_w = 86$, the moment capacity is slightly larger for the wider stiffener spacing in the plot on the left (i.e., for $D/b_f = 3$), but in the plot on the right (i.e., for $D/b_{fc} = 4.25$) the strength is reduced slightly for the wider stiffener spacing. It is likely that this behavior is related to the complex conditions which affect how much the stiffeners restrain flange local buckling (e.g., the ratio of $d_{o.in}$ and/or $d_{o.el}$ to the wave length of the flange local buckles), as well as to the magnitude of the initial curvatures introduced in the compression flange (for the shorter stiffener spacing, the initial curvatures due to the imperfections δ_{of} are larger).

- The load shedding is less abrupt in the girders that have additional inelastic restraint stiffeners. However, for $D/b_{fc} = 4.25$ and $D/t_w = 125$ and 163, the effect of the additional stiffeners is quite small (again, compare the black curves to the light-grey curves in each of the plots).

- The curves in the right-hand plot, corresponding to $D/b_{fc} = 4.25$, have a markedly reduced maximum moment capacity and ductility compared to the curves in the plot on the left, which correspond to $D/b_{fc} = 3$.

Effect of Moment Gradient (Fig. 2.11)

The plots in Fig. 2.11 show the effect of changing L/D in symmetric sections with compact flanges, d_o based solely on the $0.6V_n$ rule, and L_{b1}/r_y based on the current AASHTO

requirements. The plot on the left is for girders with $D/b_{fc} = 3$, and the plot on the right is for $D/b_{fc} = 4.25$. The black curves are for $L/D = 20$ whereas the light-grey curves are for $L/D = 30$. These plots indicate that for the combinations of parameters considered, the effects of changes in the moment gradient, or changes in the M/V ratio at the pier, are insignificant. This is contrary to the behavior that has been observed in the studies cited earlier in this chapter. It is believed that these differences in the observed behavior are due in part to the fact that the present studies are on girders with webs that are relatively slender compared to the web plates in the other studies that have considered moment gradient effects. The moment gradient effects may be larger in sections with stockier web plates. However, in many of the prior studies, the ratio of L_{b1} to the AASHTO and ASCE bracing requirements is not constant among the tests that vary the moment gradient. In some cases, the tests may be affected more by these variations in the lateral bracing parameter rather than by changes in the moment gradient. Comparison of the plots on the left and right-hand sides of Fig. 2.11 again indicates a significant effect of D/b_{fc} on the moment-rotation behavior.

Effect of Flange Slenderness (Fig. 2.12)

Figure 2.12 shows the effect of changing the flange slenderness $b_{fc}/2t_{fc}$ between 7.0 and 9.2 for girders with a cross-section aspect ratio of $D/b_{fc} = 4.25$. The span-to-depth ratio, stiffener spacing, and lateral brace spacing are all set according to the $L/D = 30$, $0.6V_n$, and AASHTO L_{b1}/r_y rules for all the curves in this plot. The black curves correspond to $b_{fc}/2t_{fc} = 7$ and the light-grey curves are for $b_{fc}/2t_{fc} = 9.2$. The maximum moment capacity is improved by about ten percent by changing from a compact flange to an ultracompact flange for the case of a compact web *($D/t_w = 86$)*, although the initial unloading from the peak moment point is very abrupt for the girder with the ultracompact flange. However, the differences in the moment capacities for $D/t_w = 125$ and $D/t_w = 163$ is much smaller. It should be noted that, although D/b_{fc} is held constant in these plots, the related parameter a_{rp} (discussed earlier in the chapter) changes significantly when $b_{fc}/2t_{fc}$ is changed. For example, a_{rp} is equal to 2.95 for test UC9 whereas it is equal to 3.87 for C15. The curves for the girders having ultracompact flanges in Fig. 2.12 (i.e., the black curves) exhibit some additional ductility, but this ductility appears to be less than that for the curves shown in other figures for girders having $D/b_{fc} = 3$.

Effect of D/b_fc (Fig. 2.13)

Figure 2.13 illustrates the effect of varying D/b_{fc} between *3* and *4.25* for girders with ultracompact flanges. This plot, along with a comparison of the plots on the left and right-hand sides of Figs. 2.10 and 2.11, supports the previous statement that the ductility and moment capacity are increased as D/b_{fc} is changed from *4.25* to *3*. The black curves are for $D/b_{fc} = 3$ and the light-grey curves are for $D/b_{fc} = 4.25$. The change in D/b_{fc} has only a small effect on the moment capacity for a compact web (although the initial load shedding beyond the peak moment is quite abrupt for $D/b_{fc} = 4.25$ and a compact web), but it has a significant effect on the moment capacity for $D/t_w = 125$ and *163*.

Effect of Depth of Web in Compression (Fig. 2.14)

Figure 2.14 contains the final set of plots, which show the effect of increasing D_{cp}/D when holding other parameters constant. As noted at the beginning of this section, the thick solid lines in these plots correspond to $D_{cp}/D = 0.5$, the thin solid lines are for $D_{cp}/D = 0.625$, and the dashed lines are for $D_{cp}/D = 0.75$. The black lines in both plots correspond to $D/b_{fc} = 3$ and the light-grey lines are for $D/b_{fc} = 4.25$. In these plots, L/D is constant at *30*, the stiffener spacing is set based on the $0.6V_n$ rule, and the lateral brace spacing is set based on the AASHTO L_{b1}/r_y equation. It should be noted that proper calculation of r_y for a nonsymmetric girder, or for a composite girder in negative bending is not addressed explicitly in the 1994 AASHTO LRFD and prior AASHTO provisions. It can be argued that the existence of a large tension flange or a relatively massive concrete deck has little influence on this behavior (this is believed to be an accurate statement unless the deck provides substantial restraint to the twisting of the steel section about the longitudinal axis and the web is reasonably compact such that distortional buckling of the cross-section does not predominate). In this work, the authors have adopted the definition that r_y is the radius of gyration of the compression flange plus one-half the total depth of the web. This is more liberal than defining r_y based on the compression flange and the depth of web in compression, for example, and it reduces to the "standard" definition used in the development of Eq. (2.2a) (Bansal 1971) for symmetric I shapes.

It can be seen from Fig. 2.14 that D_{cp}/D has a significant effect on the normalized moment capacity for all the cases. However, it should be noted that if the maximum moments are normalized by the yield moment M_y, the values do not vary as greatly. For a given flange

slenderness, the unloading portions of the curves are essentially the same shape, but are simply shifted downward along with the shift in the maximum moment capacity for larger D_{cp}/D. The unloading portions of the curves are also essentially the same shape for many of the other curves that have been presented in Figs. 2.9 through 2.14.

2.5 General Observations and Development of Design Moment-Rotation Equations

Based on the moment-plastic rotation results presented in the previous section, the following general observations may be made:

- The studies based on the AASHTO rule for L_{b1}/r_y, the $0.6V_n$ rule for the transverse stiffener spacing (i.e., no additional inelastic restraint stiffeners), and $L/D = 30$ limit may be used to lower-bound the M-θ_p behavior without significant penalty. Particularly for compact flanges and high D/b_f, use of two inelastic restraint stiffeners spaced at $D/3$ provides very little benefit.

- The parameters $2D_{cp}/t_w$, $b_{fc}/2t_{fc}$, D/b_{fc} (or a_{rp}), and D_{cp}/D have a major effect on the moment-rotation characteristics in general. Since these parameters are all associated with the girder cross-section, they are relatively simple to consider within a design and/or rating context.

- The primary effect of $2D_{cp}/t_w$ is on the moment capacity; the M-θ_p curves tend to simply shift up or down based on the magnitude of this parameter. Conversely, the effect of changes in $b_{fc}/2t_{fc}$ on the moment capacity is relatively minor over the range studied ($b_{fc}/2t_{fc} = 9.2$ to 7.0). Although a ten percent difference in the moment capacity is shown for the compact web girders in Fig. 2.12 for $b_{fc}/2t_{fc} = 7.0$ versus 9.2, this behavior is believed to be at least partly due differences in D/b_{fc} (and a_{rp}) for the separate curves.

- The moment capacities do not exceed the plastic moment capacity M_p by more than a few percent for any of the cases studied. However, all the girders are able to develop maximum moments larger than M_y. In addition to the studies presented here, the development of capacities greater than M_y is supported by experimental data and by the Q formula in the AASHTO LRFD Specifications (1994). This is discussed in detail in Chapter 3.

- The post-peak load-shedding characteristics are affected significantly by $b_{fc}/2t_{fc}$ for all cases. The use of the stockier flanges tends to result in a "plateau" in the M-θ_p response, whereas for the thinner flanges, this plateau is small or nonexistent.

- The unloading curves subsequent to any "plateau" in the M-θ_p response are very similar for all the girders.

- The variables D/b_{fc} and D_{cp}/D generally affect both the normalized moment capacity (M_{max}/M_p) as well as the load-shedding characteristics.

The authors have found that all the above attributes of the behavior may be captured reasonably well within the format shown in Fig. 2.15. As shown in this figure, the M-θ_p behavior may in general be broken into three regions: a linear pre-peak curve from zero plastic rotation at $M = 0.7M_n$ to a plastic rotation of 0.005 at M_n, where M_n is the nominal moment capacity, a plateau at the nominal moment capacity M_n from a plastic rotation of 0.005 to a value denoted by the parameter θ_{RL}, where θ_{RL} can be as small as 0.005 (in which case the girder unloads immediately upon reaching its peak moment capacity), and a quadratic unloading curve given by the equation shown in the figure.

The linear pre-peak curve is the same as the pre-peak curve specified for compact I shapes in the present LRFD Specifications (AASHTO 1994). This curve is a reasonable approximate fit to all the experimental data, as well as to the finite element data shown in this chapter. However, it should be noted that, as discussed earlier in the chapter, the residual stresses in actual prototype bridge girders are expected to be significantly smaller than those produced in the smaller sections fabricated for the experimental tests. The residual stresses modeled in the finite element studies are an approximation of the stresses that can be calculated for typical test girders using the equations from (ECCS 1976). When less severe residual stresses are included in the finite element models, the pre-peak plastic rotations are smaller and the "knee" in the moment-plastic rotation curves as the peak moment is approached is more abrupt (e.g., see (White 1994)). Although there are many factors involved, only the report on the FHWA component test (FHWA 1992) discusses the use of special restrictions to prevent an oversized weld on the small test specimens. In this test, the pre-peak plastic rotations are significantly smaller than those predicted by the pre-peak equation shown in Fig. 2.15. Based on the above reasoning, the pre-peak equation shown in the figure should be generally conservative for use in design and rating in that the pre-peak plastic rotations at the pier sections and the corresponding redistribution of moment to the positive bending sections of the girder will be somewhat over-estimated.

The authors have studied a number of approaches for developing simple equations to describe the moment capacity, including: (1) yield-line type analyses as employed by Climenhaga and Johnson (1972a) and by Kuhlmann (1989), (2) effective section approaches (discounting a portion of the web), analogous to the work by Basler and Thurlimann (1961) and to equations for Class 4 sections in Eurocode 3 (CEN 1993) but considering an effective plastic section rather than an effective elastic section (Barth 1996), and (3) direct use of strength formulas from various standards and specifications. However, the complexity of the first two approaches, and the desire to improve upon the correlation of current design formulas with the available experimental and finite element data, led the authors to quantify the moment capacity for the ranges of the parameters considered by a linear regression fit to the finite element data. Although a number of current design formulas recognize the ability of plate girders with noncompact webs to develop moment capacities greater than the yield moment M_y, none of the formulas that predict M_n greater than M_y consider the effect of D/b_{fc} and/or a_{rp}. Furthermore, all but one of the experimental tests that have been reported in the literature (and on which the current design formulas are based) have a $D/b_{fc} \leq 3.5$.

The following multiple-linear regression model represents a "best-fit" to the finite element data:

$$\frac{M_n}{M_p} = 1 + \frac{3.6}{\sqrt{\frac{2D_{cp}}{t_w}}} + \frac{1}{10a_{rp}} - 0.4\frac{M_p}{M_y} \leq 1 \qquad (2.9)$$

This model has an R^2 of 0.96. Also, the following bilinear expression for θ_{RL} was fit deterministically to the finite element data corresponding to the lower-bound values given by the current AASHTO equation for L_{b1}/r_y (Eq. (2.2a)), spacing of the transverse stiffeners solely based on the $0.6V_n$ rule, and $L/D = 30$, and considering that the "plateau" in the moment-plastic rotation characteristics is correlated predominantly with $b_{fc}/2t_{fc}$ and D/b_{fc} :

$$\theta_{RL} = 0.128 - 0.0119\frac{b_{fc}}{2t_{fc}} - 0.0216\frac{D}{b_{fc}} + 0.002\frac{b_{fc}}{2t_{fc}}\frac{D}{b_{fc}} \qquad (2.10)$$

In Chapter 3, these equations are validated against available experimental test data, including composite and all-steel tests, and in the case of the maximum moment capacity, against the strengths predicted by equations in current design standards and specifications. The correlation

with the experimental data is quite good, although it is of course not as good as the correlation with the finite element curves shown in Figs. 2.9 through 2.14. These equations produce curves that practically match the finite element test data, as shown in (Barth 1996) and Chapter 3. Figure 2.16 shows the predictions of the model for the numerical tests U6, which has the least strength and ductility of all the girders studied, UC6, which has the greatest strength and ductility of all the tests involving the lower-bound parameters for the lateral brace and stiffener spacing and L/D, and UC3, which is based on the more beneficial ASCE lateral brace spacing and has the extra inelastic restraint stiffeners adjacent to the pier section. It should be noted that the predictions relative to the least ductile curve *in Fig. 2.3* are slightly unconservative; however, the test on which this curve is based does not have any unbraced segments beyond the critical unsupported lengths L_{b1}. When additional segments are added on the ends of this test girder, the moment-rotation response (see (White 1994)) is closely approximated by Eqs. (2.9) and (2.10).

A number of the experimental tests considered in Chapter 3 involve combinations of parameters that fall outside the ranges studied in the finite element parametric studies on which the above equations are based. Based on consideration of the experimental as well as the finite element data, the following restrictions on the use of the simplified curves are recommended:

$$\frac{D}{b_{fc}} \le 4.25, \quad \frac{b_{fc}}{2t_{fc}} \le 0.4\sqrt{\frac{E}{F_{yc}}}, \quad \frac{2D_{cp}}{t_w} \le 6.77\sqrt{\frac{E}{F_{yc}}}, \quad \frac{D_{cp}}{D} \le 0.75, \quad \frac{L_{b1}}{r_y} \le \text{Eq. (2a)}, \quad \text{and} \quad \frac{V}{V_n} \le 0.6$$

With the exception of the D/b_{fc} and D_{cp}/D restrictions, limits exist in the current AASHTO provisions for all of these parameters. Furthermore, the restrictions on D/b_{fc} and D_{cp}/D are desirable from the perspective of attaining good design economy. As illustrated by the comparison to the FEA results for girder UC3 in Fig. 2.16, the curves are expected to provide a conservative representation of the "actual" M-θ_p behavior for cases in which the lateral brace and stiffener spacings are smaller than the limits for the "lower-bound" curves. Some change in the behavior is expected for different L/D ratios, but the effect of L/D appears to be small within the range of parameters studied in this work. Also, Eqs. (2.9) and (2.10) are expected to provide a conservative representation of the physical behavior in general, assuming that full-composite action is developed within the hogging-moment region. This is due to the following benefits that are neglected in the present development:

- twisting restraint provided by the bridge deck to the girder tension flange

- transverse load redistribution between the girders.

All the analyses conducted in this chapter are for Grade 50 steels. However, the F_y values measured in experimental tests with Grade 50 steels are of course not *350 MPa (50 ksi)*. Based on limited finite element studies with F_y = *480 MPa (70 ksi)* reported by (White 1994) and on comparisons to available experimental data, the above equations may be applied for F_y other than *350 MPa* by using the "equivalent" slenderness values for the web and flange plates of

$$\frac{2D_{cp}}{t_w}\sqrt{\frac{F_{yc}}{50}\frac{29\,000}{E}} \quad \text{and} \quad \frac{b_{fc}}{2t_{fc}}\sqrt{\frac{F_{yc}}{50}\frac{29\,000}{E}}.$$

At present, it is suggested that these equivalent slenderness conversions should be limited to normalization of the data from experimental tests of Grade 50 steel girders in which the nominal and actual values for the static yield strength are different. On-going studies of girders fabricated from high-performance steels with $F_y \geq 480$ MPa may lead to refinements in the suggested M-θ_p model accounting for variations in F_y and other material parameters.

2.6 Conclusions

Based on a reasonably comprehensive set of finite element parametric studies, a simple model of the M-θ_p behavior within the hogging-moment region of welded bridge girders with noncompact webs has been developed and presented. Verification and validation of this model against experimental results, and comparisons to current specification strength equations are provided in Chapter 3. These studies and the resulting model indicate clearly that sections with compact and ultracompact flanges, and which satisfy the other restrictions specified in these studies, will usually develop maximum pier moments larger than M_y. This characteristic of the behavior over the pier is already captured by the strength equations of a number of standards and specifications, such as the Q formula in the AASHTO LRFD Specifications (1994). However, none of the present specification equations account for the significance of the girder aspect ratio D/b_{fc}, or the closely related parameter a_{rp} (see Fig. 2.4). Also, these studies and the resulting M-θ_p model indicate that the effect of reducing the web slenderness is not as great as deduced in prior research. The parameter $2D_{cp}/t_w$ is only one of several terms within the "best-fit" equation presented for the nominal strength at the pier section; the terms a_{rp} and M_p/M_y in this equation are of similar importance to the prediction of the maximum strength. Furthermore, $2D_{cp}/t_w$ has

only a minor effect on the ductility of the pier section, as reflected by its absence in the equation for θ_{RL}, which represents the extent of the effective "plateau" in the moment-rotation behavior. The parameter $2D_{cp}/t_w$ is expected to have a significant effect for web slenderness values less than the minimum value considered here (i.e., $2D_{cp}/t_w = 86$), due to the web providing restraint to twisting of the compression flange. However, for the range of $2D_{cp}/t_w$ studied in this work, it appears that the compression flange always restrains the local buckling deformations of the web. It is shown in Chapter 3 that reductions in the ductility observed in specific prior experimental tests, which have been attributed to variations in $2D_{cp}/t_w$ from 86 to 163, can be attributed to changes in D/b_{fc} (or a_{rp}).

Finally, these studies show that noncompact-web bridge girders generally exhibit good ductility within the hogging-moment region, although the rotation capacity determined by traditional definitions such as Eq. (2.5) may be zero. In this regard, it is important to note that even for members that meet the most stringent compactness provisions for plastic design, a large fraction of the rotation capacity defined by Eq. (2.5) actually comes from local and/or lateral-torsional buckling deformations of the member. Local and/or lateral torsional buckling always begins to predominate within the vicinity of the maximum moment point in any moment-rotation curve. Kemp (1986) estimates the ratio $R_{ult}/(R_{max} - 1)$, where R_{ult} and R_{max} are given by Eqs. (2.5) and (2.4) respectively, to be approximately 1.7 for sections that satisfy the limits for compact and plastic design sections in American design provisions. The results of these studies show that as the web slenderness approaches the compactness limit in the AASHTO provisions (1994), this ratio can be significantly larger than 1.7. More importantly, these studies show that there is no sudden and dramatic degradation in the extent of the "plateau" in the moment-plastic rotation behavior and in the slope of the load-shedding curves as the cross-section parameters are changed such that the maximum moment capacity of a section drops below M_p. As shown in (Bansal 1971) and (Croce 1970), the rotation capacity of a continuous-span beam as a structural system (defined by Eq. (2.3) for example) may be reasonably good although the rotation capacity defined by Eqs. (2.4) or (2,5) may be quite small or undefined.

Table 2.1. Summary of FEA parametric studies, symmetric compact-flange girders
($b_{fc}/2t_{fc} = 9.2$).

Test	L_{b1}/r_y	$d_{o.in}$	L/D	D/b_{fc}	D/t_w
Initial study set					
C1	ASCE	2@D/3	30	3	163
C2	ASCE	2@D/3	30	3	125
C3	ASCE	2@D/3	30	3	86
Study the effect of ASCE versus AASHTO L_{b1}/r_y, compare to C1, C2 & C3					
C4	AASHTO	2@D/3	30	3	163
C5	AASHTO	2@D/3	30	3	125
C6	AASHTO	2@D/3	30	3	86
	>>> AASHTO bracing limit selected				
Study the effect of cross-section aspect ratio (D/b_{fc}), compare to C4, C5 & C6					
C7	AASHTO	2@D/3	30	4.25	163
C8	AASHTO	2@D/3	30	4.25	125
C9	AASHTO	2@D/3	30	4.25	86
Study the effect of stiffener spacing adjacent to the pier with low D/b_{fc}, compare to C4, C5 & C6					
C10	AASHTO	V/V_n=0.6	30	3	163
C11	AASHTO	V/V_n=0.6	30	3	125
C12	AASHTO	V/V_n=0.6	30	3	86
Study the effect of stiffener spacing adjacent to the pier with high D/b_{fc}, compare to C7, C8 & C9					
C13	AASHTO	V/V_n=0.6	30	4.25	163
C14	AASHTO	V/V_n=0.6	30	4.25	125
C15	AASHTO	V/V_n=0.6	30	4.25	86
		>>> stiffener spacing based on V/V_n = 0.6 selected			
Study the effect of moment gradient with low D/b_{fc}, compare to C10, C11 & C12					
C16	AASHTO	V/V_n=0.6	20	3	163
C17	AASHTO	V/V_n=0.6	20	3	125
C18	AASHTO	V/V_n=0.6	20	3	86
Study the effect of moment gradient with high D/b_{fc}, compare to C13, C14 & C15					
C19	AASHTO	V/V_n=0.6	20	4.25	163
C20	AASHTO	V/V_n=0.6	20	4.25	125
C21	AASHTO	V/V_n=0.6	20	4.25	86
		>>> effect of moment gradient neglected			
Check the appropriateness of the AASHTO L_{b1}/r_y limit for high D/b_{fc}, compare to C7, C8 & C9					
C22	ASCE	2@D/3	30	4.25	163
C23	ASCE	2@D/3	30	4.25	125
C24	ASCE	2@D/3	30	4.25	86

Table 2.2. Summary of FEA parametric studies, symmetric ultracompact-flange girders ($b_{fc}/2t_{fc} = 7.0$).

Test	L_{b1}/r_y	$d_{o.in}$	L/D	D/b_{fc}	D/t_w
Study effect of most beneficial L_{b1}/r_y, d_{o1} & d/b_{fc}, compare to C13, C14 & C15					
UC1	ASCE	2@D/3	30	3	163
UC2	ASCE	2@D/3	30	3	125
UC3	ASCE	2@D/3	30	3	86
Study the effect of flange slenderness for low d/b_f, compare to C10, C11 & C12; also study the effect of L_{b1}/r_y and d_{o1} for ultracompact flanges and low D/b_{fc}, compare to UC1, UC2 & UC3					
UC4	AASHTO	$V/V_n=0.6$	30	3	163
UC5	AASHTO	$V/V_n=0.6$	30	3	125
UC6	AASHTO	$V/V_n=0.6$	30	3	86
Study effect of flange slenderness for high d/b_f, compare to C13, C14 & C15; also study effect of D/b_{fc} for ultracompact flanges, compare to UC4, UC5 & UC6					
UC7	AASHTO	$V/V_n=0.6$	30	4.25	163
UC8	AASHTO	$V/V_n=0.6$	30	4.25	125
UC9	AASHTO	$V/V_n=0.6$	30	4.25	86
Check the validity of neglecting moment gradient with ultracompact flanges, compare to UC5					
UC10	AASHTO	$V/V_n=0.6$	20	3	125

Table 2.3. Summary of FEA parametric studies, unsymmetric girders -- AASHTO L_{b1}/r_y, $d_{o.in}$ based on $V/V_n = 0.6$, L/D = 30, $2D_{cp}/t_w = 163$.

Test	D_{cp}/D	D_c/D	D/t_w	D/b_{fc}	$b_{fc}/2t_{fc}$
U1	0.625	0.546	130	3	9.2
U2	0.750	0.593	109	3	9.2
U3	0.625	0.540	130	3	7.0
U4	0.750	0.582	109	3	7.0
U5	0.625	0.563	130	4.25	9.2
U6	0.750	0.621	109	4.25	9.2
U7	0.625	0.557	130	4.25	7.0
U8	0.750	0.612	109	4.25	7.0
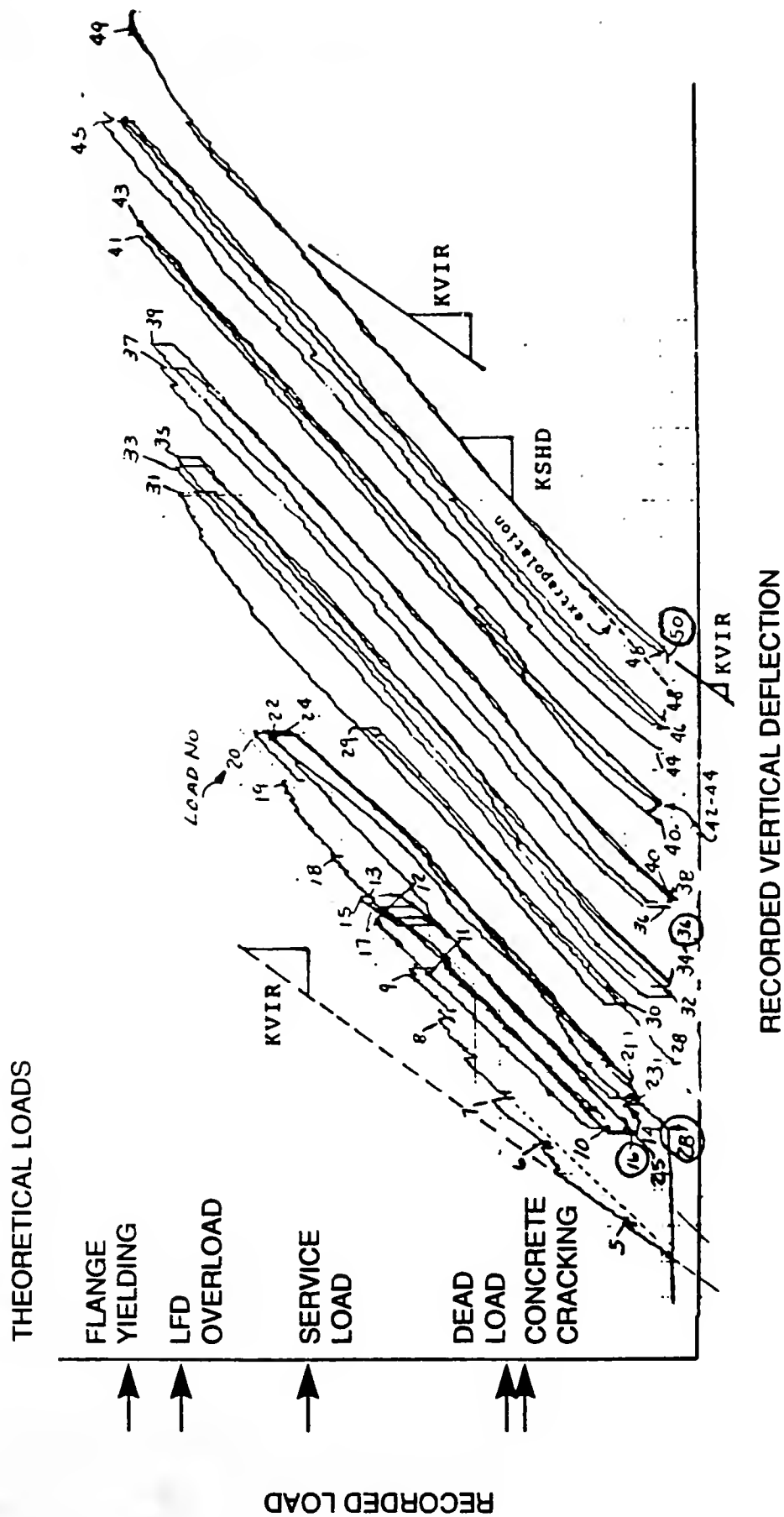
Figure 2.1. Load-deflection behavior in a hogging-moment test of a composite girder (Carskaddan 1980).
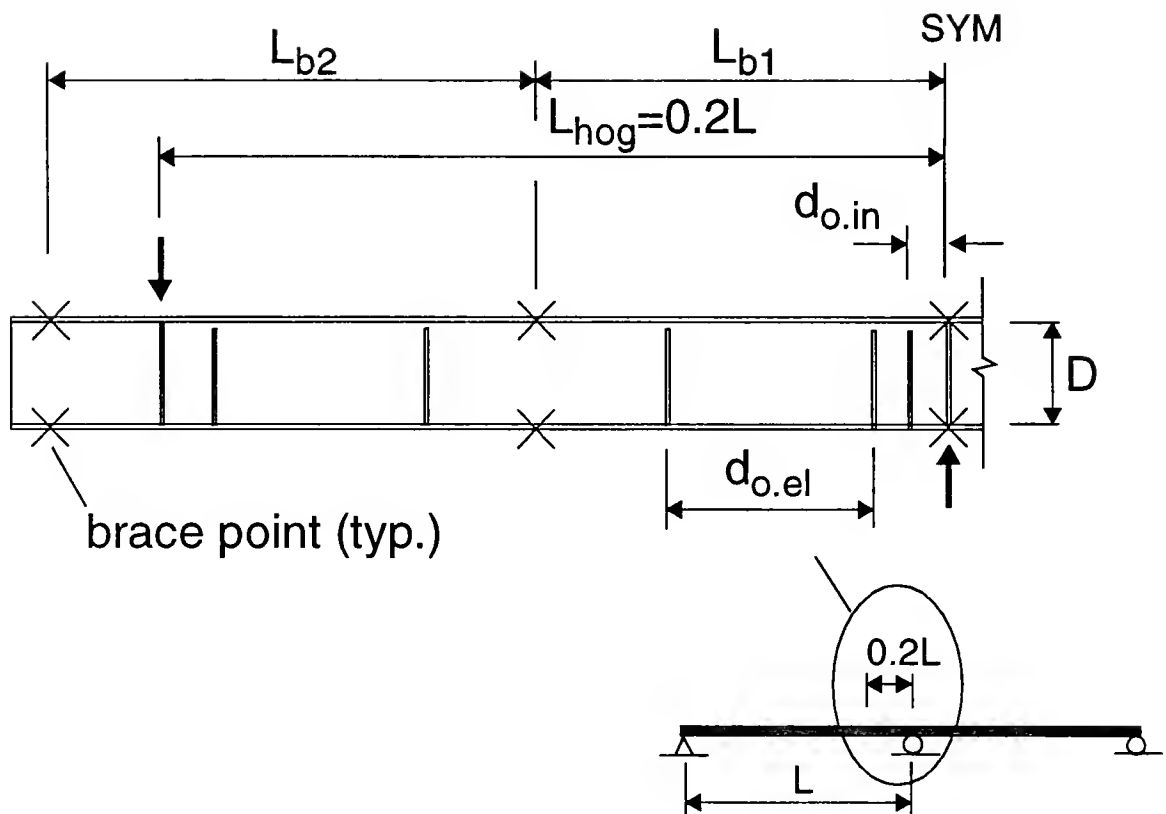
Figure 2.2. Generic test configuration.
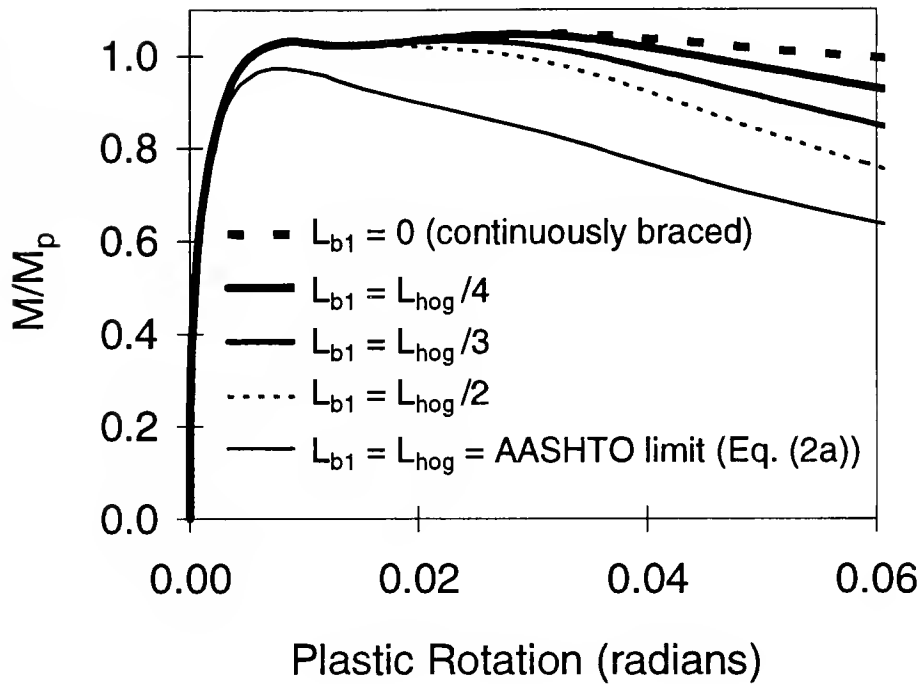
Figure 2.3. Effect of lateral brace spacing on moment-rotation response -- preliminary finite element study using a modified version of a three-point bending test conducted by Schilling and Morcos (1988) on a Grade 50 steel symmetric girder having an ultracompact flange ($b_{fc}/2t_{fc} = 6.47$) and a compact web($D/t_w = 80.7$).

$$a_{rp} = A_{wcp} / A_{fc} = (2D_{cp}t_w) / (b_{fc}t_{fc})$$

$$= [4 (D_{cp}/D) (b_{fc}/2t_{fc}) / (D/t_w)] (D/b_{fc})^2$$

For constant D/t_w, $b_f/2t_f$ & D_{cp}/D, increasing D/b_f results in a significant increase in a_{rp}

For the range of parameters considered in the studies, a_{rp} varies from 0.77 to 4.59

$D/b_{fc} = 3$

$D/b_{fc} = 4.25$
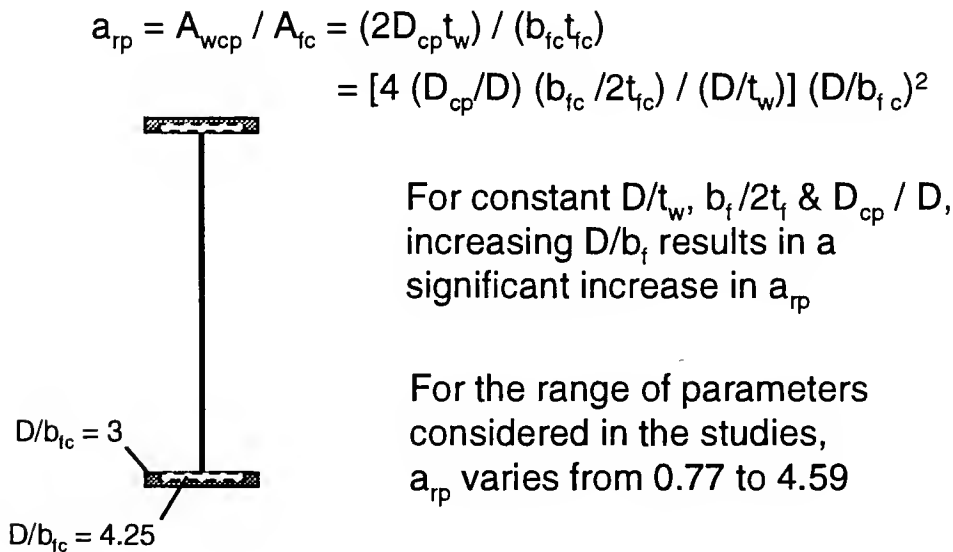
Figure 2.4. Effect of varying D/b_f while holding other parameters constant.
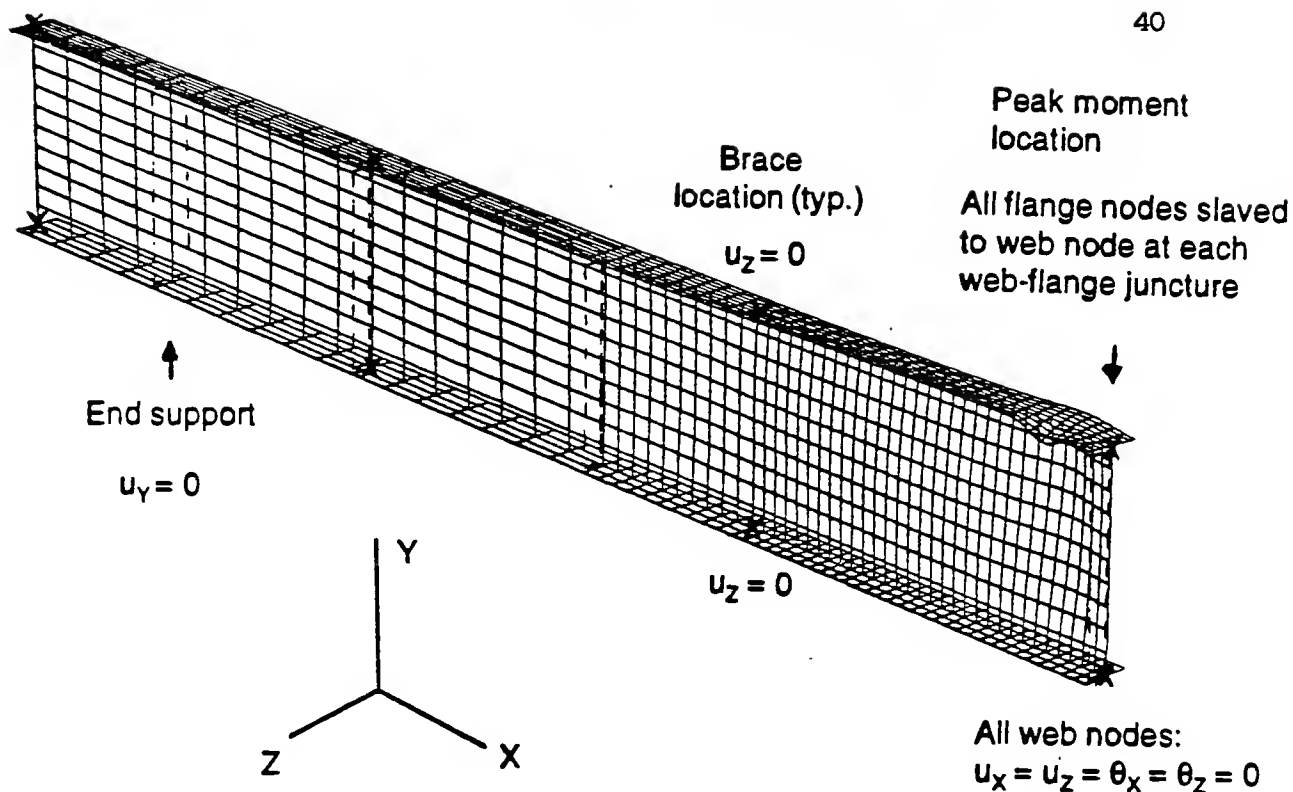
Figure 2.5. Typical finite element mesh and nodal constraints (note that the tests are conducted in an "inverted" configuration relative to that of the hogging moment region of the prototype bridge girder).
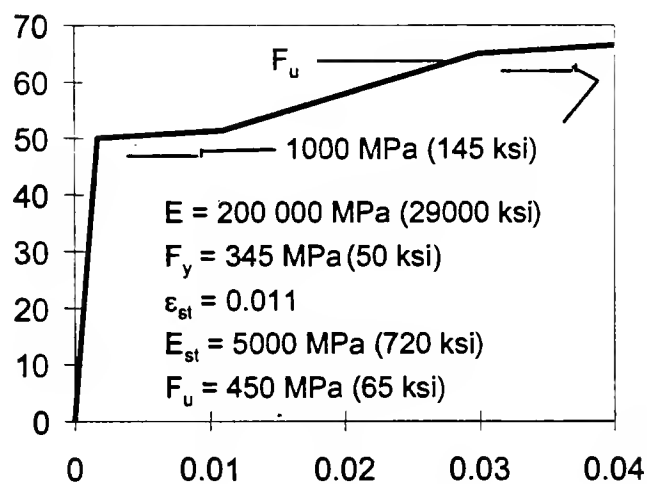
Figure 2.6. Effective stress-strain response.

0.95F$_y$ 0.95F$_y$

0.05F$_y$ 0.05F$_y$

-0.5F$_y$
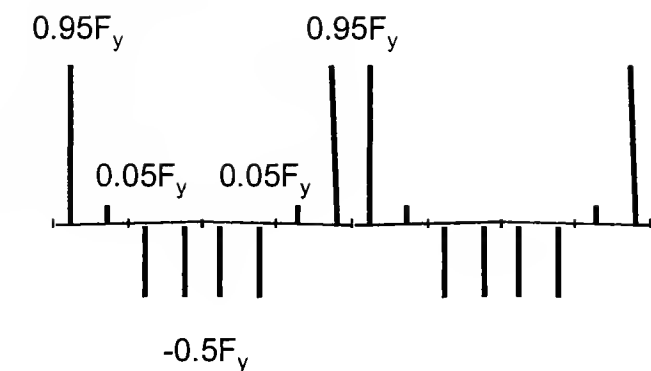
(a) Gauss point residual stresses
    in compression flange

Quadratic variation,
self-equilibrating

F$_y$

D/10

-f$_{rc}$

D/t$_w$	f$_{rc}$ / F$_y$
163	0.0631
125	0.1074
86	0.2270

0.95F$_y$

0.05F$_y$

-0.5F$_y$
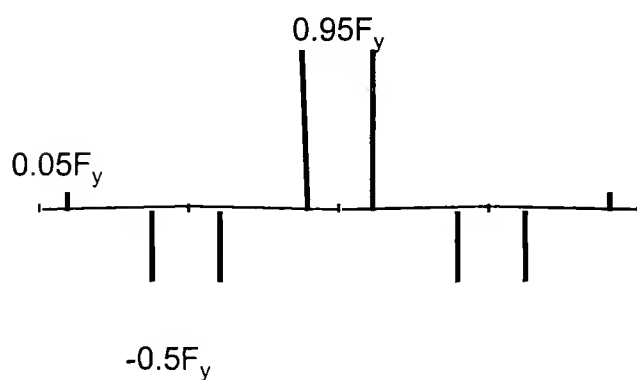
(b) Gauss point residual stresses
    in tension flange
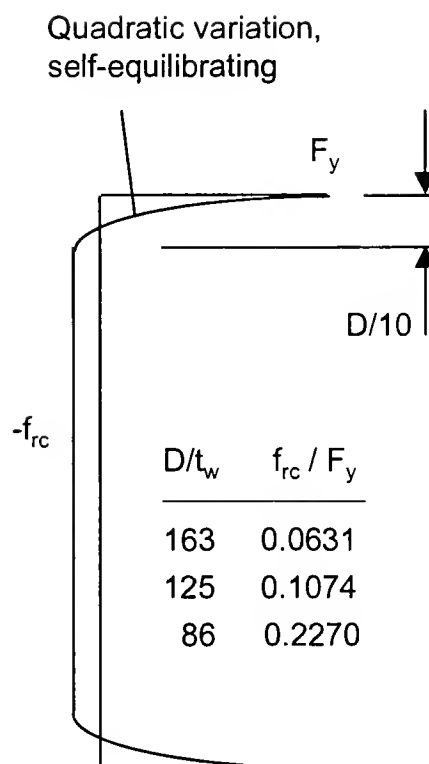
(c) Web residual stresses

Figure 2.7. Initial residual stresses.

(a) Initial out-of-flatness in each web panel

(b) Initial tilt of compression flange within each panel

(c) Initial sinusoidal sweep of the compression flange within each unbraced length
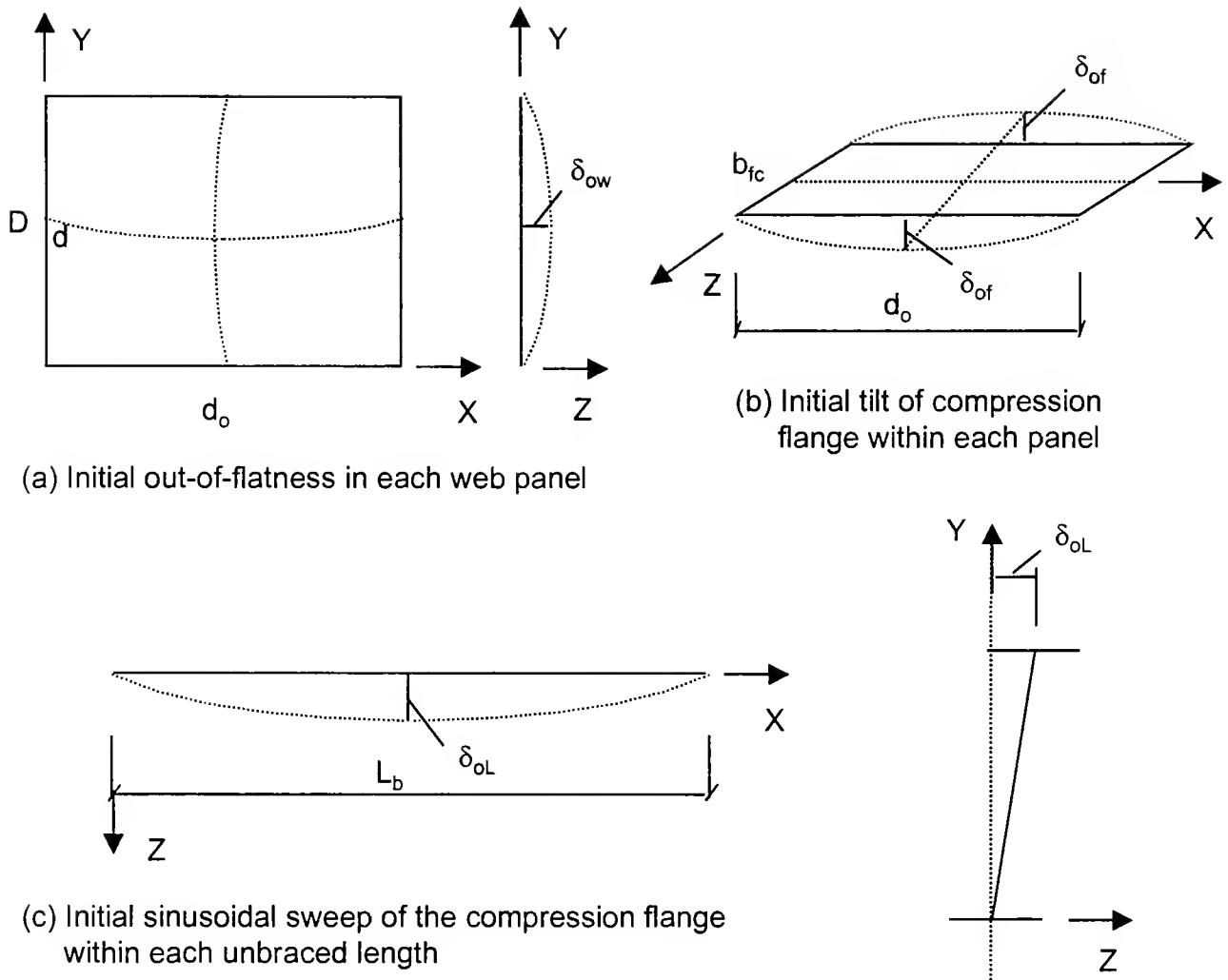
Figure 2.8. Initial geometric imperfections (out-of flatness and initial sweep are specified in alternate directions in adjacent panels and unbraced lengths).
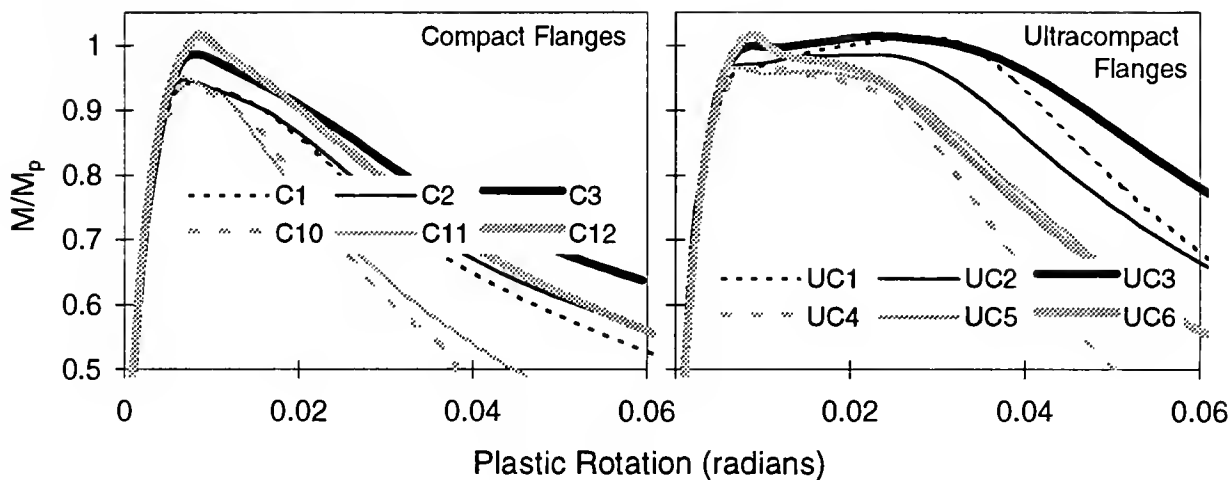
Figure 2.9. Effect of varying L_{b1} / r_y between the ASCE and AASHTO inelastic design limits plus varying the stiffener spacing in the peak moment region from 2 at $D/3$ to the spacing associated with with $V = 0.6 \, V_n$ -- symmetric sections with compact and ultracompact flanges, $L/D = 30$, $D/b_{fc} = 3$.
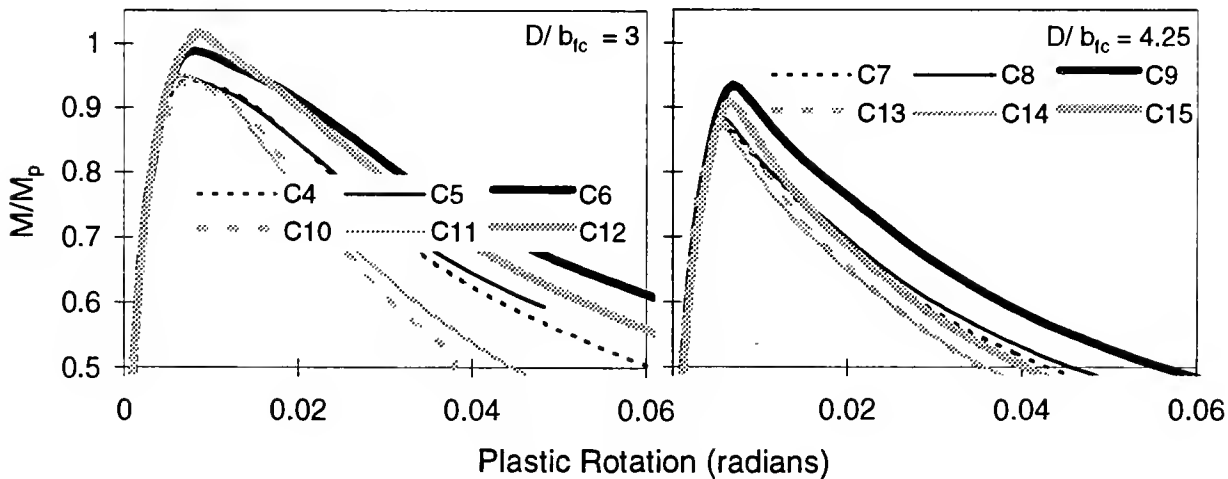
Figure 2.10. Effect of varying the stiffener spacing in the peak moment region from 2 at $D/3$ to the spacing associated with $V = 0.6 \, V_n$ - symmetric sections with compact flanges, $D/b_f = 3$ and 4.25, $L/D = 30$, L_{b1} / r_y based on current AASHTO requirements.
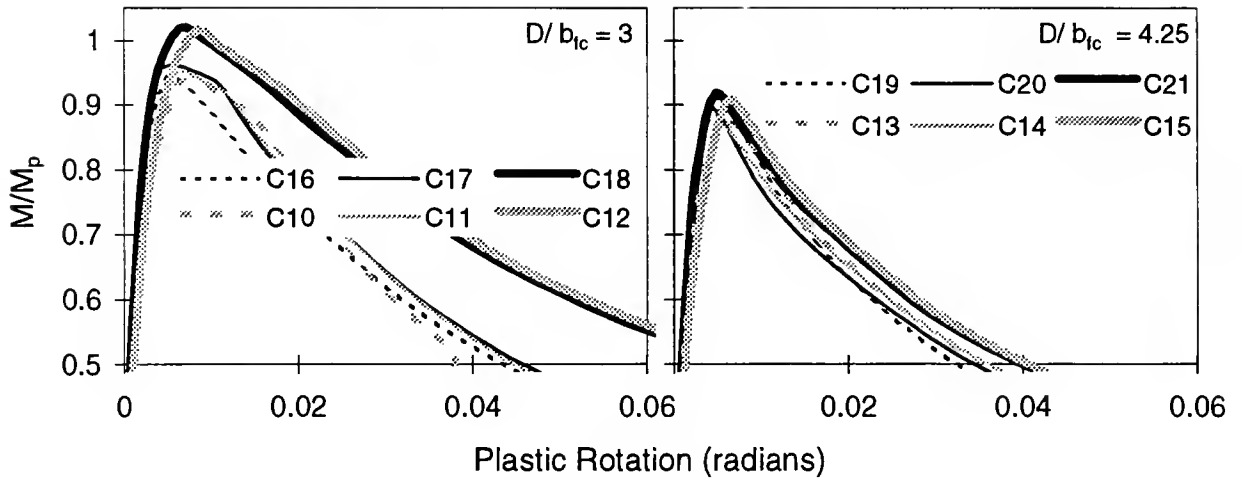
Figure 2.11. Effect of moment gradient ($L/D = 30$ versus $L/D = 20$) -- symmetric sections with compact flanges, $D/b_{fc} = 3$ and 4.25, $d_{o.in}$ based on $V = 0.6V_n$, L_{b1}/r_y based on current AASHTO requirements.
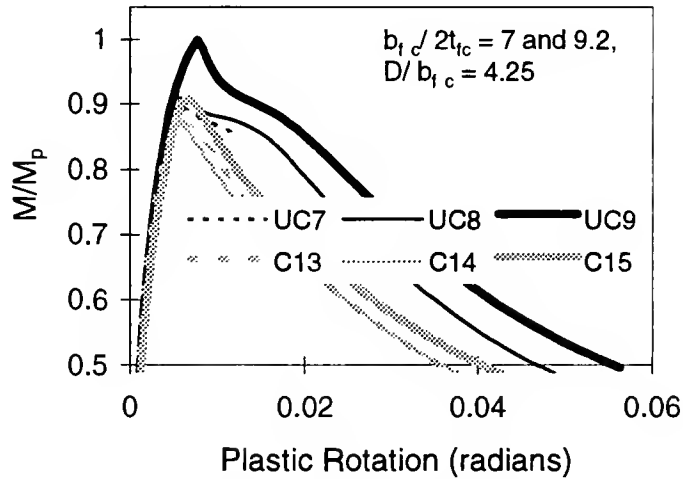
Figure 2.12. Effect of varying $b_{fc}/2t_f$ between 7 and 9.2 for sections with $D/b_{fc} = 4.25$ -- $L/D = 30$, $d_{o.in}$ based on $V = 0.6V_n$, L_{b1}/r_y based on current AASHTO requirements.
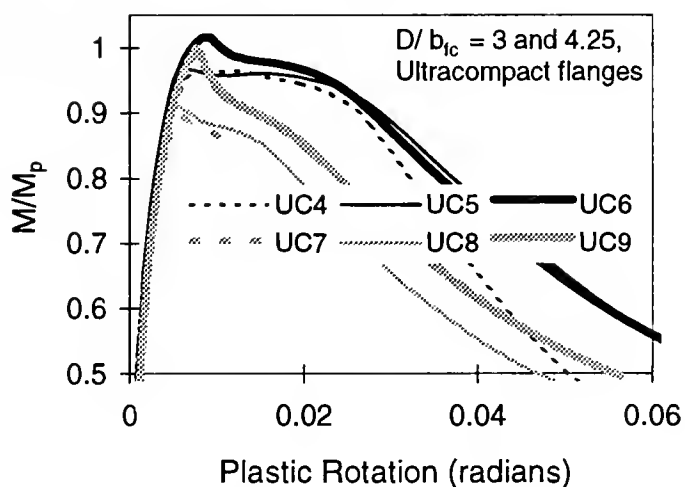
Figure 2.13. Effect of varying D/b_{fc} between *3* and *4.25* for symmetric sections with ultracompact flanges -- L/D= *30*, $d_{o.in}$ based on $V = 0.6V_n$, L_{b1} / r_y based on current AASHTO requirements.
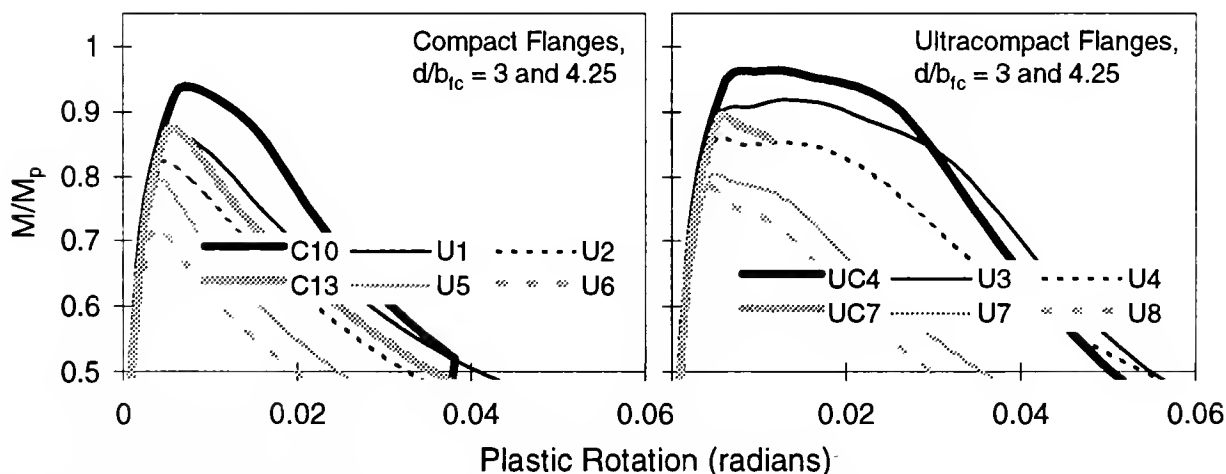
Figure 2.14. Effect of depth of web in compression for sections with compact and ultra-compact flanges, and for D/b_{fc} = *3* and *4.25*, L_{b1} / r_y based on current AASHTO requirements (r_y based on compression flange plus one-half the depth of the web).

$$\frac{M}{M_n} = 1 - 16(\theta_p - \theta_{RL}) + 100(\theta_p - \theta_{RL})^2$$

$$\frac{M}{M_n} = 0.7 + 60\theta_p$$
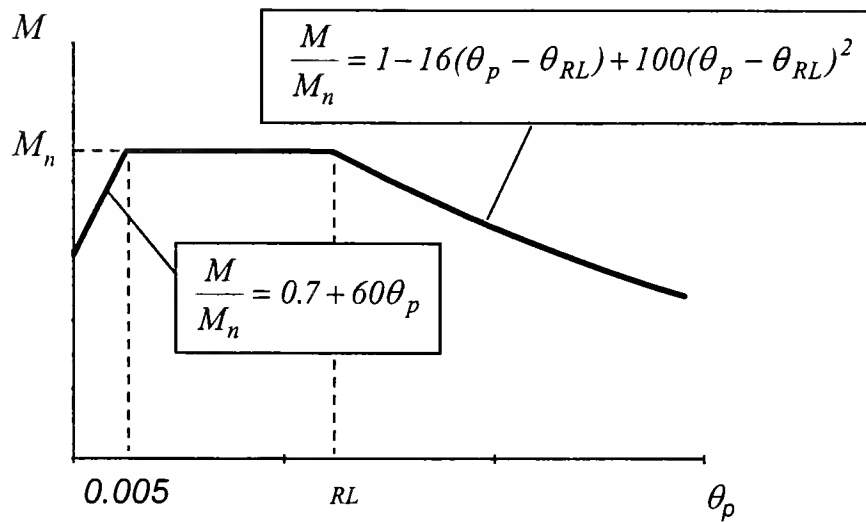
Figure 2.15. Moment-plastic rotation model.
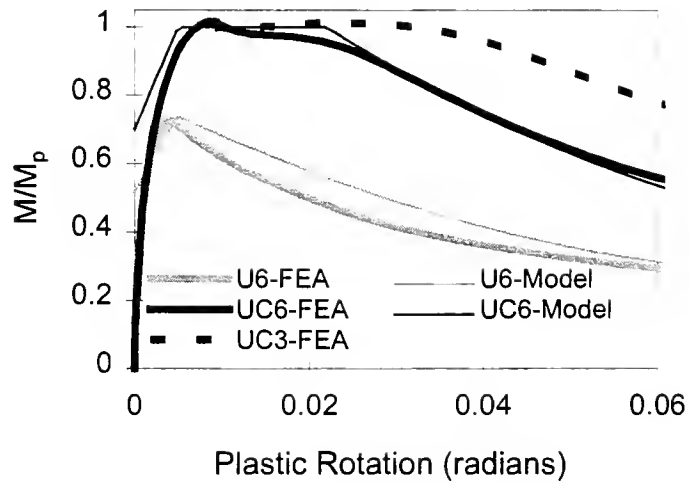
Figure 2.16. Upper- and lower-bound moment-rotation curves -- finite element analysis results and proposed moment-rotation model.

CHAPTER 3

STRENGTH AND DUCTILITY OF COMPACT-FLANGE I-GIRDERS IN NEGATIVE BENDING

Prior research studies such as (Schilling 1985), (Schilling and Morcos 1988), (Tansil 1991) and White and Dutta (1993) have shown that, as long as the flanges are compact, members with noncompact webs and $2D_{cp}/t_w \leq 163$ generally have moment capacities larger than the yield moment M_y. Furthermore, these types of girders can exhibit a significant and reliable capacity for inelastic rotation over interior pier supports. Nevertheless, these prior studies represent only a sparse sampling over the full range of possible design parameters. Consequently, additional studies are needed to develop appropriate moment-rotation data for inelastic design of the above types of members. To address this need, the authors have conducted a reasonably comprehensive parametric study using shell finite element models validated against prior and several new experimental tests. Based on this study, equations for the hogging moment-plastic rotation behavior of composite and noncomposite bridge girders with noncompact webs and compact or ultra-compact flanges have been developed. The finite element study and the development of the M-θ_p equations are summarized in Chapter 2. This chapter focuses on comparisons of this M-θ_p model with existing experimental and finite element test results, and with current American specification equations for I-girder moment capacities. Several weaknesses are found in the current American specification provisions that are avoided by the suggested M-θ_p model. Implications with respect to procedures for inelastic design of steel I-girder bridges are addressed in Chapter 4.

3.1 Overview of American Specification Strength Equations

The following subsections provide a brief overview of relevant strength provisions in the AASHTO LRFD Bridge Design (1994) and AISC LRFD Building Design (1993) Specifications. Barth (1996) assesses the Eurocode 3 (CEN 1992) rules for the types of members discussed in the introduction. In this report, the equations considered are limited to the American provisions for the sake of clarity, simplicity and succinctness of the presentation. Furthermore, the discussion is limited predominantly to equations that allow prediction of nominal girder strengths larger than the yield moment capacity M_y. Traditional plate girder design equations have often limited the nominal maximum moment capacities to M_y. However, particularly for composite and/or

unsymmetric I-girder sections, the maximum strength in many cases can be significantly larger than the yield moment capacity.

The AASHTO Q Formula

The AASHTO LRFD Specifications (1994) introduce a new equation for the flexural strength of noncompact girders with $F_y \leq 485$ MPa *(70 ksi)*, commonly referred to as the Q formula[*]. This equation accounts for the interaction between web and flange local buckling, and predicts that the flexural capacity is greater than M_y in many practical situations. The Q formula can be written as

$$M_n = \left[1 - \left(1 - \frac{0.7}{\left(\frac{M_p}{M_y} \right)} \right) \left(\frac{Q_p - Q_{fl}}{Q_p - 0.7} \right) \right] M_p \leq M_p \tag{3.1}$$

For girders with *noncompact flanges*, Q_{fl} is an estimated ratio of the elastic buckling and yield strengths of the compression flange, expressed as

$$Q_{fl} = \frac{F_{cr}}{F_{yc}} = \frac{4.45}{\left(\frac{b_{fc}}{2t_{fc}} \right)^2 \sqrt{\frac{2D_{cp}}{t_w}}} \frac{E}{F_{yc}} \tag{3.2}$$

This equation is obtained by substituting a flange-buckling coefficient of

$$k = \frac{4.92}{\sqrt{\frac{2D_{cp}}{t_w}}} \tag{3.3}$$

into the theoretical equation for the elastic plate buckling stress F_{cr}. Equation (3.3) approximates the influence of web and compression flange buckling interactions on either the elastic or *inelastic* flexural resistance, and is based primarily on the tests conducted by Johnson (1985). However, if the compression flange satisfies the AASHTO compactness limit, Q_{fl} is given by the equation

$$Q_{fl} = \frac{30.5}{\sqrt{\frac{2D_{cp}}{t_w}}} \tag{3.4}$$

---

[*] In the 1996 interim changes to the AASHTO LRFD Specifications, the usage of the Q formula is limited to $F_y = 350$ MPa *(50 ksi)*.

This formula for Q_{fl} is obtained by substituting the compact section limit $\frac{b_{fc}}{2t_{fc}} = 0.382\sqrt{\frac{E}{F_{yc}}}$

(= *9.2* for Grade 50 steels) into Eq. (3.2). Its use for girders having compact flanges is based on the observation (Bak 1992) that the girder strength is not affected significantly by the flange slenderness $b_{fc}/2t_{fc}$ for cases in which the flange elastic local buckling strength approaches or exceeds the yield stress. The term Q_p in Eq. (3.1) is the value of Q_{fl} for which it is assumed that the cross-section is capable of developing the plastic moment M_p. This limit is assumed to be equal to three for symmetric I sections, and is given by

$$Q_p = 5.47\left(\frac{M_p}{M_y}\right) - 3.13 \tag{3.5}$$

for unsymmetric sections.

Figure 3.1a illustrates the variation in the normalized flexural strength M_n versus $1/Q_{fl}$ predicted by the Q formula (*$1/Q_{fl}$ is equal to F_y/F_{cr} for a noncompact flange (see Eq. (3.2)), but it is equal to the inverse of Eq. (3.4) for compact flange girders*). The Q formula defines a linear transition in the flexural strength in terms of the parameter *$1/Q_{fl}$* from a value of *$0.7M_y$* at *$1/Q_{fl} = 1/0.7 = 1.429$* to the plastic resistance M_p at *$1/Q_{fl} = 1/Q_p$*.

AISC LRFD Flexural Strengths

The formulas provided in the AISC LRFD Specification for Structural Steel Buildings (1993) are well accepted for calculating the design strength of steel beams and girders, and as such, they are a useful benchmark against which other models for flexural strength can be assessed. The AISC LRFD flexural resistance equations are in general tied to two slenderness limits, λ_r and λ_p, for each of the three predominant types of buckling failure -- local flange, local web, and lateral-torsional buckling. The λ_r limits are slenderness values beyond which elastic buckling would theoretically govern the design resistance, whereas the λ_p limits are the slenderness values below which the plastic moment capacity M_p can be reached prior to the strength being affected by the corresponding inelastic buckling limit states.

The AISC LRFD Specification has three separate sections that pertain to calculation of the flexural resistance of I sections:

1. Chapter F, which defines the strength of doubly-symmetric compact I sections, i.e., sections that have a web and flange slenderness, $\lambda = b_{fc}/2t_{fc}$ for the flanges and $\lambda = D/t_w$ for the web, smaller than the corresponding λ_p values. The AISC LRFD limits for flange and web compactness are identical to those of the AASHTO LRFD Specifications; both specifications limit the flange and web slenderness to *9.2* and *91* respectively for Grade 50 steels. However, the web slenderness is calculated differently in these two specifications, as outlined below.

2. Appendix F, which addresses unsymmetric I shapes and I shapes with noncompact webs and/or noncompact or slender flanges. Noncompact cross-section elements are defined in the AISC LRFD Specification as having a slenderness between λ_p and λ_r, whereas slender elements are defined as having λ values greater than λ_r. The AISC Specification (1993) defines the web slenderness as $\lambda = D/t_w$ for both symmetric and unsymmetric cross-sections[†]. Consequently, the λ_r limit varies with the depth of the web in compression. The AASHTO Specifications do not have an explicit λ_r limit. Furthermore, the web slenderness is defined as $2D_{cp}/t_w$ in the AASHTO provisions.

3. Appendix G, which addresses symmetric or unsymmetric shapes with slender webs (i.e., $\lambda = D/t_w > \lambda_r$). The provisions of this appendix account for web post-buckling strength, and involve separate limit state checks for local and lateral buckling of the girder compression flange. If the slenderness of the web ($\lambda = D/t_w$) is less than λ_r, then the AISC LRFD Specifications assume that no bend buckling of the web will occur prior to developing the yield strength M_y. Since the post-buckling strength of the web is expected usually to have little positive influence on the flexural capacity for strengths between M_y and M_p, the designer is routed to Appendix F where the web post-buckling strength is not considered. However, for $\lambda = D/t_w > \lambda_r$, the AISC LRFD Specification routes the designer to Appendix G, where the web elastic post-buckling strength is included in the flexural capacity equations.

It is not feasible to present all the detailed equations for calculation of the flexural strengths from each of the above sections here. However, there are numerous characteristics of the AISC

[†] In the 1997 changes to the AISC LRFD Specification, the web slenderness is defined as $2D_{cp}/t_w$ for comparison with the compactness limit λ_p when checking members with unequal flanges. This reduces to $\lambda = D/t_w$ for symmetric I shapes. The web slenderness is still calculated uniformly as $\lambda = D/t_w$ for comparison with the λ_r equations.

LRFD equations that are important to the comparisons made in this chapter. The overall characteristics of the calculations in each of the above three sections of the LRFD Specification are summarized below to provide guidance to the interpretation of the presented results.

Figure 3.1b summarizes the provisions from all three of the above sections of the AISC LRFD Specification. In all the cases shown, the strength is defined by a constant maximum value (equal to M_p or to M_y) for $\lambda \leq \lambda_p$, by a linear transition between this strength and the nominal strength associated with elastic local flange, local web, or lateral-torsional buckling at the onset of significant inelastic response for $\lambda_p \leq \lambda \leq \lambda_r$, and by elastic buckling strengths for $\lambda > \lambda_r$. Chapter F requires $\lambda \leq \lambda_p$ for the local flange and local web buckling limit states, and therefore, the strength curves shown in Fig. 3.1b only need to be considered with respect to the lateral-torsional buckling limit state in that Chapter. In all three of the above sections of the AISC LRFD Specification, when checking lateral-torsional buckling, the strength is calculated as a capacity under uniform bending multiplied by a factor C_b to account for the beneficial effects of nonuniform moment along the unsupported length. The resulting strengths are limited to the maximum potential flexural capacity (equal to M_p in Chapter F, less than or equal to M_p in Appendix F, and less than or equal to M_y in Appendix G).

Appendix F is simply a generalization of Chapter F that addresses the effects of local flange and local web buckling as well as the strength of unsymmetric sections. In Appendix F, a separate strength is computed from curves of the form shown in Fig. 3.1b for local flange bucking, local web buckling, and lateral-torsional buckling. The smallest of these strengths is taken as the controlling nominal resistance. Potential interactions between local and lateral-torsional buckling are ignored and simple approximations are made for the restraint (positive or negative) provided to the flanges by the web and vice versa in writing separate strengths associated with flange and web local buckling. If the section is noncompact, the flexural resistance is in many cases larger than the yield moment M_y, but it is generally less than the plastic moment M_p. For symmetrical sections, the lateral-torsional buckling equations are the same as in Chapter F. However, for unsymmetrical sections, separate resistance formulas are provided that are based on the slenderness $\lambda = L_b / r_{yc}$, where r_{yc} is the radius of gyration of the compression flange about the cross-section minor axis.

Appendix G accounts for the interaction of the post-buckling resistance of slender webs ($\lambda > \lambda_r$) with potential local or lateral buckling of the compression flange. Whereas the potential

maximum strength is M_p in Chapter F and Appendix F, the strength is always less than or equal to the yield moment of the cross-section in Appendix G. Furthermore, the moment above which yielding effects are assumed to become significant is generally taken as $0.5M_y$ for the basic strength curves in Appendix G, whereas this moment is assigned larger values (denoted by the symbol M_r) in Chapter F and Appendix F. In Appendix F, M_r is reduced to account for compressive flange residual stresses in checking flange local and lateral-torsional buckling. However, no reduction for residual stresses is included in determining the M_r associated with web local buckling (i.e., in Appendix F, M_r is taken as M_y for non-hybrid girders in checking the influence of web inelastic buckling on the flexural strength).

The effect of a slender web on the strength is accounted for in Appendix G by multiplying the flexural resistance equations associated with local or lateral buckling of the compression flange by a plate girder bending strength reduction factor, R_{PG}. This factor accounts for the reduced effectiveness of the web due to bend buckling, and for the web post-buckling strength. The AISC equation for R_{PG} can be expressed as

$$R_{PG} = 1 - \frac{a_r}{1200 + 300a_r}\left(\frac{2D_c}{t_w} - 5.70\sqrt{\frac{E}{F_{cr}}}\right) \qquad (3.6)$$

This equation is based on the original formulation by Basler (1961). The term a_r is the ratio of the web area to the compression flange area, and F_{cr} is the compression flange critical stress. A similar equation is specified in the AASHTO LRFD provisions for girders with noncompact webs (the Q formula is provided as an alternative to this equation). However a_r is set equal to $2D_c\, t_w\, /b_{fc}\, t_{fc}$ in the AASHTO provisions, and the applied stress in the compression flange (f_c) is used in place of F_{cr}. Also, for symmetric girders, AASHTO uses 5.76 instead of the coefficient 5.70 in Eq. (3.6), and it reduces this coefficient to 4.64 for girders with $D_c\, /D$ larger than 0.5. For non-hybrid girders with adequate bracing and compact flanges, Appendix G predicts a nominal flexural capacity M_n equal to $R_{PG}M_y$ if first yielding occurs in the compression flange; it predicts $M_n = M_y$ if the onset of yielding is at the tension flange. Comparable equations are provided in the AASHTO Specifications that predict $M_n = R_b\, M_y$ irrespective of which flange is associated with first yielding, where R_b is similar to Eq. (3.6) but with the differences outlined above. However, this chapter focuses on the AASHTO strengths predicted by the Q formula (see Section 2.1) rather than the strengths predicted by the AASHTO equations comparable to those in AISC LRFD Appendix G, since the Q formula allows the prediction of nominal strengths greater than M_y.

The AISC LRFD equations for the compactness limit λ_p are the same throughout each of the three sections discussed above. Thus, they are the same for symmetric or unsymmetric girders and rolled or welded shapes. However, the equations for λ_r are in general different for symmetric and unsymmetric as well as for rolled and welded shapes. Furthermore, the flange local and lateral-torsional buckling λ_r values specified in Appendix G differ from those in Chapter F and Appendix F. An equation is provided in Appendix B5.1 of the AISC LRFD Specification that defines the web λ_r for the general case of symmetric or unsymmetric girders. This equation may be written as

$$\lambda_r = 1.49 \sqrt{\frac{E}{F_y}} \left[1 + 2.83 \left(\frac{D}{2D_c} \right) \right], \quad \frac{3}{4} \le \frac{D}{2D_c} \le \frac{3}{2} \tag{3.7}$$

This equation determines whether Appendix F or G is used to calculate the resistance of a section (the influence of the web on the flexural capacity equations in Appendix G is addressed by Eq. (3.6), which does not require the λ_r parameter). For symmetric sections ($D_c/D = 0.5$) and Grade 50 steels, Eq. (3.7) places a limit of *137* on D/t_w. For sections with $D_c/D > 0.5$, λ_r is less than *137*.

3.2 Moment-Plastic Rotation Model

In Chapter 2, the authors have developed a model for the moment-plastic rotation behavior of composite and noncomposite girders with noncompact webs and compact or ultra-compact flanges. This model is illustrated in Fig. 2.15. Equation (2.9) has been proposed for the nominal maximum strength M_n for use with this model, and Eq. (2.10) has been developed for the plastic rotation at which the pier-section starts to shed its moment significantly.

The suggested model a fit to a suite of finite element studies in which transverse stiffeners are placed such that the applied shear is less than $0.6V_n$ in the web, and cross frames are spaced at the inelastic limit defined in the current AASHTO Specifications (1994) (Eq. (2.2a)). In Chapter 2, it is recommend that r_y in this equation should be based on the compression flange plus one-half the total depth of the web about the minor axis of the cross-section. The limit on the applied shear V is such that potential moment-shear interaction effects are avoided for sections in which tension field action is included in determining the web shear capacity. It does not appear to pose any practical limitations on the design of compact sections (Schilling and Morcos 1988), but it can require the use of additional stiffeners beyond the minimum number required for strength in girders with webs approaching the AASHTO limits for design without longitudinal stiffeners. The suggested M-θ_p model is applicable for beams and girders that satisfy these limits plus the

restrictions $\dfrac{2D_{cp}}{t_w} \le 6.77\sqrt{\dfrac{E}{F_{yc}}}$, $\dfrac{b_{fc}}{2t_{fc}} \le 0.4\sqrt{\dfrac{E}{F_{yc}}}$, $\dfrac{D}{b_{fc}} \le 4.25$, and $\dfrac{D_{cp}}{D} \le 0.75$. The limit on

$\dfrac{2D_{cp}}{t_w}$ is the same as the current limit in the AASHTO LRFD Specifications (1994) for girders

without longitudinal stiffeners. The last three limits are based on the ranges of design parameters

encompassed by the available finite element and experimental tests, and it can be argued that they

are reasonable practical limits for economical designs. The limit on $\dfrac{b_{fc}}{2t_{fc}}$ is slightly more liberal

than the current AASHTO LRFD definition of a compact compression flange.

3.3 Summary of Validation Studies

Figure 2.2 illustrates a generic configuration employed for all the experimental and finite
element tests considered in this chapter. Tables 3.1 through 3.3 list key parameters associated
with each of the tests. The reader is referred to the notation list for definitions of the terms. An
entry of "NA" in the L_{b2}/L_{b1} column indicates that the test girder does not have any unsupported
segments beyond the "critical unbraced length" L_{b1} . An entry of "NA" in the $d_{o.in}/D$ column
indicates that no additional "inelastic restraint stiffeners" were employed in the test. The entries
for D_c/D, and $(2D_c/t_w)_{eq}$ are not listed for the symmetrical sections. The tests summarized in
Table 3.1 are grouped based on project and emphasis, and are listed chronologically in the order
from the earliest to the most recent studies. The primary focus of each of these groups of tests is
summarized below:

- **US steel tests USS2, USS3 & USS4 performed by Grubb and Carskaddan (1979) and
Carskaddan (1980).** These tests were performed under AISI project 188, Phase 3, and are
labeled as 188-3-2 through 4 within the above references. The main purpose of these tests was to
determine compactness requirements and to study the interior-support behavior of bridge beams
designed using Autostress methods. The specific objective of the first set of tests (Grubb and
Carskaddan 1979) was to qualify most of the rolled shapes at the *345 MPa (50 ksi)* yield strength
level for plastic design of continuous-span bridges. The tests showed that, although the D/t_w of the
webs was limited to *58*, the rotation capacities were essentially undefined by traditional definitions
used in plastic design (since the maximum strength did not reach the plastic moment capacity M_p).
This behavior was attributed to the fact that the D_c/D of the tests was larger than *0.5*. Test 188-3-1
is not included here because its L_{b1}/r_y is quite small compared to the bracing limit for the Q

formula (Eq. (2.2a)). As demonstrated in Chapter 2, the spacing of braces at lengths substantially smaller than Eq. (2.2a) can result in a substantial improvement in the M-θ_p response. This is the case for test 188-3-1 compared to the other tests in (Grubb and Carskaddan 1979).

Test 188-3-4 (Carskaddan 1980) was conducted to assess the service load (i.e., fatigue of stud shear connectors), overload (i.e., cracking behavior of the deck), and maximum strength characteristics of composite rolled beam sections over interior pier supports. The tests by Grubb and Carskaddan (1979) were all-steel tests, whereas 188-3-4 was a twin composite beam. The steel girders in 188-3-4 closely matched 188-3-2 in their design proportions, and they exhibited similar experimental behavior. Based on this study, Carskaddan concluded that the composite and all-steel test results were sufficiently similar to permit additional testing for compactness requirements to be performed with simpler all-steel specimens. Along with additional studies conducted using more restrictive $2D_c/t_w$ limits (Grubb and Carskaddan 1981), the above tests served as a basis for the "effective plastic moment" concepts proposed in the early Autostress design research (Haaijer et al. 1983) and adopted by the original AASHTO Guide Specifications for Alternate Load Factor Design (1986).

- **Early tests US, UL and SL performed by Schilling (1985).** These tests were conducted to investigate the pier moment-plastic rotation behavior of girders proportioned at the slenderness limits for transversely-stiffened girders in (AASHTO 1983). Based on these tests, Schilling developed a lower-bound pier moment-rotation curve for noncompact web girders. Also, this study showed that the equations for the effective plastic moment M_{pe} (Haaijer et al. 1983), which were developed for stockier rolled-beam type sections, are not applicable for more slender-web plate girder sections. That is, it was found that plate girder sections in general are not able to develop plastic rotations $\theta_p \geq 0.063$ radians prior to the bending resistance falling below that given by the rolled-section M_{pe} equation developed by Haaijer et al. (1983). However, it was concluded that the general concept of an effective plastic moment potentially could still be applied.

- **Latter tests S, M and D performed by Schilling and Morcos (1988).** These tests were conducted to develop moment-rotation curves for noncompact plate girders with improved M-θ_p characteristics compared to the girders studied by Schilling (1985). Three changes were made to improve the M-θ_p behavior: (a) the flange slenderness ratios $b_{fc}/2t_{fc}$ were reduced from the maximum limits allowed in (AASHTO 1983) to traditional plastic design limits (referred to by Schilling and Morcos as ultracompact limits), (b) the web slenderness ratios were reduced, and (c)

additional one-sided transverse stiffeners (i.e., inelastic restraint stiffeners) were placed at a distance of *0.5D* on each side of the simulated pier section. Each of these girders was a symmetric all-steel section. The D/t_w values were *81* for specimen S, *117* for specimen M, and *154* for specimen D. The moment-plastic rotation characteristics were significantly improved, particularly for the girders with the stockier webs.

- **Composite plate girder test UTC, performed by Tansil (1991).** This test, designated as UTC in Table 3.1, was conducted to determine more precisely the pier moment-rotation behavior in unshored composite bridge girders with noncompact webs (the earlier test by Carskaddan (1980) simulated shored construction conditions). The performance of the girder was evaluated both at overload and at maximum load. Specifically, the slab-cracking behavior as well as the effective slab width were evaluated at the overload and maximum load stages. The test results showed that the girder exhibited good ductility and developed a maximum flexural capacity approximately nine percent larger than the theoretical yield moment, even though the web slenderness $2D_{cp}/t_w$ was *199* ($2D_c/t_w$ was equal to *156*). It was concluded that at dead and service load, the girder behaved approximately as an uncracked section with an effective slab width of *4t_s*, whereas at overload and maximum load, the girder appeared to behave predominantly as a cracked section with an effective width of *13t_s* (the total width of the slab in this test is *18.75t_s*, and the AASHTO effective width is *12t_s*).

- **FHWA component test (FHWA 1992).** The primary purpose of this test was to determine the experimental moment-rotation characteristics for the pier section of a girder that would be used in a subsequent model bridge study. This test specimen had longitudinally post-tensioned precast modular deck panels. Block-outs were provided in the panels for installation of stud shear connectors. These block-outs were grouted to make the panels composite with the steel girders after the panels were longitudinally post-tensioned and the shear connectors were installed. The post-tensioning was designed such that zero tensile stress would be present in the deck at service load and a maximum tensile stress of $5\sqrt{f_c'}$ (psi) would be present in the deck under overload levels, including the effects of differential creep and shrinkage. Unshored construction conditions were simulated. The girder behavior was nearly linear for moments less than the theoretical yield moment M_y, calculated including the effects of initial noncomposite dead loads. Also, the maximum moment capacity exceeded M_y by approximately eight percent even though $2D_{cp}/t_w$ is equal to *138*. However, a separation of the deck panel from the steel girder occurred shortly after

the maximum load capacity was reached, and the test data indicates a degradation in the shear transfer between the deck and the girder for subsequent girder deflections (FHWA 1992). Correspondingly, the ductility of the moment rotation curve is not as good as that for Schilling's tests S, M, and D (Schilling and Morcos 1988). The test did exhibit greater ductility than Schilling's (1985) lower-bound moment-rotation curve however.

- **Tests P1 through P6 conducted by the authors (Barth 1996).** A primary objective of these tests was to study the effect of lateral brace spacing near the AASHTO limit (Eq. (2.2a)) on the moment-rotation behavior of plate girders with noncompact webs and compact or ultracompact flanges. All but one of these test girders had two unbraced segments on each side of the peak moment location, and the end reaction points were placed at the second brace location. This resulted in relatively small moment gradients in most of the tests (the authors have found lower moment gradients to be more detrimental to the M-θ_p behavior than high shear and high moment gradient, as long as moment-shear strength interaction at the pier is not a consideration (see Chapter 2 and (White 1994)). The second unbraced segment on each side of the simulated pier section provides some lateral bending restraint to the compression flange. This tends to enhance the M-θ_p characteristics, as discussed in Chapter 2. Also, two transverse stiffeners, spaced at $D/3$, were placed on each side of the pier location to restrain the local buckling distortions of the web and compression flange and thus enhance the moment-plastic rotation behavior. All the test girders exhibited good ductility, and all but one developed maximum moments greater than M_y.

- **Finite element parametric studies based on "lower-bound" L/r_y, transverse-stiffener spacing, and L/D values (Chapter 2).** These are the primary finite element "numerical tests" used to develop Eqs. (2.9) and (2.10). Important attributes of these tests include: (a) all the studies involved multiple unbraced segments on each side of the peak moment location, (b) plate local out-of-flatness values were set approximately at the AWS tolerances (AWS 1995) and residual stresses representative of those expected in typical plate girder tests were specified, (c) the lateral brace spacing was set at the AASHTO limit (Eq. (2.2a)), (d) transverse stiffeners were spaced such that $V \leq 0.6V_n$, but no additional "inelastic restraint" stiffeners were placed within the plastic hinging region to enhance the performance, (e) a relatively large span-to-depth ratio of the prototype girders ($L/D = 30$) was targeted, (f) a range of girder cross-section aspect ratios (D/b_{fc}) representative of typical values from rolled beam sections to welded plate girders were specified (only one of the experimental tests outlined above has a D/b_{fc} larger than four), and (g) a range of

D_{cp}/D values from *0.5* to *0.75* were tested. In Tables 3.2 and 3.3, these tests are labeled as C10 through C15 for symmetric girders with $b_{fc}/2t_{fc}$ set at the flange compactness limit, UC4 through UC9 for symmetric girders with ultracompact flanges, and U1 through U8 for the unsymmetric girder tests (girders with flanges proportioned both at the compact and ultracompact $b_{fc}/2t_{fc}$ limits were included in the unsymmetric studies). As discussed in Chapter 2, items (b) through (e) in the above list are reasonable limits for "lower-bounding" of the M-θ_p responses with respect to potential designs.

A number of other tests of noncompact web girders can be found in the literature. For example, important tests are documented in (Johnson 1985) and (Holtz and Kulak 1973). However, these are four-point bending tests involving an unsupported length subjected to uniform bending moment. The tests outlined in the above discussions are believed to be the most representative of conditions in the hogging moment region of continuous-span bridge girders.

3.4 Overview of Results

Figures 3.2 through 3.8 compare the flexural capacities predicted by the Q formula and by the AISC LRFD Specification, and the curves predicted by the M-θ_p model developed in Chapter 2, to the moment-plastic rotation data determined by experimental tests and/or finite element analysis. Figure 3.2 presents the results for the all-steel experimental tests performed by Schilling (1985) and by Schilling and Morcos (1988), and Fig. 3.3 shows the results from all-steel experimental tests conducted by Barth (1996). Figure 3.4 then presents the data for the composite girder tests reported in (Tansil 1991) and (FHWA 1992). Both finite element as well as experimental results are shown for all the tests in these figures, with the exception of the FHWA test. The correlation between these finite element and experimental curves gives some indication of the quality of the finite element predictions. The reader is referred to Chapter 2 for an extensive discussion of the finite element modeling issues. In the early stages of the authors' research, the tests by Schilling (1985), Schilling and Morcos (1988), and Tansil (1991) were targeted as the primary experimental base for verification of the finite element models. The FHWA (1992) test and the tests performed by Grubb and Carskaddan (1979) and Carskaddan (1980) were targeted subsequently for comparisons to the final M-θ_p model. Figure 3.5 shows the results for the all-steel tests (USS2 and USS3) conducted in the early study by Grubb and Carskaddan (1979), and for the composite girder test (USS4) performed by Carskaddan (1980). Finally, Figures 3.6 through 3.8 show the

comparisons for the subset of the finite element parametric studies from Chapter 2 outlined in the previous section.

For application of the formulas outlined in Section 2 to composite girders, the calculation of the yield moment capacity M_y is key. The yield moment is calculated in this chapter including the effects of noncomposite dead load for the tests by Tansil (1991) and FHWA (1992), since these tests simulated unshored construction. However, Carskaddan's test (1980) simulated shored construction, and therefore M_y is calculated assuming that all the loads are applied to the composite section for this girder. For the FHWA girder, which had a longitudinally post-tensioned concrete deck, M_y is determined based on the uncracked cross-section using a modular ratio of 6.6 as reported in (FHWA 1992) since this is clearly the reported behavior of the girder at first yielding in this test. However, for the other composite tests, M_y is based on a cracked section analysis at the pier section. In all the composite girder tests, the plastic moment capacities are determined based on a cracked pier section, including all the longitudinal post-tensioning tendons and/or reinforcing steel within the AASHTO effective width of the slab (AASHTO 1994). However, it should be noted that the finite element analysis of Tansil's test assumed that all the longitudinal reinforcing within the concrete deck was effective (approximately 70 percent of the longitudinal reinforcing steel was located within the AASHTO effective width in this test).

The AISC LRFD (1993) equations discussed in Section 2.2 are directed predominantly at prediction of the strength of all-steel girders, i.e., the strength of composite girders in negative bending is not addressed directly within this specification. As shown in Figs. 3.4 and 3.5, Appendix G governs for Tansil's girder and for the FHWA test, and Chapter F governs for Carskaddan's test (the governing Sections of the AISC LRFD Specification are shown in the labeling of the strengths in the plots). In determining the AISC LRFD strengths for Carskaddan's test, the radius of gyration of the compression flange r_{yc} was used in the Chapter F lateral-torsional buckling provisions, similar to the AISC LRFD requirements of Appendix F for unsymmetric girders. For the FHWA girder, the uncracked section was used to determine D_c, and the moment capacity was calculated by reducing M_y of the uncracked section, including noncomposite dead load effects, by R_{PG} (Eq. (3.6)) (the compression flange of this girder is compact and the section is adequately braced such that neither local nor lateral-torsional buckling affect the strength by AISC LRFD). For Tansil's girder, the effect of the reinforcing steel within the cracked effective width of the slab was included in calculating D_c, and the moment capacity was calculated by reducing

M_y of the cracked section, including noncomposite dead load effects, by R_{PG} (Eq. (3.6)) (the compression flange of this girder is also compact, and the section is adequately braced such that local and lateral buckling strength checks do not apply). Yielding of the tension flange and the reinforcing steel were considered in both the FHWA girder and in Tansil's specimen, but these checks did not control the strengths.

3.5 Assessment of Strengths

The following items summarize the results for the predicted, measured, and computed moment capacities illustrated in Figs. 3.2 through 3.8:

- With the exception of P4, US, UL and SL, the experimental and finite element results all show moment capacities greater than or equal to M_y. However, in tests US, UL and SL, the equivalent web slenderness values are somewhat larger than the limits generally permitted for girders without longitudinal stiffeners, the compression flange slenderness exceeds the AASHTO compactness limit, and the web shear force was larger than 60 percent of the web shear capacity including tension field action. Nevertheless, the experimental strengths for UL and SL (see Fig. 3.2) are only one percent smaller than M_y.

- The finite element results in Fig. 3.2 indicate that US would not develop M_y, but that the yield moment can be developed in tests UL and SL. The finite element analyses overpredict the experimental strengths by three percent for girder US, and by six percent for tests UL and SL. However, the initial residual stresses specified in these finite element models (White 1994) were not as severe as those considered in the current research (Chapter 2). This is expected to have a small effect on the finite element strength predictions.

- In test P4 (Fig. 3.3), the finite element analysis predicted a capacity larger than M_y whereas a maximum moment of only $0.91M_y$ was measured experimentally. However, the strength predictions of the finite element model, the Q formula, the AISC LRFD equations, and the M-θ_p model are all reasonably well correlated with each other for this test. The AISC LRFD strength is somewhat smaller than the other predictions, and it is expected that this strength should provide a conservative estimate of the experimental capacity for this test (since it is limited by the web local buckling strength without any consideration of post-buckling behavior). Also, it is interesting that the shape of the experimental M-θ_p curve is very similar to the finite element based curve. All these considerations indicate that the low values of

M/M_p measured in the experiment may be in error and that the finite element $M\text{-}\theta_p$ curve is more representative of the correct physical response. Unfortunately, the authors are not able to ascertain a specific cause of these low M/M_p values. However, they forward that the above factors merit the exclusion of the experimental curve of test P4 from further consideration.

- The strengths predicted by AISC LRFD Appendix G (for the tests to which it applies) are reasonably accurate compared to the experimental and/or finite element analysis strengths for the all-steel tests that have *both* large $2D_c/t_w$ (or $2D_{cp}/t_w$) *and* large D/b_{fc} values (see tests US, D, C13, UC7, U5 and U7). However, Appendix G underestimates the capacity of the other all-steel tests for which it applies from four to seven percent (see tests SL, P1, P2, C10, UC4, U1 and U3)[‡]. One common attribute of each of these tests is that D/b_{fc} is less than or equal to three. Also, tests P1 and P2 only slightly exceed the λ_r web limits for application of Appendix F. If the Appendix F equations are used for these girders, the predicted strengths are similar to the strengths predicted by the Q formula (see Fig. 3.3). In all these tests, the flexural capacity either approximately meets or exceeds M_y.

- It is interesting to note that the AISC LRFD Specification requires the consideration of a flexure-shear interaction effect in determining the strengths for girders US and SL. The theoretical strength reduction due to this effect is quite small for girder US. However, for girder SL, this reduction is significant. Curiously, the AISC M_n estimate without the moment-shear interaction effect corresponds approximately to the peak moment attained in the test whereas the reduced strength corresponds roughly to the plateau in the experimental post-buckling response.

- The strengths predicted by AISC LRFD Appendix F are accurate compared to the experimental and/or finite element analysis strengths for most of the tests. However, the Appendix F predictions underestimate the experimental strengths of girders M, P3 and P6 by nine, six and five percent respectively. Each of these girders is near the AISC λ_r web limit. The AISC reduction in strength associated with web local buckling neglects the web post-buckling strength in these girders. Also, the flanges of these girders are ultracompact, thus permitting development of some strain hardening in the flanges prior to flange local buckling.

[‡] For the girders that have been tested experimentally, the percentage errors are reported relative to the experimental data.

- The strengths for tests P4 and U6 are significantly overestimated by the AISC LRFD Appendix F equations. The experimental results for test P4 have already been discussed and dismissed. Test U6 is the maximum error case of an Appendix F trend in overestimating the capacities for unsymmetric girders illustrated in the right-hand side plots of Fig. 3.8. For non-hybrid girders, Appendix F uses the yield moment M_y for M_r in determining the strength associated with web bend buckling. Also, as noted previously, the web slenderness λ is expressed as D/t_w in the AISC Specification, and λ_r is adjusted to account for the depth of the web in compression. Apparently, the linear interpolation between M_r (= M_y) and M_p (see Fig. 3.1) tends to be somewhat liberal when based on these definitions in the case of girders with $D_c/D > 0.5$. The unconservative error of Appendix F for test U6 is twelve percent.

- Chapter F controls the AISC LRFD strength predictions for girders S, USS3 through USS4, C12 and C15, and UC6 and UC9, and in each of these girders, the predicted moment capacity is M_p. Girder S is symmetric and has a low D/b_{fc}, ultracompact flanges, close transverse stiffener spacing within the plastic hinge length, and a lateral brace spacing that is significantly smaller than the AASHTO limit. As a result, this girder is capable of developing substantial strain hardening within the plastic hinge length, and thus M_p is a conservative estimate of the maximum flexural capacity. The US Steel tests all have D_{cp}/D significantly larger than 0.5. As a result, only test USS2, which has the shortest L/D and a small L_{b1}/r_y relative to the AASHTO limit (Eq. (2.2a)), is capable of developing the plastic moment. Test USS3 and the composite girder test USS4 fall five and eleven percent short of M_p. Also, test C15, which has a large D/b_{fc} falls far short of the plastic moment (the maximum moment is only $0.91M_p$ in the finite element solution for this member). It should be noted however that the capacities of these girders are each significantly larger than M_y.

- The Q formula is an accurate predictor of the maximum strengths of the all-steel girders with the exception of four cases: (1) It overestimates the experimental strengths for tests P4 and P5. As noted previously, the small measured capacities for test P4 are dismissed. Equation (2.2a) is significantly exceeded (by 16 percent) for test P5. It is believed that this is the main cause of the overprediction of the strength by the Q formula for this test. (2) It underestimates the strength of girder UC4 by six percent. This girder has a small D/b_{fc} and the smallest a_{rp} of all the girders considered in the finite element studies reported in Chapter 2. (3) It underestimates the strength of the unsymmetric girders with small D/b_{fc} and small a_{rp}, i.e., girders U1 through

U4, by three, five, six and seven percent respectively. (4) It significantly overestimates the capacities of girders C14, C15 and UC8, with respective unconservative errors of ten, nine and five percent. These girders all have large D/b_{fc} and correspondingly large a_{rp} values. With respect to the composite girder strengths, the Q formula performs well for the FHWA and USS4 tests, but it is somewhat conservative for Tansil's UTC test, underpredicting the strength by eleven percent.

- Equation (2.9) of the M-θ_p model is an accurate predictor of the flexural capacity for all the girders studied, with the exception of girders P4 and P5. The reason for the overestimates in these cases is believed to be the same as that explained above for the Q formula.

3.6 Summary of Weaknesses in American Strength Equations

Several flaws in current specification strength equations are apparent from the above observations and from consideration of the calculations outlined in Section 2:

- With the exception of sections in which the strength is controlled by Appendix G in the AISC LRFD equations, neither the Q formula nor the AISC LRFD equations capture any sensitivity of the maximum strength to D/b_{fc} or a_{rp}. However, the test data clearly shows some sensitivity to these parameters. In the studies conducted in this research, the largest unconservative error due to this simplification is nine percent for the AISC LRFD Appendix F formulas (test C15) and ten percent for the Q formula (test C14).

- The equations in Appendix F of the AISC LRFD Specification (1993) tend to overpredict the capacity of girders with $D_{cp}/D > 0.5$ (see tests U2, U4, U6 and U8 in Fig. 3.8). This error appears to come from the approximation that $M_r = M_y$ in checking the influence of web local buckling on the flexural capacity for these types of sections. The maximum unconservative error in the studies presented here is twelve percent.

- The equations of Appendix G of the AISC LRFD Specification (1993) underestimate the flexural capacity of noncompact web girders for all the cases in which these equations are applicable. For the girders where D/b_{fc} is approximately equal to three, the capacities are underestimated by as much as seven percent. However, for the larger D/b_{fc} cases, the predictions of the strengths by Appendix G (approximately equal to M_y in all cases) are reasonably good. Similar results would be expected for the comparable AASHTO strength formulas. The differences between the AISC LRFD R_{PG} formula (Eq. (3.6)) and the

comparable AASHTO plate girder modification formula would be relatively minor for the range of girder parameters considered. It should be emphasized however that the AISC LRFD Appendix G formulas are applicable only for slender web girders. The comparable AASHTO LRFD formulas are applicable also for girders with stockier noncompact webs[§], thus giving a maximum design resistance of only M_y for these types of sections. The conservatism of using a base maximum strength of M_y for these types of girders is significant.

- The strength of steel I-girders with a noncompact web and compact or ultracompact flanges is apparently dominated by the *inelastic buckling* behavior of the *compression flange*, with a possible destabilizing effect due to the flange providing restraint to bend-buckling of the web and a partial loss of effectiveness of the web due to bend-buckling deformations. The Q formula captures this behavior reasonably well, but it does not account for the apparent effect of the ratio of the area of the web in compression to the flange area associated with the parameter a_{rp}. The maximum unconservative error associated with this simplification is ten percent. Furthermore, the accuracy of the Q formula for girders with compact or ultracompact flanges requires that Q_{fl} must be independent of the flange slenderness $b_{fc}/2t_{fc}$, as reflected in Eq. (3.4) (Bak 1992). That is, the flexural strength of girders with compact flanges is not highly correlated with elastic local buckling of the compression flange. Also, the formulas for the flange buckling coefficient proposed by Johnson (1985), which are similar to Eq. (3.3), appear to have been developed by dividing moment capacities which are larger than the yield moment M_y by the elastic section modulus of the girder to obtain a flange critical stress. Although, Eq. (3.3) appears to provide reasonable values for the flange buckling coefficient associated with the restraint (positive or negative) provided to the *inelastic* compression flange by the web, it is theoretically awkward to use this coefficient in an *elastic* flange buckling equation (Eq. (3.2)) that is subsequently used in a linear interpolation formula for the *inelastic* flexural strength (Eq. (3.1)). Equation (2.9) is somewhat simpler to apply than the Q formula and the AISC LRFD equations, yet it more accurately represents the behavior of girders with compact and ultracompact flanges, and noncompact webs.

[§] The comparable AASHTO parameter to R_{PG} is equal to one for $2D_{cp}/t_w$ less than *139* and *112* for girders with $D_{cp}/D \leq 0.5$ and $D_{cp}/D > 0.5$ respectively, assuming that the compression flange is stressed to F_y due to the factored loading. If the applied stress f_c is less than F_y this parameter is taken equal to one for even higher web slenderness values.

- Equation (2.9) has the limitation that it is applicable essentially only to girders with compact or ultra-compact flanges (i.e., $b_{fc}/2t_{fc} \leq 0.4\sqrt{E/F_{yc}}$). However, the Q formula loses its advantage relative to the more traditional AASHTO calculations that are similar to Appendix G of the AISC LRFD Specification as the flanges become more and more noncompact. Within the context of the AASHTO LRFD Specifications, Eq. (2.9) would appear to be preferable to the Q formula within the range that it is applicable. Use of this equation would retain the advantage of the Q formula in predicting nominal strengths greater than M_y for girders with compact and ultra-compact flanges. The traditional AASHTO flexural capacity formulas should be adequate for other cases. Alternatively, ongoing research by a number of investigators may produce improved formulas that address girders with both compact and noncompact flanges. Within the context of the AISC LRFD Specification, it should be possible to adjust the current equations to account for the unconservative errors in Appendix F pertaining to unsymmetric girders. However, consideration of the effects of adjustments to the Appendix F equations is beyond the scope of the current research.

3.7 Assessment Of Moment-Rotation Model

With the exception of the FHWA test (1992), the M-θ_p model developed in Chapter 2 provides conservative to excellent predictions of the complete moment-rotation characteristics for the girders studied. As discussed previously, the post-peak characteristics of the FHWA test were degraded by the loss of the shear interconnection between the deck and the steel girder shortly after the maximum flexural capacity was reached. The M-θ_p curve predicted by the model is certainly a plausible one for this girder, supposing that the shear connection between the steel girder and the slab had been sufficient.

In general, the M-θ_p model is somewhat conservative for situations in which the lower-bound parameters selected in its development are set at more beneficial values. For example, girder S (see Fig. 3.2) has a compact web, an extra "inelastic restraint" transverse stiffener placed at $D/2$ on each side of the pier section, an L/D of 21.2 in the prototype bridge span, and a lateral brace spacing that is 0.71 of the AASHTO limit (Eq. (2.2a)). Each of these attributes in general can produce improved moment-plastic rotation characteristics relative to the girders analyzed in the development of the M-θ_p relations. However, the influence of these attributes appears to become less important for larger $2D_{cp}/t_w$ values. This plus the fact that the lateral brace spacing is closer

to the AASHTO limit for girders M and D helps explain why the suggested M-θ_p model is more accurate for these girders. If the web $2D_{cp}/t_w$ is reduced significantly from the smallest values considered in this report, it is apparent that the web will tend to provide significant torsional restraint to the compression flange (Kuhlmann 1989; Johnson 1985; ASCE 1971), and the suggested M-θ_p model will tend to be conservative. With the exception of tests P4 and P5, for which the over-prediction of the strengths has already been discussed, the M-θ_p model tends to be somewhat conservative for the girders tested experimentally by Barth (1996). It is believed that this can be attributed to the use of the transverse stiffeners at $D/3$ within the plastic hinging region in Barth's tests.

For composite bridge girders, it is believed that the M-θ_p model will often be a conservative representation of the actual behavior because of the restraint provided by the bridge deck to twisting of the girder tension flange about its longitudinal axis, and due to potential tension stiffening behavior of the concrete deck. Of course, the benefit of the twisting restraint provided to the tension flange is diminished by distortional buckling of the girder cross-section as the web becomes more and more slender. The twisting restraint offered by the deck in the UTC and FHWA tests (see Fig. 3.4) is probably small, since only a single composite girder was tested. However, in the USS4 study (see Fig. 3.5), a twin-girder system with girders having relatively small $2D_{cp}/t_w$ values was tested. In this case, it is expected that twisting restraint from the deck was quite beneficial. The authors believe that this is evidenced in Fig. 3.5 by the flatter slope on the load-shedding portion of the experimental M-θ_p curves compared to the model prediction. The model prediction for girder USS3 (Fig. 3.5) is quite good, with only the latter portion of the unloading curve being somewhat different in the experiment. Girder USS2 is identical to USS3, but with a larger moment gradient and a smaller value for the ratio of the lateral brace spacing to the AASHTO bracing limit.

The model post-peak moment-rotation curves are slightly liberal for tests U5 through U8, which all have a high D/b_{fc}; however, the authors judge these predictions to be acceptable.

Figure 3.9a compares the predictions of the M-θ_p model to the finite element and experimental curves for Schilling's test S (Schilling 1988), and to the effective plastic moment for this girder (AASHTO 1994). This girder is the most ductile of all those studied in this chapter, and since its web slenderness meets the AASHTO compactness requirements, the original effective plastic moment concept (Haaijer et al. 1983) should be valid for this girder. By definition, the effective

plastic moment (M_{pe}) corresponds to the moment at which a plastic rotation of $\theta_p = 0.063$ radians is reached on the post-peak unloading portion of the moment-plastic rotation curve (Haaijer et al. 1983). Figure 3.9a illustrates that $M_{pe} = 0.84M_p$, calculated according to the AASHTO (1994) equations, matches well with $\theta_p = 0.063$ for girder S. The suggested M-θ_p model underpredicts the actual ductility of the test girder, although it does predict that the girder is able to develop M_p for a substantial plastic rotation. It is believed that the underprediction of the ductility for this test is due to the fact that girder S was braced at only 0.71 of the AASHTO limit (Eq. (2.2a)). Figure 3.9b shows finite element results for a modified version of this test in which the L_{b1} is increased such that it is equal to the AASHTO bracing limit. It was found that the girder web could be unstiffened for this modified test and still satisfy the limit of $V < 0.6V_n$; therefore, only bearing stiffeners were included in the modified finite element study. This figure shows that the M-θ_p model approximates the behavior of the modified girder reasonably well, although the modified girder is not capable of developing M_p. White (1994) shows that if end restraint from an adjacent unsupported segment is added to this girder, the ductility is increased. The M-θ_p model is an excellent predictor of the behavior of this final version of girder S. Chapter 2 shows additional curves that illustrate that the ductility of the modified girder S can be improved substantially by adding intermediate brace points to shorten the critical unsupported length.

3.8 Implications on Ductility, Development of M_p, and Development of M_y

Many measures of the flexural ductility of beams and girders, often termed inelastic rotation capacity, have been employed in the literature. Chapter 2 reviews several definitions that are closely related to the AASHTO and AISC LRFD provisions. One of the most frequently used definitions is based on the total plastic rotation that has been achieved over the plastic hinging length when the moment drops below M_p within the post-peak portion of the response. If a girder's maximum strength is less than M_p, the rotation capacity is undefined by this measure. This is the case for most of the test results that have been presented. However, it can be argued that all of the tests exhibit acceptable ductility for inelastic redistribution of excessive moments from the pier sections of continuous-span girders. Equations for an effective plastic moment $M_{pe} < M_p$ could be developed based on a required inelastic rotation capability such as in (Haaijer 1983). However, more recent Autostress-type procedures utilize the predicted M-θ_p relations directly, and therefore should provide a more realistic assessment of the behavior.

It is important to note that, if the rotation capacity is defined as the inelastic rotation where the moment falls below a certain value along the load-shedding part of the M-θ_p curve, much of this capacity often comes from local and/or lateral buckling deformations. This is true either for highly-compact traditional plastic design type sections or for noncompact web plate girders such as those considered in this work. It can be argued that the load-shedding portion of the M-θ_p response, represented by the portion of the M-θ_p model in which θ_p is larger than θ_{RL} might be avoided under service II conditions in the AASHTO LRFD provisions, where the primary consideration is limiting of permanent deflections. This is because the inelastic local and lateral-torsional buckling distortions tend to increase rapidly as the pier section begins to shed its moment. However, for consideration of maximum strength load conditions, the inelastic deformations associated with $\theta_p > \theta_{RL}$ should be acceptable.

If the suggested M-θ_p model is accepted as a reasonable representation of the hogging moment behavior, it is informative to assess the implications of Eq. (2.9) versus the Q formula (Eq. (3.1)) on the ability of the section to develop the plastic moment capacity. Figure 3.10 shows plots of the maximum limit on $2D_{cp}/t_w$ versus M_p/M_y implied by Eqs. (2.9) and (3.1) for the section to be able to develop M_p. The Q formula gives one curve for this limit, independent of the parameter a_{rp}. However, Eq. (2.9) shows a significant dependency of the girder maximum strength on this parameter that is evident in the studies that have been performed. It can be observed that the $2D_{cp}/t_w$ required for the girder to develop M_p is larger by nearly a factor of two for a_{rp} values of 0.8 versus values of three to five. Both the curve developed from Eq. (3.1) and the curves developed from Eq. (2.9) exhibit similar trends in terms of a reduction in the maximum $2D_{cp}/t_w$ values for girders with large M_p/M_y ratios; however, the curves based on Eq. (2.9) have slightly smaller slopes than the curve derived from the Q formula.

Finally, it is informative to consider the requirements on $2D_{cp}/t_w$ implied by Eqs. (3.1) and (2.9) for a section with a compact or ultracompact flange to be able to develop the yield moment M_y. The Q formula implies a limit of $2D_{cp}/t_w = 170$, indicating that all unstiffened or transversely-stiffened girders, designed by AASHTO LRFD with compact flanges ($b_{fc}/t_{fc} \leq 9.2$ for Grade 50 steels), are capable of developing at least M_y. If the AASHTO limit of $2D_{cp}/t_w = 163$ for transversely-stiffened webs is assumed, and the flanges are allowed to be noncompact, the Q formula requires that the flanges must have a $b_{fc}/2t_{fc} \leq 9.3$ for the section to be capable of developing M_y. This correlates well with the results of the finite element parametric study

reported in Chapter 2, for which all the girders developed a maximum flexural capacity of at least M_y. The $2D_{cp}/t_w$ limit obtained by Eq. (2.9) that is comparable to the *170* limit of the Q formula varies with a_{rp}, and if plotted shows that the limit may need to be significantly smaller than *170* for large a_{rp} and small M_p/M_y values. However, it is practically impossible to obtain cross-section a_{rp} and M_p/M_y values that violate these limits (and if the limits are violated, they are only violated slightly). None of the girders considered in the experimental and finite element analysis tests violate these limits. Therefore, as a practical matter, Eq. (2.9) is in agreement with the Q formula in expressing that for web slenderness values within the AASHTO limits for transversely-stiffened webs, steel I-girders are generally able to develop strengths greater than or equal to the yield moment capacity.

3.9 Concluding Remarks

The finite element and experimental tests documented in this chapter all indicate that, within the limits for which longitudinal stiffeners are not required by the AASHTO LRFD provisions (i.e., $2D_{cp}/t_w \leq 163$ for Grade 50 steels), I-girders with compact or ultra-compact flanges are for all practical purposes always capable of developing flexural capacities greater than or equal to the yield moment M_y. Furthermore, it has been shown that these types of girders exhibit a reliable capacity for inelastic rotation over interior pier supports, even though the inelastic rotation capacity is undefined by some traditional definitions. The M-θ_p equations developed in Chapter 2 appear to give an excellent prediction of the girder strength and ductility for cases that match the lower-bound limits associated with their derivation. The most significant of these limits appears to be a lateral brace spacing set at the AASHTO LRFD limits (Eq. (2.2a)) and the use of no additional transverse stiffeners beyond the minimum required such that the maximum applied shear is less than *60* percent of the web shear capacity. When braces are spaced closer than the AASHTO limit and/or additional inelastic restraint stiffeners are placed within the plastic hinging region, the suggested M-θ_p equations tend to be somewhat conservative. Also, these equations would tend to be conservative whenever extremely stocky flanges or webs are employed. The suggested M-θ_p equations are simpler and more accurate than the current AASHTO LRFD Q formula; however, they are limited to sections with compact or ultra-compact flanges. Although the advantage of equations that can predict $M_n \geq M_y$ over traditional AASHTO flexural capacity equations that predict $M_n \leq M_y$ is reduced for sections with noncompact flanges, further research by various investigators may result in improved flexural capacity equations that are more

comprehensive. The current American specification formulas in the AASHTO LRFD (1994) and AISC LRFD (1993) Specifications were found to be reasonably accurate compared to the test data for most of the cases. However, significant unconservative errors were encountered in the Appendix F provisions of the AISC LRFD Specification for girders with $D_{cp}/D > 0.5$ and in both of these specifications for symmetrical girders with both the web and the flanges at the compactness limits and large D/b_{fc} values (equal to *4.26*).

Although the accuracy of the finite element models employed in this research is supported by comparisons with the available experimental data, it is important to note that the specific tests for which the current American Specifications exhibit significant unconservative errors have not been corroborated by experimental testing. Ideally, several focused experimental tests should be conducted to further affirm or refute these findings. Furthermore, the current studies have focused on the behavior of I-girders composed of Grade 50 steels. Additional studies are needed to extend the equations reliably to girders composed of steels with higher yield strengths.

Table 3.1. Summary of parameters for experimental tests considered in this research.

Test	$(b_{fc}/2t_{fc})_{eq}$	D/b_{fc}	$a_{rp} = (2D_{cp}t_w)/(b_{fc}t_{fc})$	$(2D_{cp}/t_w)_{eq}$	M_p/M_y	L_{b1}/r_y vs. AASHTO limit	L_{b2}/L_{b1}	$d_{o,in}/D$	$d_{o,el}/D$	$V_{max}/V_{n,el}$	L/D	F_{yc} (MPa)	F_{yw} (MPa)	D_{cp}/D	D_c/D	$(2D_c/t_w)_{eq}$	F_y (MPa)	F_{yrs} (MPa)	F_{yps} (MPa)
USS2	8.45	2.49	2.33	83	1.22	0.62	1.00	NA	2.36	0.39	23.6	383	345	0.678	0.569	70	F_{yc}	NA	NA
USS3	8.45	2.49	2.33	83	1.22	0.72	2.00	NA	2.36	0.25	35.4	383	345	0.678	0.569	70	F_{yc}	NA	NA
USS4	8.45	2.49	2.85	102	1.30	0.62	1.00	NA	2.36	0.41	23.6	383	345	0.833	0.607	74	F_{yc}	520	NA
US	9.84	4.70	5.08	174	1.47	0.80	NA	NA	1.50	0.62	8.9	410	450	0.712	0.616	150	F_{yc}	NA	NA
UL	9.86	2.61	1.58	171	1.26	0.61	NA	NA	1.50	0.74	16.6	401	450	0.707	0.573	138	F_{yc}	NA	NA
SL	9.84	2.94	1.00	171	1.16	0.54	NA	NA	1.50	0.82	15.8	342	450	0.500	-	-	F_{yc}	NA	NA
S	7.23	2.44	0.98	87	1.10	0.71	NA	1@0.5	1.36	0.72	21.2	405	387	0.500	-	-	F_{yc}	NA	NA
M	7.15	3.44	1.33	127	1.10	0.82	NA	1@0.5	0.86	0.64	16.3	405	387	0.500	-	-	F_{yc}	NA	NA
D	7.11	4.39	1.65	166	1.11	0.93	NA	1@0.5	0.61	0.56	13.8	405	387	0.500	-	-	F_{yc}	NA	NA
UTC	7.19	3.08	1.03	178	1.19	0.63	1	3@0.6	1.73	0.56	36.0	337	354	0.579	0.500	154	371	500	NA
FHWA	7.13	3.40	2.07	140	1.30	0.60	1.00	NA	1.32	0.67	13.2	356	310	0.664	0.456	96	310	454	1753
P1	9.41	2.92	1.14	141	1.13	1.13	1	2@0.33	2.92	0.52	35.9	427	483	0.500	-	-	F_{yc}	NA	NA
P2	9.35	2.94	1.15	141	1.14	0.89	1.36	2@0.33	1.95	0.49	30.9	427	483	0.500	-	-	F_{yc}	NA	NA
P3	7.13	3.50	1.28	137	1.15	1.03	1.09	2@0.33	1.95	0.51	27.4	427	483	0.500	-	-	F_{yc}	NA	NA
P4	9.33	2.95	1.21	134	1.14	1.17	NA	2@0.33	1.36	0.39	26.2	427	483	0.500	-	-	F_{yc}	NA	NA
P5	9.40	2.31	0.92	109	1.12	1.16	1	2@0.33	4.18	0.60	48.5	427	483	0.500	-	-	F_{yc}	NA	NA
P6	7.01	2.75	0.98	109	1.13	1.05	1	2@0.33	2.97	0.52	36.5	427	483	0.500	-	-	F_{yc}	NA	NA

Table 3.2. Summary of parameters for symmetric finite element tests.

Test	$(b_{fc}/2t_{fc})_{eq}$	D/b_{fc}	$a_{rp} = (2D_{cp}\,t_w)/(b_{fc}\,t_{fc})$	$(2D_{cp}/t_w)_{eq}$	M_p/M_y	L_{b1}/r_y vs. AASHTO limit	L_{b2}/L_{b1}	$d_{o.in}/D$	$d_{o.eff}/D$	$V_{max}/V_{n.eff}$	L/D	F_y (MPa)
C10	9.20	3.00	1.02	163	1.09	1.00	1.00	NA	1.32	0.52	30.0	345
C11	9.20	3.00	1.32	125	1.11	1.00	1.00	NA	2.67	0.53	30.0	345
C12	9.20	3.00	1.93	86	1.14	1.00	1.00	NA	6.00	0.36	30.0	345
C13	9.19	4.26	2.04	163	1.14	1.00	1.21	NA	2.50	0.41	30.0	345
C14	9.19	4.26	2.66	125	1.17	1.00	1.30	NA	6.00	0.54	30.0	345
C15	9.19	4.26	3.87	86	1.22	1.01	1.43	NA	6.00	0.22	30.0	345
UC4	7.00	3.00	0.77	163	1.08	1.00	1.00	NA	0.79	0.53	30.0	345
UC5	7.00	3.00	1.01	125	1.10	1.00	1.00	NA	1.67	0.53	30.0	345
UC6	7.00	3.00	1.46	86	1.13	1.00	1.00	NA	6.00	0.44	30.0	345
UC7	7.00	4.26	1.56	163	1.12	1.00	1.13	NA	2.28	0.49	30.0	345
UC8	7.00	4.26	2.03	125	1.15	1.00	1.20	NA	3.00	0.39	30.0	345
UC9	7.00	4.26	2.95	86	1.19	1.00	1.33	NA	6.00	0.28	30.0	345

Table 3.3. Summary of parameters for singly-symmetric finite element tests.

Test	$(b_{fc}/2t_{fc})_{eq}$	D/b_{fc}	$a_{rp} = (2D_{cp}\,t_w)/(b_{fc}\,t_{fc})$	$(2D_{cp}/t_w)_{eq}$	M_p/M_y	L_{b1}/r_y vs. AASHTO limit	L_{b2}/L_{b1}	$d_{o.in}/D$	$d_{o.eff}/D$	$V_{max}/V_{n.eff}$	L/D	F_{yc} (MPa)	F_{yw} (MPa)	D_{cp}/D	D_c/D	$(2D_c/t_w)_{eq}$
U1	9.20	3.00	1.59	163	1.19	1.00	1.00	NA	1.71	0.46	30.0	345	F_{yf}	0.625	0.546	142
U2	9.20	3.00	2.29	163	1.27	1.00	1.00	NA	3.00	0.46	30.0	345	F_{yf}	0.750	0.593	129
U3	7.00	3.00	1.21	163	1.16	1.00	1.00	NA	1.17	0.50	30.0	345	F_{yf}	0.625	0.540	141
U4	7.00	3.00	1.74	163	1.24	1.00	1.00	NA	1.83	0.48	30.0	345	F_{yf}	0.750	0.582	127
U5	9.19	4.26	3.19	163	1.28	1.00	1.23	NA	2.50	0.33	30.0	345	F_{yf}	0.625	0.563	147
U6	9.19	4.26	4.59	163	1.39	1.00	1.24	NA	3.00	0.28	30.0	345	F_{yf}	0.750	0.621	135
U7	6.99	4.26	2.43	163	1.24	1.00	1.16	NA	2.50	0.39	30.0	345	F_{yf}	0.625	0.557	145
U8	6.99	4.26	3.49	163	1.34	1.00	1.17	NA	3.00	0.35	30.0	345	F_{yf}	0.750	0.612	133

(a) Q formula (AASHTO, 1994)   (b) AISC LRFD (1994)
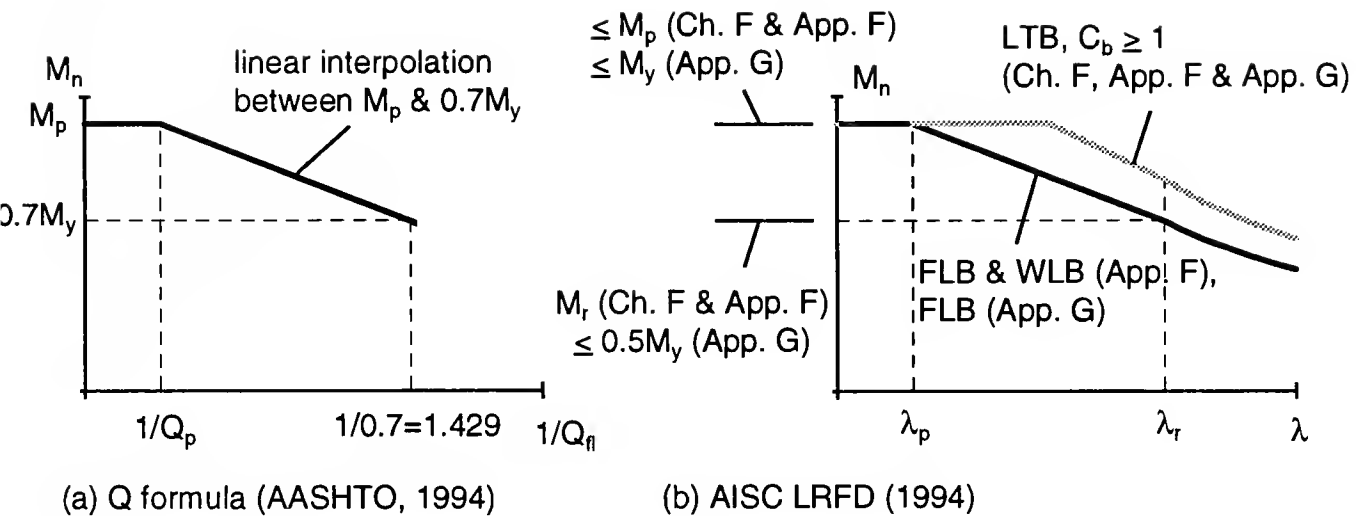
Figure 3.1. AASHTO LRFD (1994) and AISC LRFD (1993) approaches for calculation
            of flexural strength.
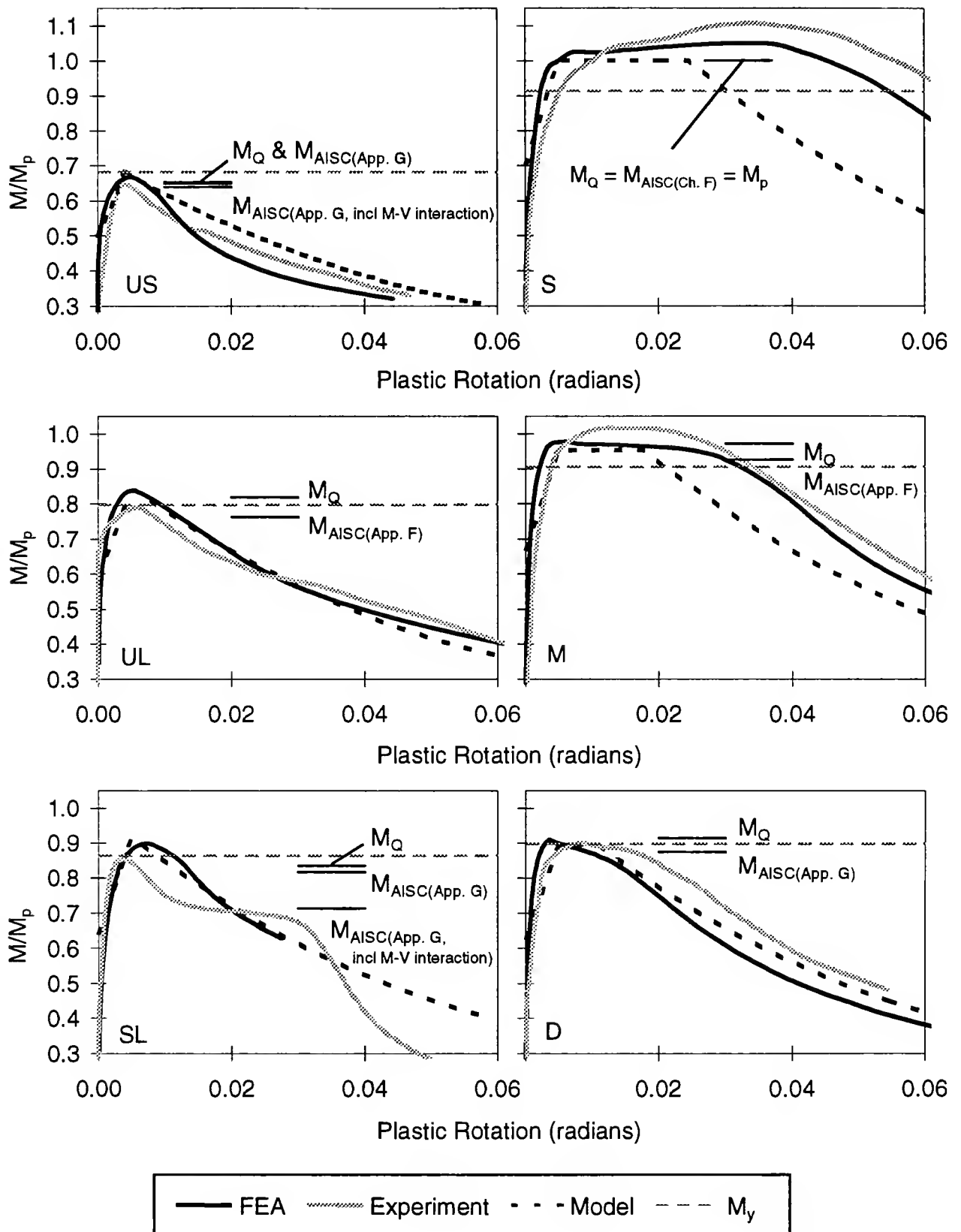
Figure 3.2. Experimental tests conducted by Schilling (1985) and Schilling and Morcos (1988).
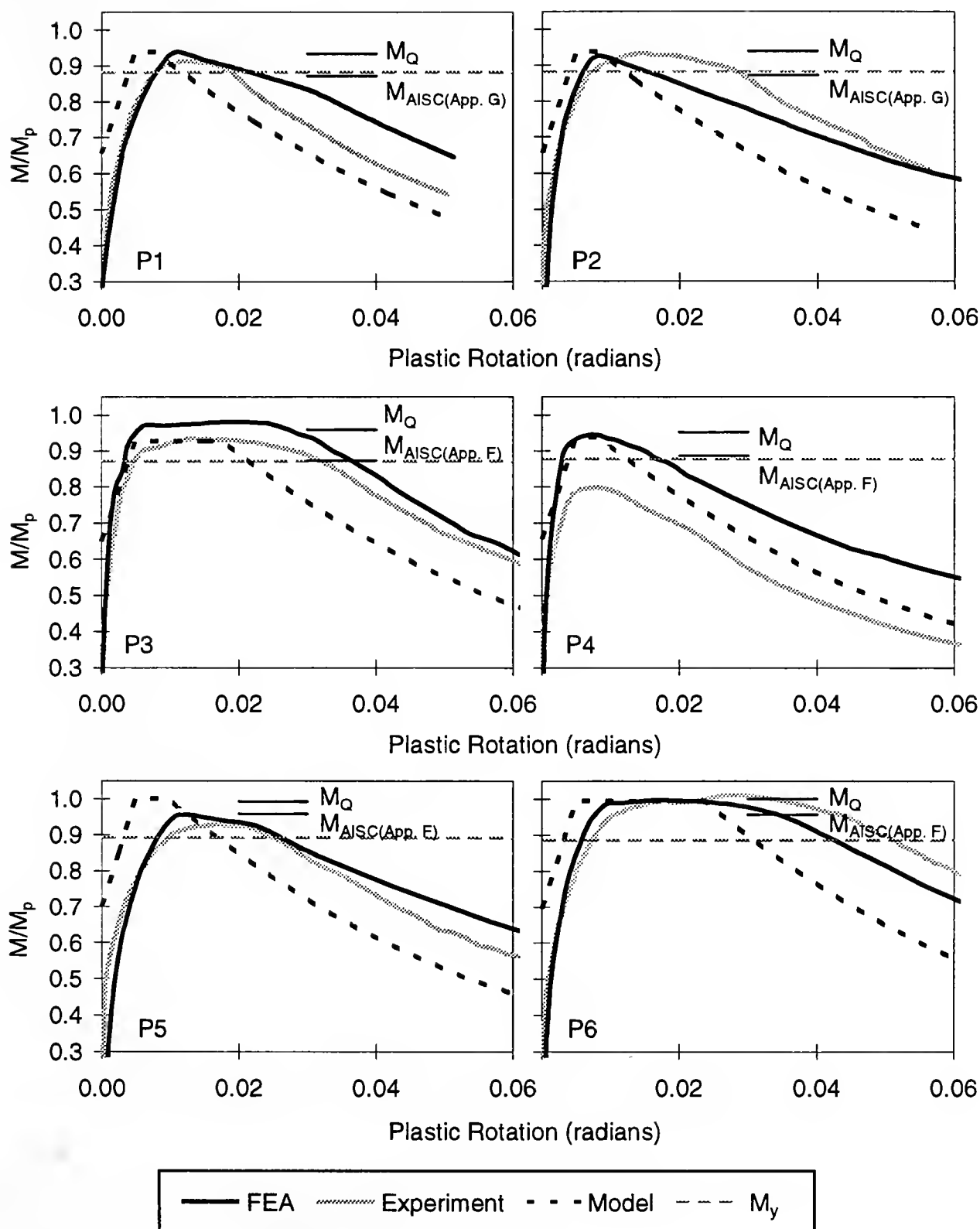
Figure 3.3. Experimental tests conducted by Barth (1996).
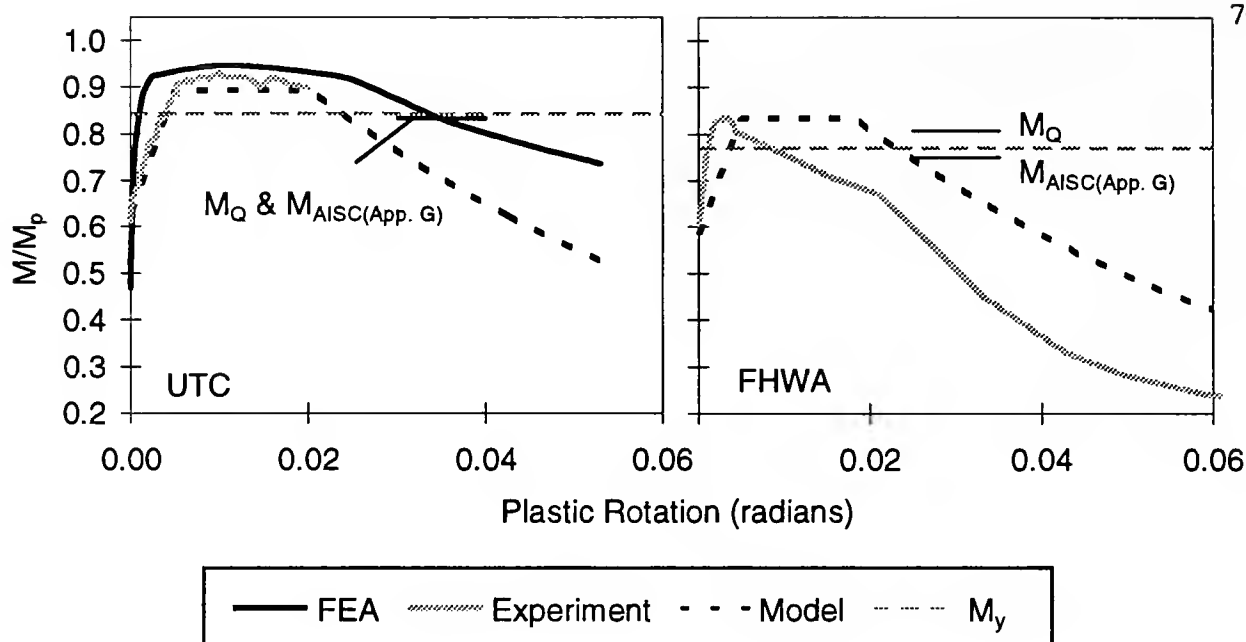
Figure 3.4. Composite girder tests conducted by Tansil (1991) and FHWA (1992).
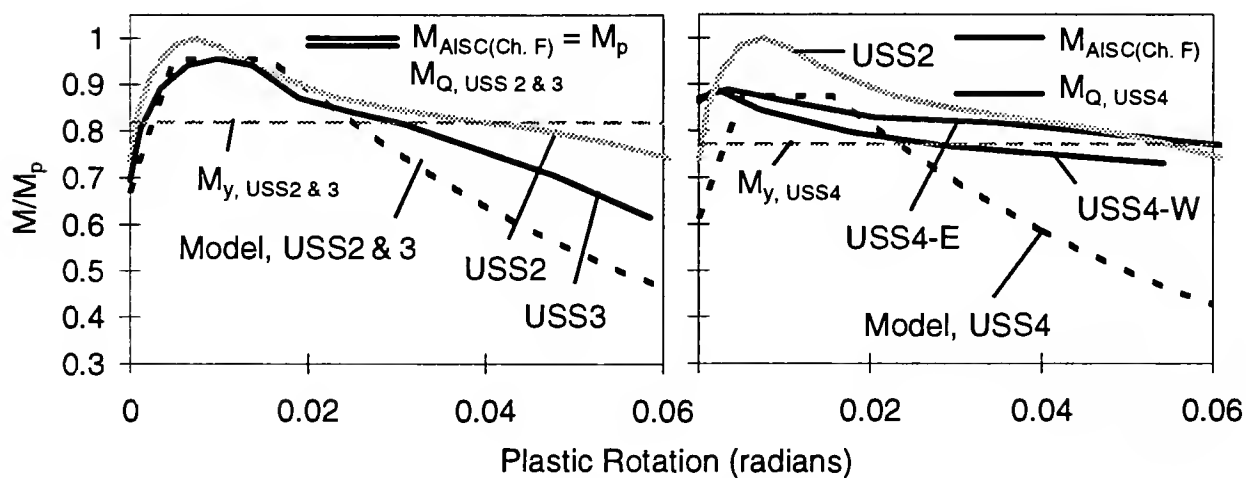
Figure 3.5. Experimental tests conducted by Grubb and Carskaddan (1979)
and by Carskaddan (1980).
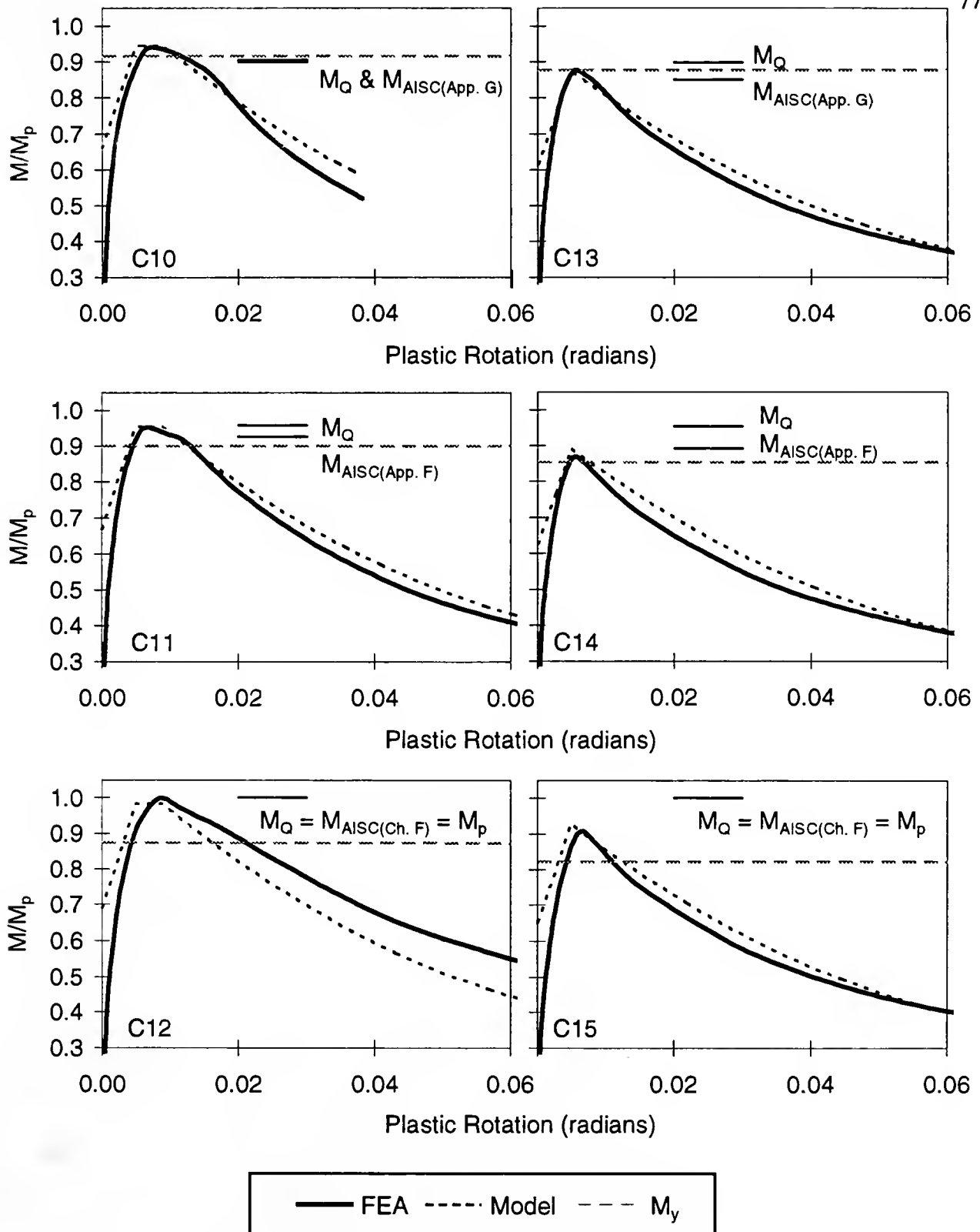
Figure 3.6. Finite element studies of symmetric girders with compact flanges.
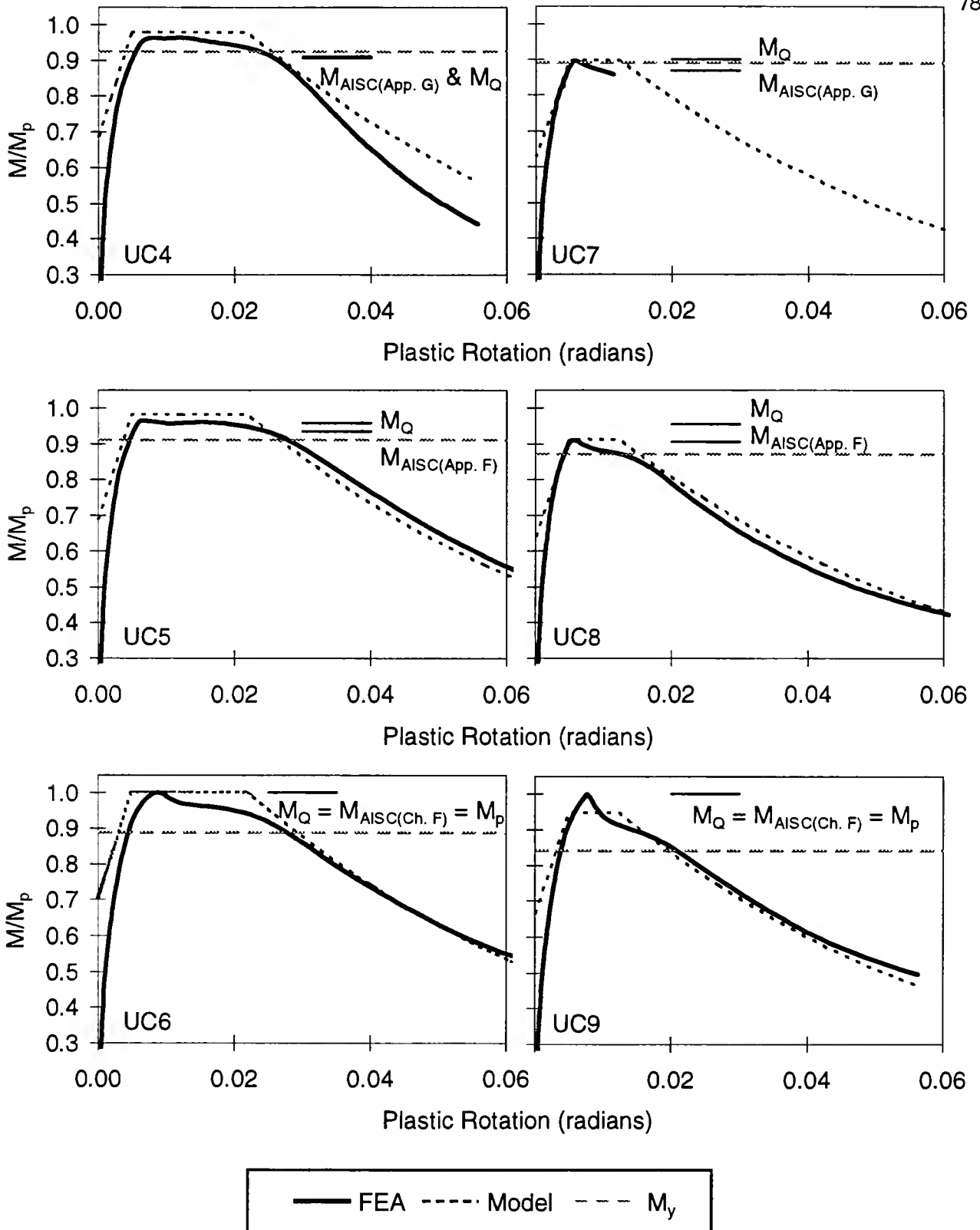
Figure 3.7. Finite element studies of symmetric girders with ultracompact flanges
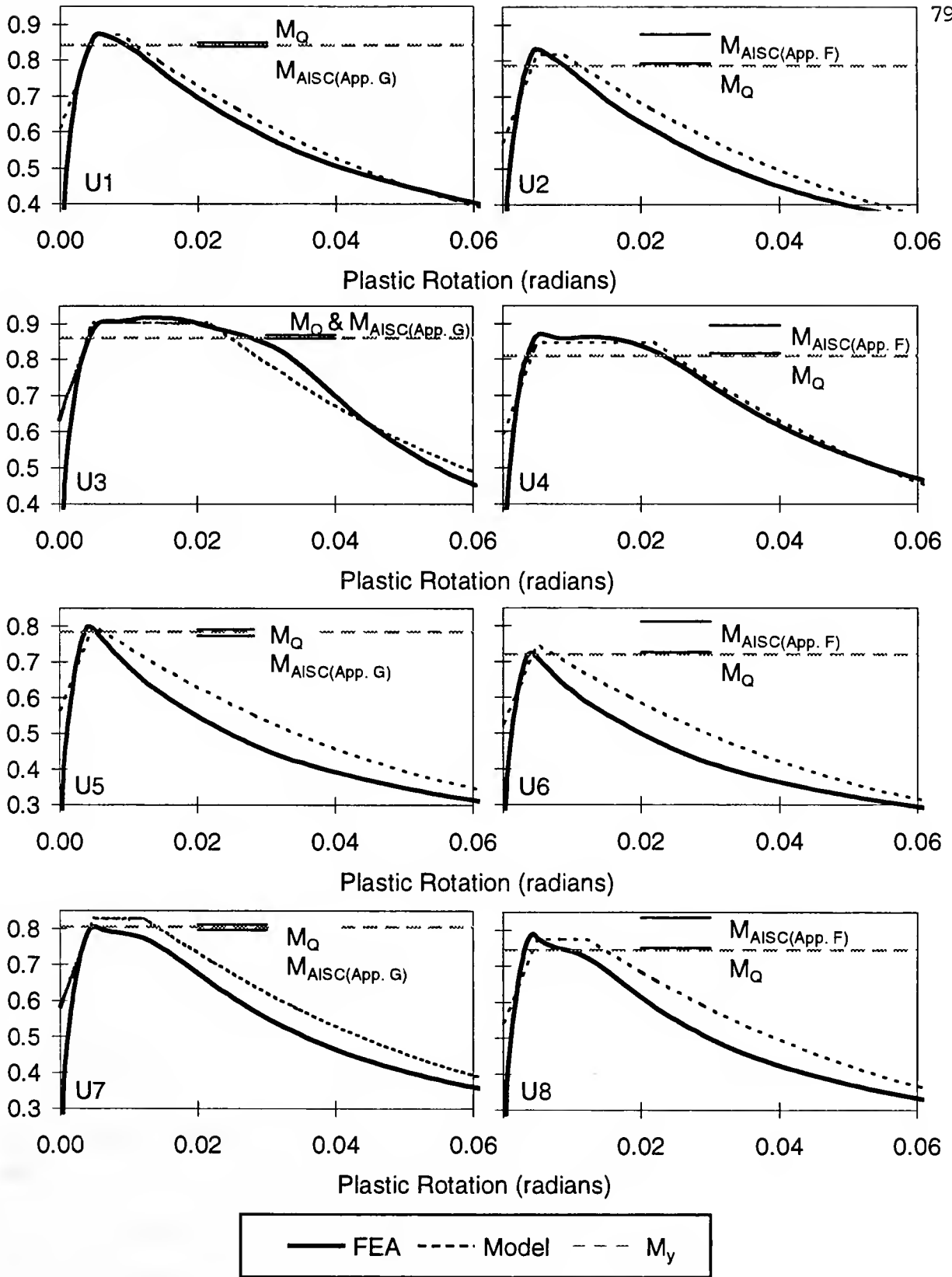
Figure 3.8. Finite element studies of unsymmetric girders.
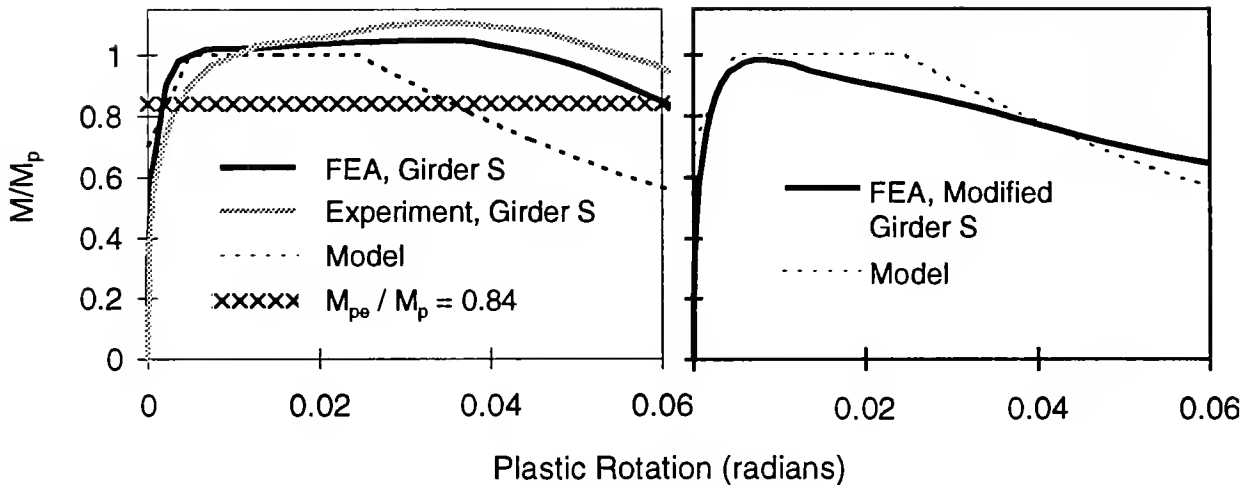
Figure 3.9. Upper-bound moment-rotation relations -- Schilling's girder S, and girder S unstiffened and with L_b set at the AASHTO limit.
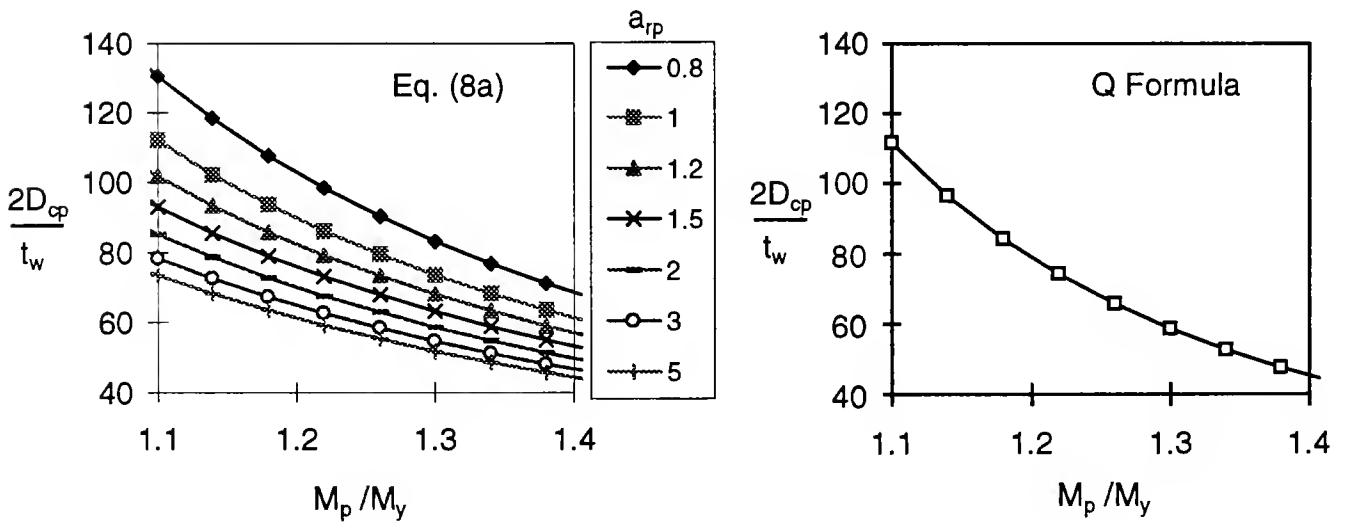
Figure 3.10. Web compactness limits as per Eq. (8a) and the Q formula.

CHAPTER 4

INELASTIC DESIGN OF STEEL I-GIRDER BRIDGES

During the last twenty years, numerous research studies have been conducted to gain a detailed understanding of the inelastic negative moment-rotation (M-θ_p) behavior of compact and noncompact-web I girders. In the current research, reasonably comprehensive finite element parametric studies have been completed, and simple design expressions have been developed that characterize this behavior (see Chapter 2). This M-θ_p model has been validated against experimental and finite element test results, and against American specification equations for I-girder moment capacities in Chapter 3. Based on parallel research, Schilling et al. (1996) have recently recommended improvements to the AASHTO inelastic LRFD provisions that account for the general performance of both compact and noncompact section members. These recommended inelastic design procedures are summarized in (Schilling 1997).

This chapter presents a detailed trial design of a three-span continuous composite plate-girder bridge using the approach proposed by Schilling (1997) along with the refined M-θ_p model suggested in Chapters 2 and 3 Various advantages, limitations and implications of the recommended procedures are observed based on this study. The bridge selected for the trial design is one in which the detailed elastic AASHTO LRFD calculations have already been published (AISI 1995). Since the format of many of the calculations is the same for both the elastic and recommended inelastic approaches, the AISI (1995) report is referenced for details that are the same for either approach. It is assumed that the reader is already familiar with the AASHTO elastic LRFD procedures. This chapter focuses on the inelastic design calculations, and on the differences between the elastic and inelastic designs and design procedures. One objective is to show that the additional calculations required for the inelastic design are relatively minor. Therefore, there is really no reason for bridge engineers not to take advantage of the recommended inelastic procedures to achieve potential economies in steel plate-girder bridge construction.

4.1 Overview of Elastic and Inelastic Designs

The specific bridge considered in this chapter is Example 3 of the *LRFD Design Examples of Steel Highway Bridges, SI Units* (AISI 1995). This is a tangent three-span continuous composite I girder bridge with spans of 43 000 mm – 53 000 mm – 43 000 mm. AASHTO M270M, Grade 345W (ASTM A709M, Grade 345W) uncoated weathering steel with $F_y = 345\ MPa$, a concrete deck with

$f'_c = 28\ MPa$ and a modular ratio of $n = 8$, and AASHTO M31M, Grade 400 (ASTM A615M, Grade 400) slab reinforcing steel are used. A typical cross-section of the bridge is illustrated in Fig. 4.1, and the framing plan of the elastic design (AISI 1995) is shown in Fig. 4.2a. The corresponding framing plan for the inelastic design presented in this chapter is detailed in Fig. 4.2b. These plans are identical with the exception that the cross frame spacing adjacent to the piers is shorter in the inelastic design to facilitate the development of controlled plastic rotations at the pier sections. The spacing between the other cross frames is made slightly longer in the inelastic design such that the total number of cross frames is the same in both designs.

The design calculations in both this chapter and in (AISI 1995) focus on the exterior girders. Figure 4.3a shows an elevation of the exterior girders obtained using the elastic LRFD procedures. These girders are slightly modified from the (AISI 1995) design example – a 30 mm thick bottom flange is detailed in the maximum positive moment region in Fig. 4.3a whereas the design developed in (AISI 1995) specifies a 38 mm thick bottom flange. In (AISI 1995), the size of this flange was controlled by the fatigue limit states check of the base metal at the connection plate weld to the bottom flange at 60 percent of the end-span length from the end support. As discussed later in this chapter, the calculation of the fatigue stress range at this location is modified to justify a reduced bottom flange size within this region in the current designs. Ratios of the calculated to the corresponding allowable design values are provided based on the modified stress range calculations as well as using the approach adopted in (AISI 1995), and the implications of the modified stress range calculations are discussed.

An elevation of the inelastic exterior girder design is shown in Fig. 4.3b. Key differences relative to the elastic design are:

- The girder cross-section is changed only at the bolted field splice locations.
- Only three plate thicknesses are used (14 mm, 20 mm and 30 mm) versus five plate thicknesses for the elastic design (14 mm, 20 mm, 25 mm, 30 mm and 45 mm).

This should lead to significant savings in fabrication costs (AISC Marketing 1994). Savings in the overall mass of structural steel are also achieved (the mass of structural steel is approximately 128 kg/m^2 of deck area for the inelastic design versus 133 kg/m^2 of deck area for the elastic example). However, the cost savings resulting from the reduction in the mass of structural steel are expected to be minor relative to the savings associated with the fabrication of the girder. A large percentage of the steel mass is within the web, which is the same size in both designs. Ten intermediate one-sided

transverse stiffeners are required within the full length of the exterior girders in addition to the cross-frame connection plates in both the elastic and inelastic designs.

4.2 Overview of Similarities and Differences Between the Inelastic and Elastic Design Calculations

The calculations for the above designs differ predominantly only in the following way. The elastic design does not permit any nominal yielding of the cross-sections over the piers (i.e., the elastic flange bending stresses are generally limited to values less than F_y). Conversely, the inelastic design involves the calculation of controlled inelastic rotations at the pier sections and the determination and consideration of the effects of the corresponding redistribution forces. The additional calculations required to determine the pier section inelastic rotations and redistribution forces are relatively minor, and can be handled easily with typical spreadsheet or mathematical manipulation software packages. These calculations are based on shakedown under repeated application of the moving design loads, and involve the direct use of ordinary elastic moment envelopes. No successive application of the design loadings, as specified in some of the prior AASHTO LRFD inelastic procedures, is required.

The inelastic design calculations do not impose any direct requirement on the pier section bending capacities. Instead, the pier sections are proportioned to provide an inelastic bending resistance that minimizes the section size in the maximum positive moment regions, within the constraints of changing the girder section only at the field splice locations and limiting the number of plate thicknesses required in the design. Furthermore, the pier sections are required to satisfy certain plate slenderness limits, and the cross frames adjacent to the pier sections are located based on inelastic bracing requirements, to ensure ductile behavior of the girders. Also, the web shear stresses are limited to *60* percent of the web capacity based on tension-field action within the unsupported lengths adjacent to the piers, such that potential moment and shear capacity interactions are avoided.

In the inelastic design, the permanent deflection of the girders is checked by limiting the bending stresses within the positive moment composite sections to $0.95F_y$ under SERVICE II conditions, including the effects of the inelastic pier rotations that would be achieved at the shakedown of the bridge under these loadings. Therefore, this check is the same as in the elastic design procedures except that the elastic approach also applies the above limit at the pier sections, and therefore does not require calculation of redistribution stresses. Furthermore, in addition to the above limit on the positive bending stresses, the inelastic pier rotations under SERVICE II conditions are limited in the inelastic design such that: (1) objectionable cross-section distortions will not occur within the steel

girder at the pier section, and (2) the reinforcing steel in the deck will remain elastic over the piers. For practical reasons to be discussed later, the designer may wish to restrict the amount of yielding in the positive moment regions under the STRENGTH loading conditions as well. The implications and significance of potential positive moment yielding under STRENGTH loadings are discussed within the presentation of the detailed calculations in the subsequent sections of the chapter.

All the loading conditions and associated design philosophies, STRENGTH I through STRENGTH V (for checking of adequate structural capacity under infrequent very heavy loadings), SERVICE II (for checking of permanent deflections under overload conditions), optional loading conditions for checking of live load deflections as outlined in AASHTO LRFD (1994) Articles 3.6.1.3.2 and 2.5.2.6.2, and the vehicular loading specified by AASHTO LRFD for checking of fatigue, are the same for both the elastic and inelastic designs. These loading conditions are summarized in (AISI 1995). The girder elastic section properties assumed for the inelastic design are the same as for the elastic LRFD procedures (AISI 1995) except as noted in the sections that follow. Also, the AASHTO live-load distribution and multiple-presence factors calculated for the elastic design in (AISI 1995) are used for the inelastic design.

Separate analyses were conducted to obtain the nominal moment and shear envelopes for the inelastic exterior girder design detailed in this chapter. The resulting graphs are shown in Fig. 4.4. The envelopes shown in (AISI 1995) were used for checking the modified elastic design.

4.3 Summary of Detailed Calculations

The results of the calculations for each of the primary limit states checks of the inelastic and modified elastic designs are summarized in Table 4.1. These results are presented in terms of a performance ratio, defined as the ratio of the calculated values to the corresponding allowable values. For the elastic design, Table 4.1 is parallel to a similar table in (AISI 1995). In the original elastic design (AISI 1995), the STRENGTH I checks controlled over the other STRENGTH limit states by a wide margin. Therefore, of the STRENGTH limit states, only STRENGTH I is considered here. All the other limit states checks for fatigue, live load deflection, permanent deflection, and constructability considered in (AISI 1995) are addressed in Table 4.1. The shaded entries in the table are ratios that are influenced by the redistribution forces calculated in the inelastic design.

As noted above, the inelastic design calculations differ from the elastic ones primarily in that one must determine the inelastic pier rotations and associated redistribution moments. These calculation procedures are addressed in the following subsections, followed by the consideration of specific limit

states checks. The discussion focuses on the specific inelastic design calculations and the differences with corresponding elastic procedures.

Pier Moment-Plastic Rotation Equations

It is generally accepted that the inelastic rotations and redistribution forces in continuous-span beams and girders can be approximated with sufficient accuracy by assuming that all yielding is concentrated at plastic hinges of zero length. For compact-section beams and girders, traditional plastic design procedures assume that the moment-rotation behavior at a plastic hinge is elastic-perfectly plastic. That is, the cross-section behavior is assumed to be fully elastic until the plastic moment capacity (M_p) is reached, after which the member behaves as if a pin were inserted at the hinge location for further increases in the loads. However, this assumption is not sufficient for noncompact beams and girders, since these types of members are not able to sustain moments greater than or equal to M_p over the range of plastic hinge rotations that may be required at maximum load or overload levels. Furthermore, in the current AASHTO Autostress type procedures, it is considered desirable to account for potential inelastic rotations that may occur over the supports prior to reaching the maximum pier section capacities.

In this chapter, the M-θ_p relationships developed in Chapter 2 are adopted to characterize the behavior of the pier sections for the trial inelastic design. In the use of this model, it should be noted that M_y is computed as the yield moment of the pier cross-section, taken as the sum of the moments due to the factored loads at the applicable limit state, applied separately to the steel, long-term composite, and short-term composite sections to cause first yield in either steel flange (see article A6.2 of (AASHTO 1994)). For a slab that is not post-tensioned within the negative moment regions, such as in the trial inelastic design, the long- and short-term composite sections are both taken as the steel member plus the reinforcing steel within the AASHTO effective width of the slab. That is, the slab is assumed to be fully cracked for the composite loadings in calculating M_y at the pier sections.

Extensive comparisons of the above M-θ_p model with available experimental and finite element data as well as with current American specification strength equations are made in Chapter 3. The proposed M-θ_p model gives conservative to excellent predictions of the experimental and finite element data within the limits defined for its application. It provides the same advantages as the AASHTO LRFD (1994) Q formula in that it predicts maximum strengths that are generally larger than M_y, yet it is simpler to apply and provides slightly better correlation with the experimental and finite element test data. Substantial economy can be realized, particularly for composite I girders in

negative bending, by recognizing that the flexural strength (within the above limits on the design parameters) can be substantially larger than the nominal moment at first yielding of one of the flanges. The suggested M-θ_p model tends to provide a conservative characterization of the pier-section behavior particularly for cases in which the lateral brace spacing is smaller than that required by Eq. (2.2a), and for members in which the web slenderness is significantly smaller than the

AASHTO web compactness limit (i.e., $\dfrac{2D_{cp}}{t_w} \leq 3.76\sqrt{\dfrac{E}{F_{yc}}}$). Also, the effect of torsional restraint

provided by the bridge deck to top flange of the girder is neglected within the development of the suggested M-θ_p model. This restraint can significantly enhance the pier section M-θ_p behavior in certain cases.

Calculation of Redistribution Moments

After the M-θ_p behavior is established for the pier sections as suggested in the previous section, then if it is assumed that any yielding in the positive moment regions is negligible, the inelastic pier rotations and redistribution moments produced by repeated applications of a set of design live loads moving across the bridge may be determined as follows. The effects of positive moment yielding under maximum strength loading conditions are addressed later in the consideration of the STRENGTH I limit states checks in positive bending. The calculations start with the maximum elastic pier moments associated with the design loadings, as expressed by ordinary elastic moment envelopes. This is illustrated as step (1) in Fig. 4.5 for a generic three-span girder. The maximum elastic pier moments are denoted by the symbols M_{1e} and M_{2e} in the figure. If these elastic pier moments are smaller than the minimum moments required to induce plastic rotations at the piers (assumed equal to $0.7M_n$ in Fig. 2.15), the girder behavior is fully elastic under all the loading conditions (assuming that no significant yielding occurs at other positions within the girders), and the necessary calculations are completed. However, if the elastic pier moments are large enough to induce plastic rotations at a given pier section, an angular discontinuity will be formed at this section. In order to form this permanent angular discontinuity, the plastic hinge must apply equal and opposite moments to the idealized elastic girder on each side of the pier. These moments produce the associated redistribution moments within the girder spans shown in steps (2) and (3) for piers 1 and 2 (Fig. 4.5). The term m_{1p1} under step (2) is the moment required to develop a unit permanent angular discontinuity (i.e., plastic rotation) at pier 1, and the term m_{2p1} is the moment at pier 2 corresponding to the unit plastic rotation at pier 1. These coefficients can be determined by artificially breaking the

continuity of the girder over pier 1 and applying unit equal and opposite moments to the girder cross-sections on each side of the pier. The values m_{1p1} and m_{1p2} are then obtained by dividing the corresponding pier moments by the angular discontinuity over pier 1 caused by the above applied moments. The redistribution moments at piers 1 and 2, associated with a specific inelastic rotation over pier 1 (θ_{p1}), are equal to $m_{1p1}\theta_{p1}$ and $m_{2p1}\theta_{p1}$ respectively. A similar set of pier redistribution moments, $m_{1p2}\theta_{p2}$ and $m_{2p2}\theta_{p2}$, is produced within the girder due to the inelastic rotation over pier 2 (θ_{p2}). The total redistribution moments are obtained by summing the moments associated with the plastic rotations at each of the pier locations (see step (4) in Fig. 4.5). It is interesting to note that these moments must vary linearly between the piers, since the assumption of zero vertical displacements at these points is required to "lock in" the redistribution moments. The total redistribution moments are added to moments from the elastic envelopes at any location along the length of the girder to obtain the total internal maximum (or minimum) moments that would be developed after the girder has shaken down to a completely elastic response under the design loadings.

The information shown in Fig. 4.5 alone is not sufficient to calculate the redistribution moments. The pier plastic rotations θ_{p1} and θ_{p2} also must be determined. Given the total internal pier moments, these rotations can be obtained by considering the pier section M-θ_p relationships. Since the total pier moments in Fig. 4.5 are equal to $(M_{1e} + m_{1p1}\theta_{p1} + m_{1p2}\theta_{p2})$ and $(M_{2e} + m_{2p1}\theta_{p1} + m_{2p2}\theta_{p2})$ (see step 5), a unique solution for the pier inelastic rotations and redistribution moments is obtained by equating these expressions to the moments obtained from the M-θ_p relationships at each of the piers (i.e., see Fig. 2.15). The resulting equations can be solved simultaneously to determine each of the pier plastic rotations associated with shakedown under the specified design loading conditions. However in the case of a three-span tangent continuous bridge girder with equal end spans, all the above quantities are the same at piers 1 and 2; therefore, only one set of equations needs to be solved to determine the inelastic pier rotations. Specific forms of these calculations are referred to as the "unified autostress method" by Schilling (1993) and as the "residual deformation method" by Dishongh and Galambos (1992). Detailed discussions of the shakedown behavior and analysis of bridge girders are provided in (Schilling 1997) and (Schilling et al. 1996).

Analysis Results for the Trial Inelastic Design

For the trial design considered in this chapter, the solution of the above single equation for the STRENGTH I limit state can be illustrated most simply in the form of a traditional beam-line plot, as

shown in Fig. 4.6. Several specific M-θ_p curves are shown in this figure. The functional form of these curves is that shown in Fig. 4.6. The middle M-θ_p curve in Fig. 4.6 (denoted by the dashed black lines) is the nominal curve expressed by Eqs. (2.9) and (2.10) along with the equations shown in Fig. 2.15. For the design shown in Fig. 4.3b, the pier section plastic moment capacity M_p (based on the steel section plus the reinforcing steel within the slab effective width) is $1.73 \cdot 10^{10}$ N·mm, the yield moment M_y based on the STRENGTH I loading conditions is $1.20 \cdot 10^{10}$ N·mm, D_{cp}/D is 0.47, $2D_{cp}/t_w$ is 142, a_{rp} is 1.69, and M_n is $1.36 \cdot 10^{10}$ N·mm. Also, D/b_{fc} is 3.82 and $b_{fc}/2t_{fc}$ is 9.17. These parameters are input to Eq. (2.10) to produce a θ_{RL} of 0.0064.

The top M-θ_p curve in Fig. 4.6 (denoted by the solid black line) corresponds to the nominal response with the moments scaled by a design ϕ factor of 1.1. Schilling (1997) and Schilling et al. (1996) recommend $\phi = 1.1$ for checking of the STRENGTH limit states. This is based on the fact that the design assessment is based on static shakedown of the girder under repeated application of the infrequent, very heavy, STRENGTH load combinations. The shakedown loading is generally smaller than the hypothetical static loading that would be required to fail the bridge in a single extreme event. Also, due to the dynamic nature of yielding, the design live loads would have to be applied to the bridge and held constant in magnitude and position for several minutes to fully stabilize the internal forces and deflections for each possible position of the live load within the inelastic range. Therefore, only a small amount of the yielding theoretically predicted for a given design loading will occur during a single passage of that loading across the bridge (Schilling 1997; Schilling et al 1996). Furthermore, as noted previously, the proposed nominal M-θ_p tends to be conservative due to torsional restraint provided to the top flange of the steel girder by the bridge deck, and as discussed below, the elastic girder stiffnesses recommended for the inelastic design calculations are expected to overpredict the plastic rotations and redistribution moments that would be generated in the actual bridge. The bottom M-θ_p curve in Fig. 4.6 is based on the use of M_y for the capacity of the section over the pier rather than the strengths predicted based on Eq. (2.9). The inelastic design checks are performed for the trial design using each of the above three M-θ_p curves to illustrate the significance of the assumptions regarding the pier moment capacities. The authors suggest that the analysis results based on the top M-θ_p curve shown in Fig. 4.6 (i.e., with $\phi = 1.1$) are the most appropriate for checking the adequacy of the inelastic design for STRENGTH.

Since the coefficients from Fig. 4.5 may be written as $M_{1e} = M_{2e} = M_e$, $\theta_{p1} = \theta_{p2} = \theta_p$, $m_{1p1} = m_{2p2}$ and $m_{1p2} = m_{2p1}$ for the trial inelastic design, the equations for each of the total pier moments in step (5) of this figure may be written as

$$M_{pier} = [M_e + (m_{1p1} + m_{1p2}) \; \theta_p] \qquad\qquad (4.1)$$

The two thin grey lines in Fig. 4.6, which may be referred to as beam lines for the trial design girder, represent this equation for two different assumed elastic girder stiffnesses. The lower beam line is based on the use of the short-term composite section properties, including the contribution from the concrete slab throughout the positive and negative moment regions. This assumption is recommended for the calculation of the elastic live load moment and shear envelopes in the current AASHTO LRFD Specifications (1994). The intersection of this beam line with the vertical axis of the plot gives the elastic pier moment M_e (i.e., zero θ_p). Conversely, the intersection of this beam line with the horizontal axis gives an estimate of the plastic rotation that would be required for zero total moment at the pier sections. This rotation is determined by setting the total pier moment in Eq. (4.1) to zero. It is interesting that the maximum pier rotations for the lower beam line shown in the figure are somewhat smaller than might generally be expected. It can be argued that the use of the uncracked composite section throughout the entire bridge length would likely provide an upper bound for the possible elastic girder stiffnesses. Conversely, the use of only the steel section plus the longitudinal slab reinforcing steel between the field splices would likely provide a lower bound on the girder stiffness properties associated with the inelastic pier rotations. The upper beam line in Fig. 4.6 is based on this assumption. The authors prefer the upper beam line since it should provide a conservative estimate of the pier plastic rotations and redistribution moments. However, they suggest that the use of the all-steel girder sections for noncomposite dead load, the long-term uncracked composite sections throughout the length of the bridge for composite dead loads, and the short-term uncracked composite sections throughout the length of the bridge for live loads are sufficient for determining the maximum elastic factored moments. This leads to some additional conservatism in the prediction of the pier plastic rotations and redistribution moments, since if the cracked composite section is used within the hogging moment regions for the elastic moment calculations, the STRENGTH I elastic pier moments will be reduced slightly from the value shown in Fig. 4.6 (the revised beam line curve would be parallel to the top beam line shown in the figure, but would intersect the vertical and horizontal axes at a smaller values of M/M_y and θ_p).

The results shown in Fig. 4.6 are based on the STRENGTH I loading conditions. Similar solutions for the inelastic pier rotations and redistribution moments can be obtained for the SERVICE

II conditions, which represent a slightly larger loading than the maximum expected during the life of the bridge. The AASHTO LRFD load factor on the live load model for SERVICE II is 1.30 whereas the maximum live load expected during the life of the bridge is about 25 percent above the specified unfactored loadings (Nowak 1995); this observation applies specifically only to simple spans. A ϕ factor of *1.0* on the pier M-θ_p relationships is considered most appropriate for assessing the design behavior under these loading conditions, since $\phi=1.0$ is commonly used in the AASHTO LRFD Specifications (1994) for checking of service limit states (Schilling 1997; Schilling et al. 1996).

The results for the inelastic pier rotations (θ_p), the normalized pier redistribution moments (M_r/M_e), and the associated normalized total pier moments (M_{pier}/M_e) are summarized in Table 4.2 based on (1) the nominal M-θ_p curve and SERVICE II conditions, and (2) the three different M-θ_p curves shown in Fig. 4.6 and STRENGTH I conditions. The girder stiffnesses based on the cracked section (i.e., the steel beam plus the longitudinal reinforcing steel) in the pier regions between the field splices, and the uncracked short-term composite section properties in the positive bending regions, are used in determining the coefficients m_{1p1} and m_{2p1} to obtain these results. It is interesting that under the SERVICE II conditions, which are used to check permanent deflections, the beam line intersects the pier M-θ_p curve within the pre-peak range of the response, and the pier inelastic rotations are quite small. However, under the STRENGTH I conditions, the beam line intersects the pier M-θ_p curves within the post-peak range of the response. As a result, the inelastic pier rotations and redistribution moments are somewhat sensitive to the assumed M-θ_p behavior. Also, these results are somewhat sensitive to the elastic pier moments determined from the ordinary moment envelopes. For instance, if the moment envelopes from (AISI 1995) are used as an approximation for checking the inelastic design, the inelastic rotations and redistribution moments are substantially increased since the elastic pier moments are somewhat larger due to the large pier sections in the elastic design.

The various flexural limit states checks for the STRENGTH I loading conditions, based on the elastic design envelopes plus the above redistribution forces, are considered in the next two sections. Table 4.3 presents the performance ratios that depend on the calculated redistribution moments for the three different M-θ_p idealizations used in checking these limit states. This is followed by a discussion of the SERVICE (permanent and nominal live load deflection) and FATIGUE limit states checks.

STRENGTH I Limit States Checks in Negative Flexure

The inelastic limit states checks for the pier sections include only the "slenderness" checks to ensure adequate ductility, as outlined in the earlier discussions:

- $\dfrac{2D_{cp}}{t_w} \le 6.77\sqrt{\dfrac{E}{F_{yc}}}$ (web plate slenderness),

- $\dfrac{b_{fc}}{2t_{fc}} \le 0.4\sqrt{\dfrac{E}{F_{yc}}}$ (compression flange plate slenderness), and

- $\dfrac{L_b}{r_y} \le \left[0.124 - 0.0759\dfrac{M_{min}}{M_{max}}\right]\left(\dfrac{E}{F_{yc}}\right)$ (lateral slenderness of the compression flange).

The performance ratios for these checks are summarized in Table 4.1. No direct section capacity calculations are required within the negative moment regions, unless there is a transition to a smaller cross-section than that over the piers. These checks are simpler than the elastic design checks for the negative moment region. The negative bending performance ratios for the modified elastic girder, also summarized in Table 4.1, are the same as in (AISI 1995). The reader is referred to the AISI report for discussion of the elastic design calculations.

STRENGTH I Limit States Checks in Positive Flexure

For composite beams and girders in positive bending, the AASHTO LRFD (1994) Specifications give the bending strength M_n as the lesser of the plastic moment capacity of the composite section (M_p) or the capacity associated with reaching the crushing strain at the top of the concrete slab. These checks are modified slightly and expressed in greater detail in the AASHTO LRFD 1996 Interims. For continuous-span girders, the positive-moment bending capacities are further limited to a maximum of $1.3 R_h M_y$ if the pier sections are noncompact (where R_h is the hybrid girder factor, equal to 1.0 if the web and flange plates have the same F_y), unless a detailed analysis is performed that accounts for the moments at the piers that are "concurrent with the maximum positive bending stresses." These provisions are intended to limit the amount of yielding in the positive moment regions, and thus limit the bending moments that would be redistributed to the adjacent noncompact pier sections due to the positive moment yielding. A ϕ factor of 1.0 is employed in all the above calculations. In (AISI 1995), the simpler of the above procedures (referred to as Method A in Section 6.10.5.2.2a of the AASHTO LRFD Specifications (1994)) is employed. The resulting positive bending strengths are $1.3M_y$ for the modified elastic design (Fig. 4.3a), although the positive-moment

composite sections are theoretically able to develop *97* percent of their plastic moment capacity (M_p = *1.49M$_y$*) prior to crushing of the concrete at the top of the slab.

The above elastic design limit of *1.3M$_y$* might also be applied to check the positive moment regions of the inelastic design. However, it is prudent to consider the effects of positive moment yielding more rigorously before adopting this approximation. The positive bending M-θ_p behavior obtained from a composite-girder experimental test conducted by Vasseghi and Frank (1987) is shown in Fig. 4.7 along with the M-θ_p response for the trial design predicted by a positive moment M-θ_p model suggested by Galambos et al. (1993) and Schilling et al. (1996). The M-θ_p model illustrated in Fig. 4.7 is considered to be a conservative linearization of the actual moment rotation results from many tests of composite girders in positive bending (Galambos et al. 1993). In the development of the linearized M-θ_p curve, it is assumed that positive moment yielding can be neglected for bending moments smaller than the nominal initial yield moment of the composite sections M_y, which should be acceptable as a reasonable approximation. However, the plastic rotations required to develop the moment capacity of *1.3M$_y$* are quite large both for the specific experimental curve obtained by Vasseghi and Frank (1987) and for the linearized model.

It is informative to consider the effect of a hypothetical shakedown θ_p of *0.002* radians in positive bending within the center span of the trial inelastic design. This is a rough estimate of the actual plastic rotations that might be expected within this region if the positive girder moments were limited to the yield moment M_y. The effect of this plastic rotation on the girder behavior can be obtained by breaking the continuity of the girder at the center of the middle span, and applying equal and opposite moments to each side of this hinge to induce a permanent angle change of *0.002* radians. The execution of and results from this analysis are summarized in Fig. 4.8. The elastic pier moments shown in this figure can be added to the pier moments $M_{1e} = M_{2e} = M_e$ in Figs. 4.5 and 4.6 to account for the effects of the above plastic rotations in positive bending. This increase in the elastic pier moments shifts the beam line in Fig. 4.6 upward, but does not change the slope of this line (Carskaddan et al. 1984). If the elastic girder stiffnesses employed in the calculation of the moment envelopes (i.e., the short-term composite uncracked properties throughout the length of the girder) are used for these calculations, the intersection of the beam line with the vertical axis in Fig. 4.6 is raised from M_e/M_y = *1.43* to M_e/M_y = *1.50*. If the plastic rotations in positive bending within the center span are increased to *0.004* radians, the elastic pier moments are increased to M_e/M_y = *1.58*. These increases in M_e/M_y produce a larger θ_p at the intersection of the beam lines with the pier M-θ_p curves

in Fig. 4.6. This in turn produces larger redistribution moments over the piers, and larger positive bending moments within hogging moment regions of the girders.

Physically, the above calculations show that if the pier sections have already experienced significant plastic rotations, the capacity of the bridge is exhausted very rapidly once significant plastic rotations start to occur within the positive bending regions. Therefore, as a practical matter, the authors suggest that it is reasonable to limit the elastic moments in the hogging-moment regions to values close to M_y. The procedure of Article A6.2 of the LRFD Specifications should be applied for the calculation of this yield moment, i.e., the all-steel, short-term composite, and long-term composite section properties are employed as appropriate for the corresponding loadings. Also, as detailed in Section 6.10.11.2.4c of the LRFD Specifications (AASHTO 1994), the long-term composite section properties should be used for calculation of the stresses due to the redistribution moments. The use of the uncracked composite properties throughout the entire bridge length for calculation of the elastic moments along with the use of the long-term composite properties in positive bending for calculation of the hogging-moment stresses due to the redistribution moments is conservative. Also, the use of the fully-cracked section over the piers in calculating the pier plastic rotations and redistribution moments (Fig. 4.6) is conservative. In view of the conservatism of these calculations, and also considering the dynamic nature of yielding as discussed previously, an appropriate limit for the maximum moments in the positive bending regions under the STRENGTH loading conditions and shakedown might be $1.1M_y \leq M_n$. This value is used for all the positive bending STRENGTH I checks shown in Table 4.1 (i.e., for the elastic as well as the inelastic design performance ratios). This limit on the positive bending capacity might be refined based on further research, but it is viewed by the authors as a safe and practical limit based on the research that has been performed to date. The positive moment region within the center span is marginally under-designed based on this assessment and using a ϕ factor of 1.1 on the pier-section M-θ_p curves. Table 4.3 shows that the more conservative pier M-θ_p idealizations result in a substantial violation of the above positive bending capacity limit.

The performance ratios corresponding to the 1996 LRFD Interim checks for ductility in positive bending are also shown in Table 4.1. The format of these checks is the same as that shown in (AISI 1995), and the elastic and inelastic design ratios are the same to within three significant digits.

Service Limit States Checks

As explained earlier, the elastic stresses in positive bending are limited to $0.95F_y$ in the trial design under SERVICE II conditions to limit the transverse deflections of the girders to acceptable values under loads that are slightly larger than the maximum that would be expected during the life of the bridge. The pier plastic rotations reported in Table 4.2 are only 0.0035 radians, and the maximum pier moments are only $1.02M_y$ for these checks, which are based on the nominal M-θ_p curves for the pier sections with $\phi = 1$. The performance ratio for the maximum girder stresses in positive bending (located at the middle of the center span) is only 0.794 (see Table 4.1). It should be noted that the permanent deflections due to the above pier-section plastic rotations could be compensated for within an initial camber of the girders. However, since the deflections due to these pier rotations are relatively inconsequential, and since the above predicted pier rotations are expected to be larger than the pier rotations that would be achieved in the physical bridge girders, the inelastic pier rotations can be neglected in any camber calculations.

As a general rule the pier plastic rotations under SERVICE II conditions should be limited to the value θ_{RL} at which the pier sections begin to shed moment (see Fig. 2.15). This is because the post-peak M-θ_p behavior is generally associated with significant inelastic distortions of the girder. In most cases, the moments will be in the pre-peak range of the pier M-θ_p curves under these loading conditions, and thus the satisfaction of this rule usually should not present any problems. Also, the stresses in the reinforcing steel over the pier section should be limited to F_y under SERVICE II conditions, to limit the cracking in the composite slab under negative bending. This rule is also seldom violated, and thus is not required in the current AASHTO LRFD (1994) provisions. The performance ratios for the above two checks are shown in Table 4.1. Furthermore, the results of the optional AASHTO nominal live load deflection checks, which are the same format as detailed in (AISI 1995), are shown in the table. It can be observed that the trial inelastic design easily satisfies all of the above service limit state checks.

Fatigue and Fracture Limit States Checks

The AASHTO LRFD Specifications (1994) generally require that the contribution of the composite concrete deck should be neglected when calculating stresses associated with negative flexure. Conversely, the Specifications state that the stresses associated with transient-loading positive bending moments are to be calculated using the short-term composite section. Therefore, in the example three-span continuous elastic design developed in (AISI 1995), the stress ranges due to

the fatigue loading are calculated using the first of these assumptions for negative fatigue-load moments and the second for positive fatigue-load moments. The above stiffness assumptions are expected to be adequate and appropriate in many cases. However, in the example design (AISI 1995), the flange sizes within the maximum hogging-moment region of the end spans were controlled by the fatigue check for the base metal at the bottom-flange connection-plate weld at the cross-frame located at *0.6* of the span from the end bearing. The maximum nominal tension stress in the concrete at these locations (due to negative fatigue-load moment acting on the short-term composite section minus the positive composite dead-load moment acting on the long-term composite section) is only *0.409* MPa. The maximum nominal tension stress due to the fatigue-load moment alone is only *0.555* MPa. These stresses are far below an estimated concrete cracking stress of $0.5\sqrt{f_c'}$ (MPa) = *2.64* MPa. In light of these nominal stress calculations, and considering that field tests of composite continuous bridges have shown that there is considerable composite action in negative bending regions (Baldwin et al. 1978; Roeder and Eltvik 1985), the authors suggest that it is appropriate to calculate the negative bending stresses due to the fatigue loading at the above critical location based on the short-term composite section. If this approach is accepted, the tension flange of the elastic design can be reduced from *38* to *30* mm. thickness. The performance ratios for the fatigue checks conducted in this manner are shown in Table 4.1 along with the ratios of the nominal maximum tension stress in the concrete deck at the critical locations to the theoretical cracking stress. The performance ratios for the fatigue checks based on the current AASHTO provisions are shown within the parentheses () for comparison purposes.

In checking the fatigue and fracture limit states within the negative moment region over the piers, it is found that the net stresses in the concrete slab due to the negative composite dead load plus the maximum *positive* fatigue-load moments over the piers are still tensile. Therefore, the performance ratios listed in Table 4.1 for the fatigue checks at the interior pier sections are based on the cracked composite section (steel plus rebar) for all the stress calculations. This is slightly different than the approach in (AISI 1995), which used the short-term composite section properties including the concrete for calculation of the stresses due to the positive fatigue-load moments over the piers. The performance ratios for the interior pier section fatigue checks are relatively low, and also the positive fatigue-load moments over the piers are relatively small. Therefore, this change in the calculations for the fatigue stress-ranges over the piers has no effect on the designs.

Other Limit States Checks

The STRENGTH I shear capacity checks and the other FATIGUE checks of the girder web plate are essentially the same as in the elastic design. The reader is referred to (AISI 1995) for details of these calculation procedures. The only differences in the inelastic design are that the applied shear forces are limited to *60* percent of the web shear capacity within the unsupported segments adjacent to the piers, such that potential flexure and shear capacity interactions are avoided. As noted previously, this provision did not change the required number of transverse stiffeners between the elastic and inelastic designs. The inelastic redistribution shears should not be included in checking the web strength at the end supports, since these reduce the total applied shear at these locations.

The CONSTRUCTABILITY checks are the same for the elastic and inelastic designs. The performance ratios for the *elastic* flexural capacities over the pier under the construction loading conditions are listed in Table 4.1 although these ratios are not critical and were not listed in (AISI 1995). These values are listed here to emphasize that the pier section is designed to remain elastic under the construction loading conditions. The deck-casting sequence detailed in (AISI 1995) was assumed in checking the modified elastic and inelastic designs.

4.4 Key Observations and Recommendations

Key points that can be drawn from the above discussions are:

- The inelastic I-girder design presented in this chapter is cleaner than the corresponding elastic design, and should provide significant savings in fabrication costs.
- The inelastic design calculations do not differ substantially from the elastic design checks. The inelastic design of the interior pier sections is arguably simpler. The calculation of the interior pier section plastic rotations and redistribution moments starts with the pier moments obtained from ordinary elastic envelopes, and can be performed using ordinary commercial spreadsheet or mathematical manipulation packages. The resulting inelastic redistribution moments are simply added to the factored elastic moments for the girder design.

It is expected that the inelastic pier rotations would vary significantly over the wide range of potential beam and girder bridge designs. Parameters that can have a major influence on these inelastic rotations include: (1) the ratio of the elastic pier moments to the pier-section moment capacities, M_e/M_n, and (2) the pier section load-shedding characteristics, which are characterized predominantly by the term θ_{RL} in the suggested M-θ_p. Schilling et al. (1996) and Schilling (1997) suggest a simplified procedure for calculating redistribution moments that is based on the assumption

of elastic-perfectly plastic pier section behavior at an effective plastic moment M_{pe}. The effective plastic moment is determined as the ordinate on the "actual" cross-section $M\text{-}\theta_p$ curve obtained at a maximum rotation expected in design practice. Plastic rotations of *0.03* and *0.009* radians are suggested as upper-bound values that would be associated with the STRENGTH and SERVICE II loading conditions respectively. With this approach, the pier redistribution moments are calculated as $|\phi M_e| - |M_{pe}|$. For the trial inelastic design presented in this chapter, the pier plastic rotations are substantially smaller than the above upper-bound values, and therefore $|\phi M_e| - |M_{pe}|$ would be substantially larger than the redistribution moments that have been estimated directly from the $M\text{-}\theta_p$ curves. Since the calculations shown in Fig. 4.6 can be easily automated using generic commercial software, the authors suggest that the direct use of the pier-section $M\text{-}\theta_p$ curves should be preferred. This approach is referred to by Schilling (1997) as a rigorous check. The authors recommend that the elastic girder stiffnesses based on the short-term composite sections in positive bending and the cracked composite sections (steel section plus rebar) in the hogging moment regions should be used for calculating the pier inelastic rotations. Also, it is recommended that the pier $M\text{-}\theta_p$ relationships should be factored by $\phi = 1.1$ for checking of STRENGTH limit states and by $\phi = 1$ for SERVICE II conditions.

It should be noted that for the STRENGTH loading conditions, the ratios of the redistribution moments to the elastic pier moments (M_r / M_e) shown in Table 4.2 are substantially larger than the traditional *10* percent allowed for compact-section members (AASHTO 1994). This is due to the post-peak load-shedding characteristics of the noncompact pier sections, which are modeled conservatively by the proposed $M\text{-}\theta_p$ relationships. Consideration of the fact that the pier maximum nominal moment capacity (M_n) can be significantly larger than the moment associated with first yielding of one of the flanges (M_y), as is accomplished by using the Q formula in the current AASHTO LRFD Specifications (1994), can have a significant impact on the design economy.

Fatigue considerations may control the design proportions in certain cases. It is suggested that the calculation of fatigue-loading stresses should be based on the short-term composite sections, including the contribution of the concrete deck, whenever the maximum net tensile stresses under the fatigue loading conditions are smaller than the concrete cracking stress. In the elastic and inelastic designs considered in this chapter, this results in a significant savings in the required positive bending sections. Considerable composite action has been observed even within the hogging-moment regions in field tests, e.g., (Baldwin et al. 1978) and (Roeder and Eltvik (1985), and this behavior is presently

accounted for in the stiffnesses suggested by the AASHTO LRFD Specifications (1994) for the calculation of girder elastic moments.

This chapter and the three-span continuous example in (AISI 1995) both focus on designs based on an ordinary line-girder analysis. There is a need for incorporation of inelastic pier M-θ_p models, such as the ones employed in this study, into three-dimensional analysis software for straight beam and girder bridges. In actuality, it is expected that the concrete deck and the cross-frames may participate significantly in distributing internal forces transversely between the girders in a bridge such as the one considered here. Transverse redistribution of forces may significantly limit the inelastic rotations that are experienced over the piers. A three-dimensional analysis of the bridge system under the design loadings is needed to better understand the implications of transverse load distribution on cross frame forces and performance.

Table 4.1. Performance ratios for modified elastic and inelastic designs.

	Elastic	Inelastic
POSITIVE MOMENT SECTIONS		
STRENGTH I Limit States		
Flexure, end spans, compact section (1996 Iterims, 1.1M$_y$ limit)	0.779	0.943
Flexure, interior span, compact section (1996 Iterims, 1.1M$_y$ limit)	0.721	1.038
Ductility (1996 Interims)	0.274	0.274
Shear, stiffened web end bearing	0.890	0.873
Fatigue and Fracture Limit States		
Base metal at connecton-plate weld to bottom flange (at cross-frame closest to mid-span)	0.968 (1.108)[*]	0.980 (1.083)
Maximum concrete tensile stress / cracking stress (at above location)	0.162	0.068
Web requirements, flexure	0.337	0.422
Web requirements, shear end bearing	0.492	0.479
Service Limit States		
Live-load deflection, end span	0.328	0.351
Live-load deflection, center span	0.345	0.359
Permanent deflection, tension flange (SERVICE II)	0.746	0.794
Constructability		
Web slenderness	0.692	0.657
Compression flange slenderness	0.698	0.730
Compression flange bracing	0.815	0.760
Shear in second panel from end bearing	0.274	0.267
INTERIOR PIER SECTION		
STRENGTH I Limit States, non-compact section		
Web slenderness	0.924	0.871
Compression flange slenderness	0.544	0.952
Compression flange bracing	0.924	0.930
Flexure, compression flange	0.912	NA
Flexure, tension flange	0.953	NA
Fatigue and Fracture Limit States		
Shear conn. weld to top flange	0.607	0.805
Bearing stiffener/connection plate weld to top flange	0.485	0.659
Web requirements, flexure	0.626	0.720
Web requirements, shear	0.888	0.590
Service Limit States		
θ_p / θ_{RL}	NA	0.547
Elastic reinforcing steel stresses	NA	0.445
Constructability		
Flexure, tension flange	--	0.661

• Values in parentheses are based on the steel section only for calculation of stresses due to negative moments.

Table 4.2. Results of inelastic analyses.

	Service II Loads & $M_{max}^- = M_n$	Strength I Loads & $M_{max}^- =$		
		$1.1M_n$	M_n	M_y
θ_p (radians)	0.0035	0.0123	0.0242	0.0321
M_r / M_e	0.074	0.208	0.408	0.541
M_{pier} / M_e	1.02	1.13	0.85	0.66

Table 4.3. STRENGTH I inelastic design performance ratios for different $M\text{-}\theta_p$ idealizations.

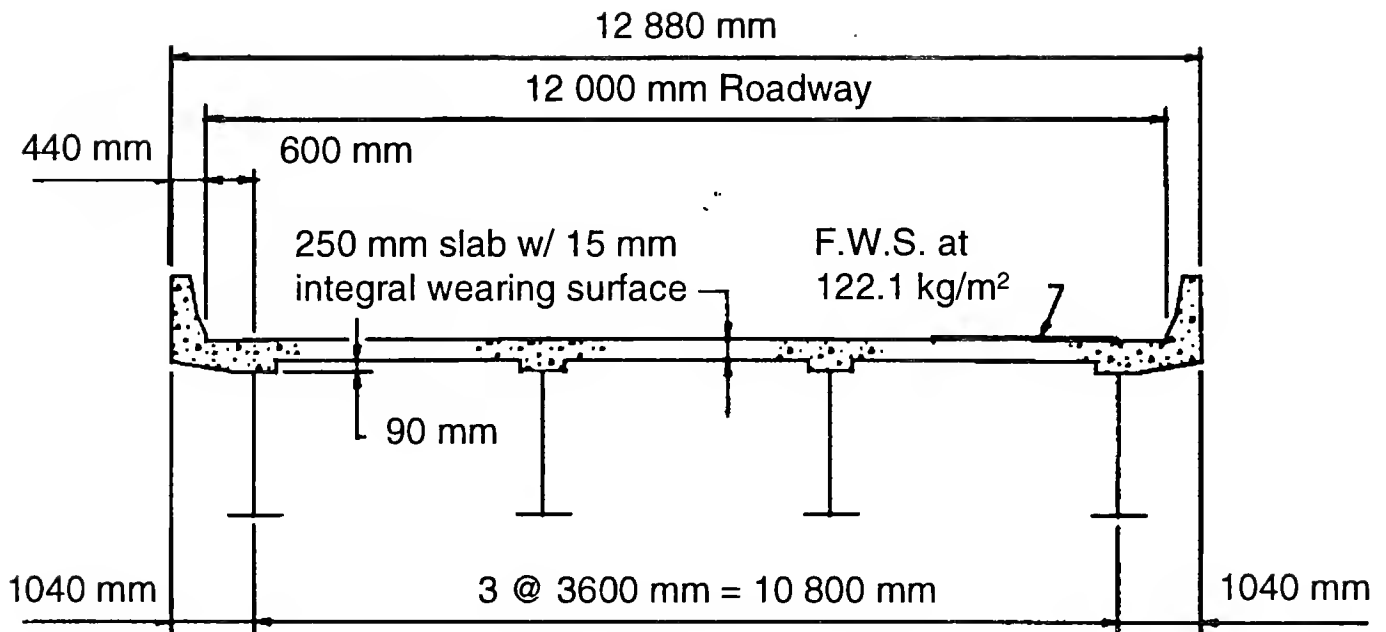|	$M_{max}^- =$		
	$1.1M_n$	M_n	M_y
POSITIVE MOMENT SECT.			
Flexure, end spans, compact section ($1.1M_y$ limit)	0.943	1.081	1.181
Flexure, interior span, compact section ($1.1M_y$ limit)	1.038	1.327	1.534
Web requirements, flexure	0.422	0.535	0.610
INTERIOR PIER SECTION			
Compression flange bracing	0.930	0.840	0.757

Figure 4.1. Typical bridge cross-section (AISI 1995).
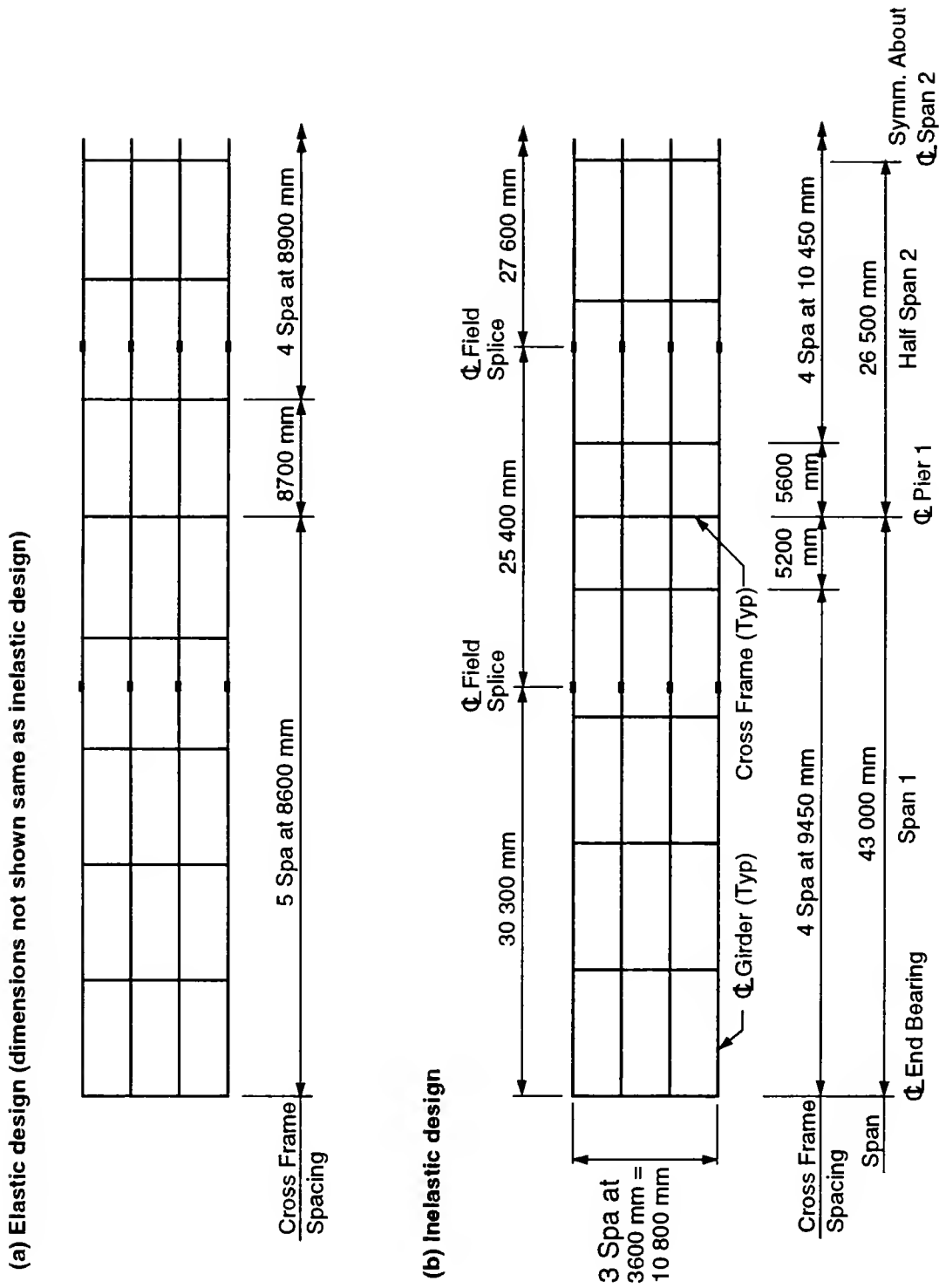
Figure 4.2. Framing plan, elastic and inelastic designs.

103

(a) Modified elastic design
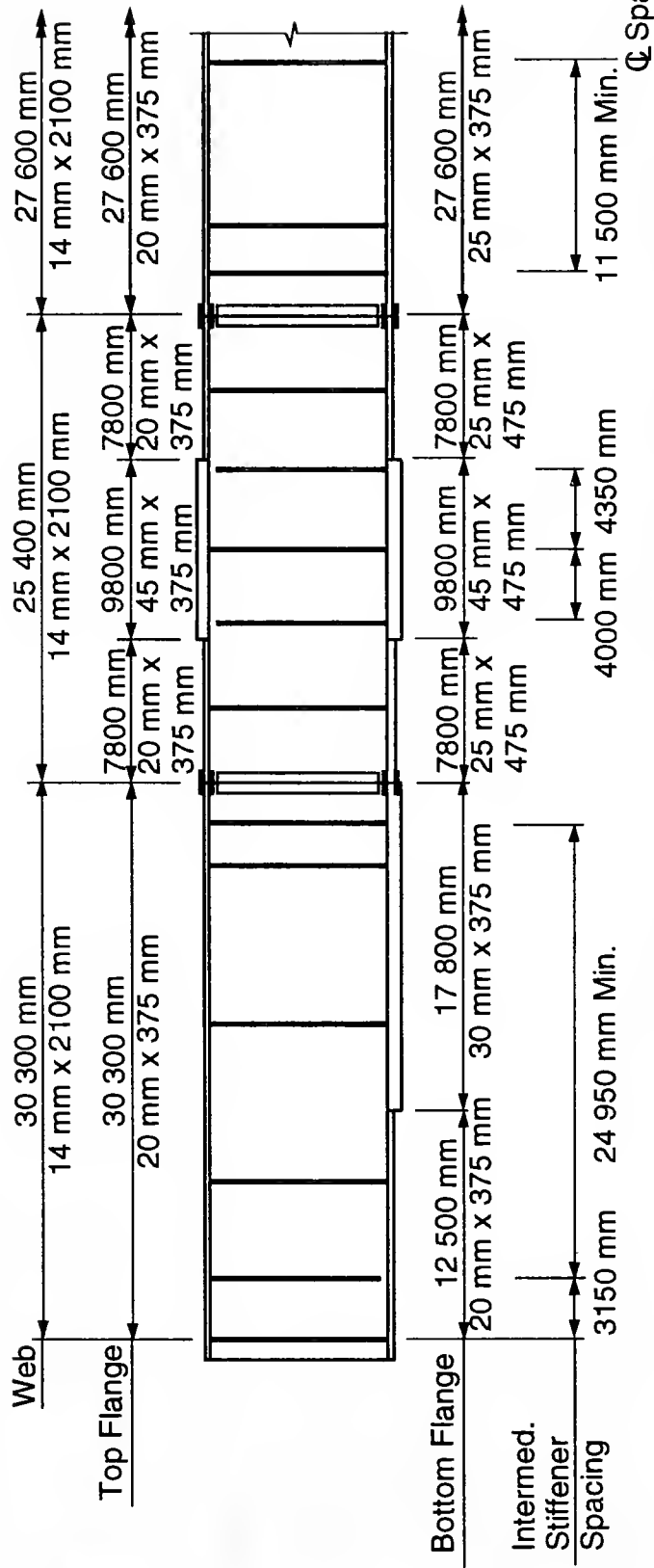
Figure 4.3. Elevation of exterior girders, modified elastic and inelastic designs.

(b) Inelastic design
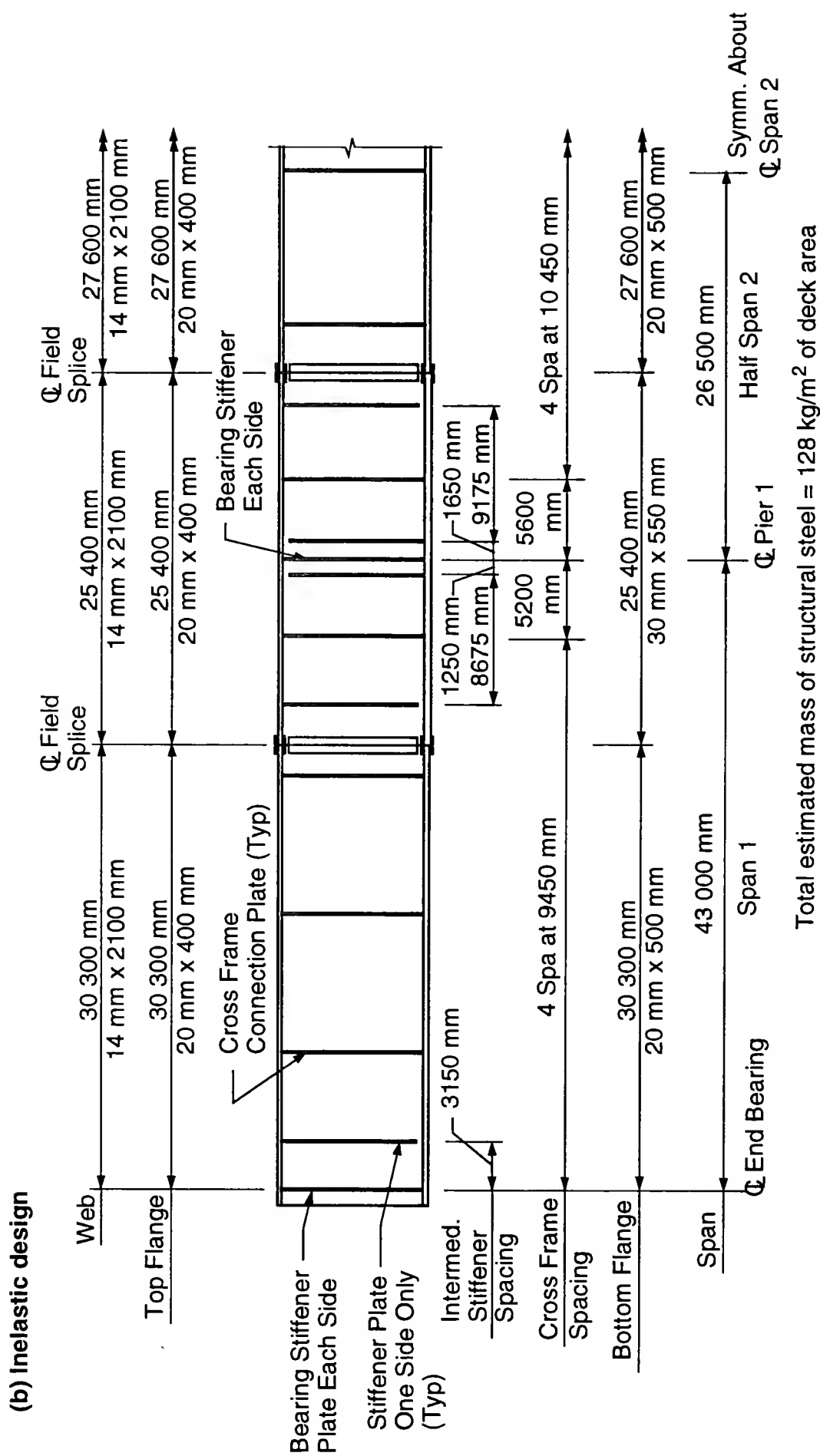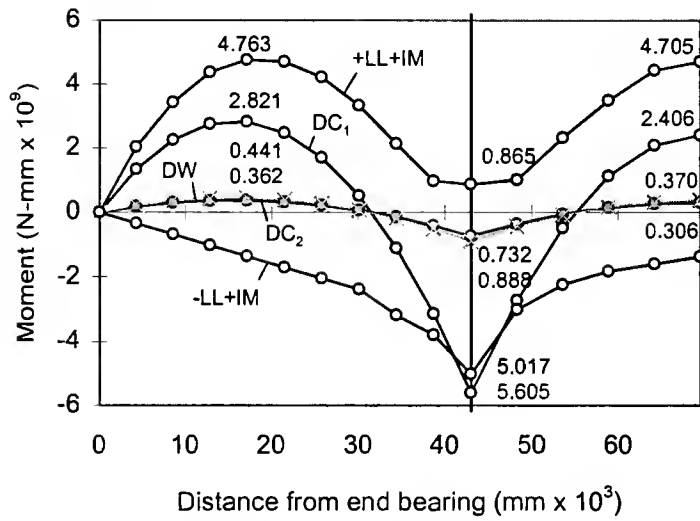

Figure 4.3 (cont'd). Elevation of exterior girders, modified elastic and inelastic designs.
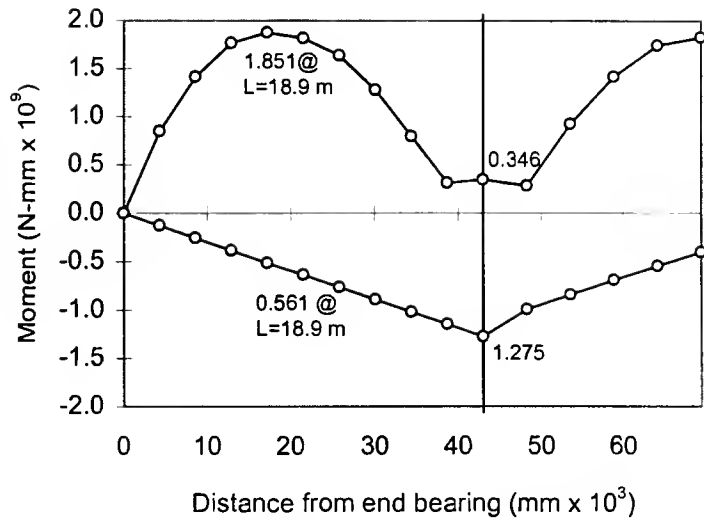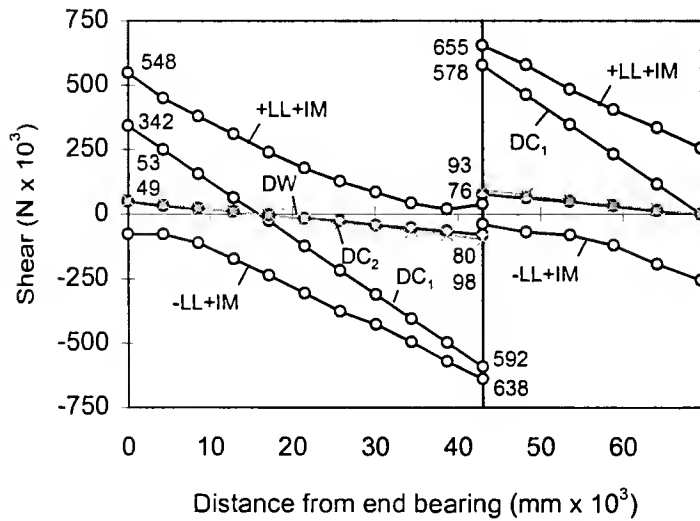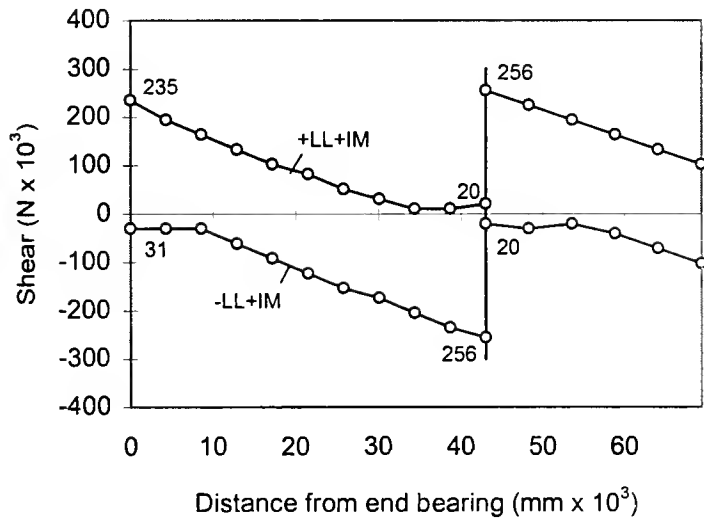
Figure 4.4. Unfactored moment and shear envelopes, inelastic design.

Pier 1   Pier 2

M_{1e} M_{2e}

(1) Maximum elastic pier moments from moment
envelopes and controlling load combination

θ_{p1}

$m_{1p1}\,\theta_{p1}$ $m_{2p1}\,\theta_{p1}$

(2) Redistribution moments due to
plastic rotation at pier 1

θ_{p2}

$m_{1p2}\,\theta_{p2}$ $m_{2p2}\,\theta_{p2}$

(3) Redistribution moments due to
plastic rotation at pier 2

θ_{p1} θ_{p2}

$m_{1p1}\,\theta_{p1} + m_{1p2}\,\theta_{p2}$ $m_{2p1}\,\theta_{p1} + m_{2p2}\,\theta_{p2}$

(4) Total redistribution moments

$M_{1e} + m_{1p1}\,\theta_{p1} + m_{1p2}\,\theta_{p2}$ $M_{2e} + m_{2p1}\,\theta_{p1} + m_{2p2}\,\theta_{p2}$

(5) Total pier moments

Figure 4.5. Procedure for calculation of pier inelastic rotations and redistribution moments.

Figure 4.6. Pier beam-line plots for STRENGTH I loading conditions.

Figure 4.7. Moment-plastic rotation curves for positive bending.

Figure 4.8. Calculation of elastic pier moments due to a plastic rotation of *0.002* radians at the center of the middle span.

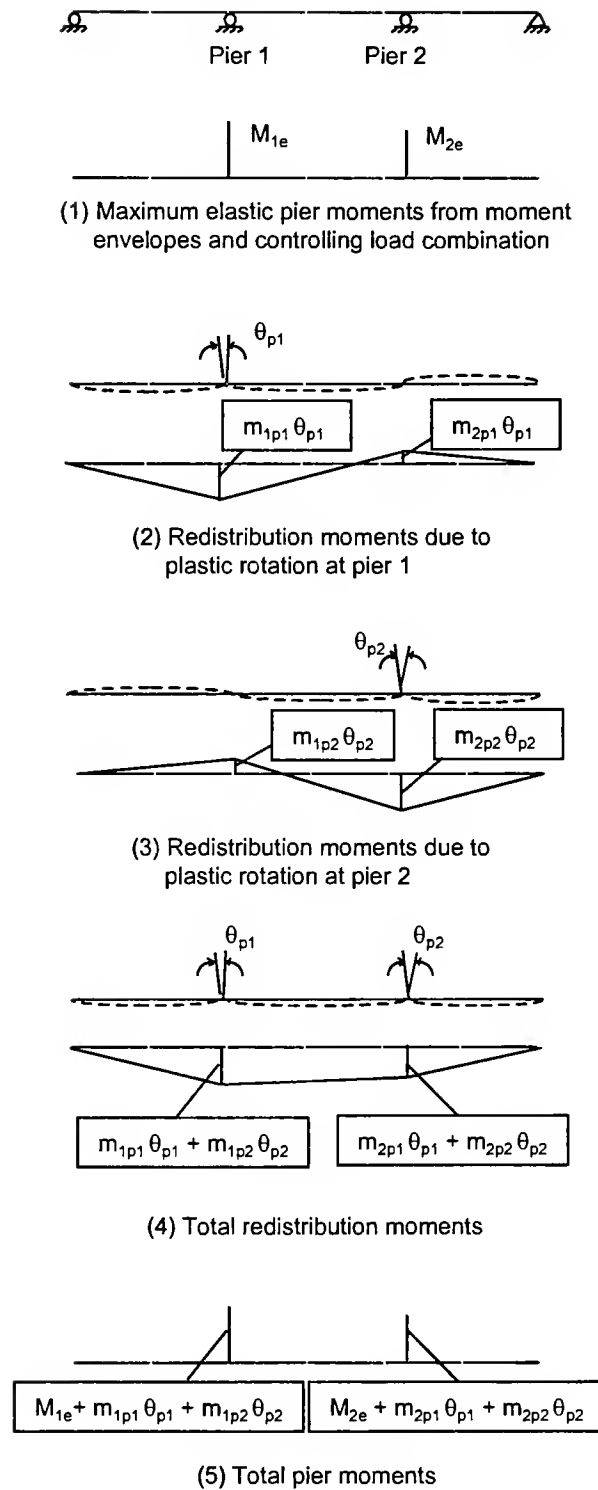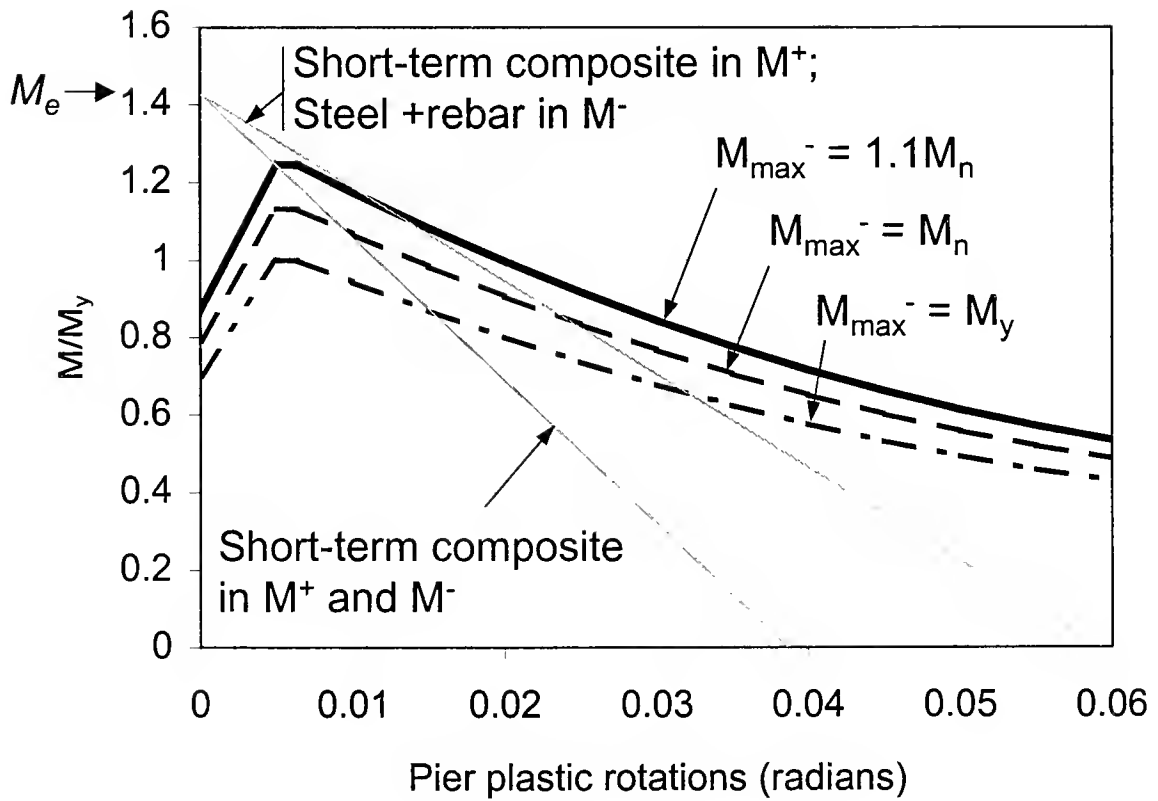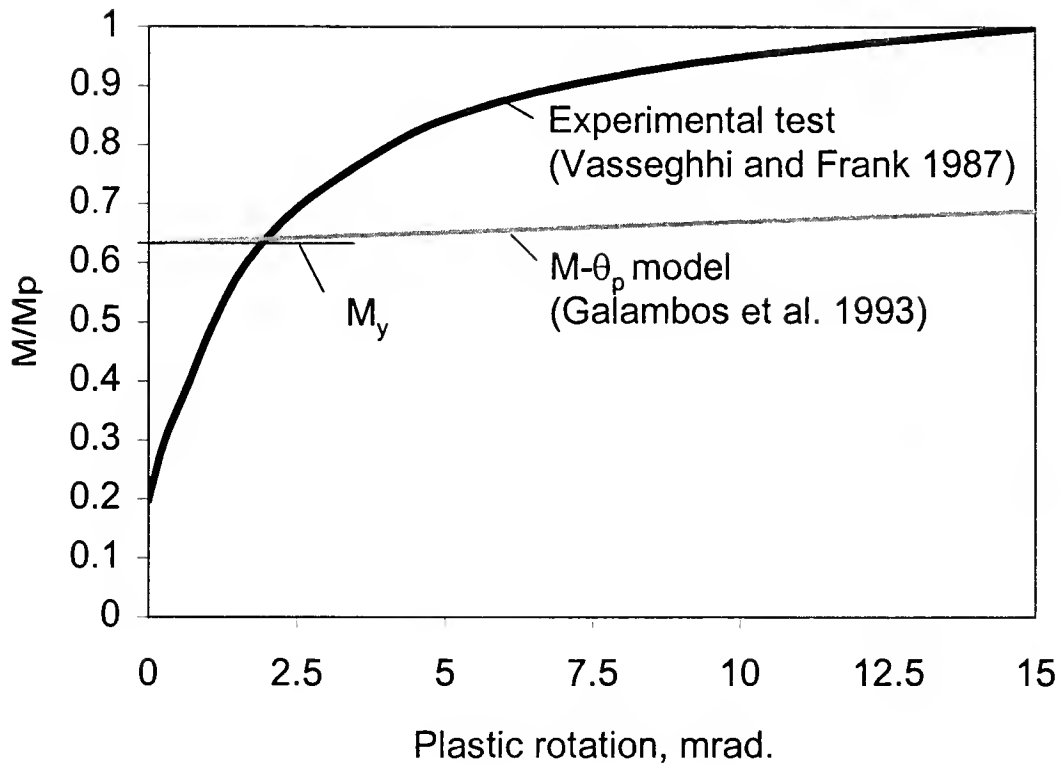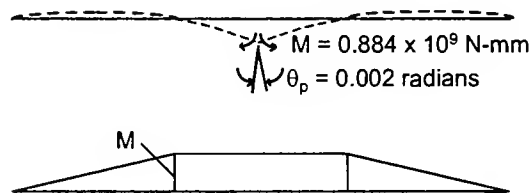# CHAPTER 5

SUMMARY AND IMPLEMENTATION

This research has provided information on the moment-rotation (M-θ_p) characteristics necessary for application of autostress-type design procedures to both continuous-span compact-beam and non-compact transversely-stiffened plate girder bridges. Simple M-θ_p expressions have been developed which can be incorporated directly in new suggested procedures for AASHTO inelastic design of continuous-span beam and plate-girder bridges (Schilling 1997; Schilling et al. 1996). The potential cost savings through use of these types of design methodologies are well documented in the technical literature, with savings in steel weight as large as *15* percent in practical designs in addition to savings in fabrication costs (e.g., Schilling 1989). These savings can be achieved to a certain extent with the same and even improved serviceability performance (i.e., deflections, fatigue, etc.). An example three-span continuous plate-girder design has been presented which illustrates the key savings associated with these methods – simplicity of the fabrication by reducing the number of plate thicknesses required in a design and by eliminating section transitions at locations other than field splices, while also achieving some reduction in steel weight. Furthermore, the inelastic methods addressed and extended in this research offer the potential for more realistic assessment of actual structural capacities. This can greatly benefit the evaluation and rating of bridge structures, as inelastic rating procedures such as those addressed in (Galambos et al. 1993) become standardized.

5.1 Cost-to-Benefit Ratio

Specific cost-to-benefit ratios have not been addressed within this research. An estimate of typical cost-to-benefit ratios for the approaches developed and illustrated in this research can be inferred from cost comparisons performed by Wasserman and Holloran (1992). These Tennessee DOT engineers conclude in their paper that, on relatively equal projects, the steel for a rolled-beam bridge designed by Autostress procedures would cost approximately 30 percent less than that for a Load Factor designed welded plate-girder bridge. The largest portion of the savings is in fabrication costs. It is

expected that savings of this order also can be realized with potential AASHTO LRFD inelastic plate-girder designs, compared to the same bridge designs using AASHTO elastic design methods.

5.2 Recommendations for Implementation

This research complements a parallel National Science Foundation study by Schilling et al. (1996) on the inelastic design of steel girder bridges. It is recommended that the M-θ_p equations developed in this research should be incorporated into the inelastic design provisions developed in (Schilling 1997; Schilling et al. 1996). This requires little change to the proposed provisions other than the replacement of effective plastic moment (M_{pe}) equations in these provisions by the M-θ_p model developed in this work. As discussed in detail in Chapter 4, the use of the direct M-θ_p equations requires minor additional effort on the part of the engineer, since the calculations can be easily implemented in existing ordinary spreadsheet or mathematical manipulation software. Use of the explicit M-θ_p relationships avoids the conservatism introduced by M_{pe} equations that are based on an upper-bound of the expected pier plastic rotations anticipated over a wide range of designs. Also, the explicit M-θ_p relationships should be more useful for potential future three-dimensional bridge analysis software that can account for the inelastic redistribution of excess elastic moments from interior pier sections. For the resulting provisions to be available for design use, they will then need to be accepted by AASHTO as changes to the existing inelastic design provisions of the AASHTO LRFD Specifications (1996).

5.3 Future Work

Research efforts by US steel plate producers have recently resulted in the availability of new High Performance Steels (HPS) of grades 70W and 100W (i.e., *70* and *100* ksi yield strengths). These steels offer many advantages over conventional steels in providing high toughness and weldability. However, due to their different material stress-strain characteristics, particularly the fact that these steels typically have a larger yield ratio (F_y/F_u) than steels used predominantly in current steel bridge construction, it is necessary to assess the applicability of current AASHTO provisions to design with these new steels. It is expected that the M-θ_p model developed in this research provides a reasonable approximation of the behavior for I girders fabricated from the above HPS

materials. However, further research is needed to better understand the implications of the HPS material properties on the strength and ductility of I girders, and to generate potential improvements to the proposed $M\text{-}\theta_p$ model.

Although the accuracy of the finite element models employed in this research is supported by comparisons with the available experimental data, it is important to note that the specific tests for which the current American Specifications exhibit significant unconservative errors (see Chapter 3) have not been corroborated by experimental testing. Ideally, several focused experimental tests should be conducted to affirm or refute these findings. The key cases involve a high web depth to compression flange width ratios (D/b_{fc}) of *4.25*, which is a reasonable proportion for bridge plate girders, and large depths of the web in compression *(D_{cp} /D > 0.5)*.

There is a need for incorporation of inelastic pier $M\text{-}\theta_p$ models, such as the one developed in this research, into three-dimensional analysis software for straight beam and girder bridges. In actuality, it is expected that the concrete deck and the cross-frames may participate significantly in distributing internal forces transversely between the girders in a bridge such as the one considered in Chapter 4. This transverse redistribution of forces may significantly limit the inelastic rotations that are experienced over the piers. A three-dimensional analysis of the bridge system under the design loadings is needed to better understand the implications of transverse load distribution on cross frame forces and performance.

REFERENCES

AISC (1993), *Load and Resistance Factor Design Specification for Structural Steel Buildings*, 2nd Ed., American Institute of Steel Construction, Chicago, Illinois.

AISC Marketing (1994), *Myths and Realities of Steel Bridges*, American Institute of Steel Construction, Chicago, IL, 23 pp.

AISI (1995), *Four LRFD Design Examples of Steel Highway Bridges, SI Units*, Vol. II, Ch. 1A, Highway Structures Design Handbook, American Iron and Steel Institute, 380 pp.

AASHTO (1994), *AASHTO LRFD Bridge Design Specifications*, 1rst Ed., SI Units, American Association of State Highway and Transportation Officials, Washington, D.C.

AASHTO (1986), *Guide Specifications for Alternate Load Factor Design Procedures for Steel Beam Bridges Using Braced Compact Sections*, American Association of State and Highway Transportation Officials, Washington D.C., 35 pp.

AASHTO (1983), *Standard Specifications for Highway Bridges*, 13th ed., American Association of State Highway and Transportation Officials, Washington, D.C.

Alpsten, G.A. (1972), "Variation in Mechanical and Cross-Sectional Properties of Steel," International Conference on Planning and Design of Tall Buildings, Lehigh Univ., ASCE-IABSE International Conference Preprints: Reports 1b-9, pp. 1-51.

ASCE (1971), *Plastic Design in Steel, A Guide and Commentary*, 2nd ed., joint committee of the Welding Research Council and the American Society of Civil Engineers, American Society of Civil Engineers, New York, NY, 336 pp.

AWS (1995), *Bridge Welding Code*, ANSI/AASHTO/AWS D1.5-95, joint publication of American Association of State Highway and Transportation Officials and American Welding Society, 236 pp.

Bak, C.-O. (1992), "Ultimate Load Capacity of Continuous Composite Plate Girders," Ph.D. dissertation, University of Texas, Austin, TX, 127 pp.

Baldwin, J.W., Salame, H.J., and Duffield, R.C. (1978), "Fatigue Test of a Three-Span Composite Highway Bridge," Report 73-1, Dept. of Civil Engrg., Univ. Missouri, Columbia, MO.

Bansal, J.P. (1971), "The Lateral Instability of Continuous Steel Beams," Ph.D. dissertation, University of Texas at Austin, Austin, TX, 128 pp.

Barth, K.E. (1996), *Moment-Rotation Characteristics for Inelastic Design of Steel Bridge Beams and Girders*, Ph.D. dissertation, Purdue Univ., W. Lafayette, IN, 311 pp.

Basler, K. and Thurlimann, B. (1961), "Strength of Plate Girders in Bending," *Journal of the Structural Division*, ASCE, 87(ST6), 153-181.

Carskaddan, P.S. (1980), "Autostress Design of Highway Bridges, Phase 3: Interior-Support-Model Test (AISI Project 188)," Technical Report 97-H-045(019-5), United States Steel Corporation Research Laboratory, 52 pp.

Carskaddan, P.S. (1991), "Concrete Cracking in the Autostress Method," internal memorandum, AISC Marketing, Inc., Oct. 2, 1991, 4 pp.

Carskaddan, P.S., Haaijer, G. and Grubb, M.A. (1984), "Adjusting the Beam-Line Method for Positive-Moment Yielding," *Engineering Journal*, AISC, **21(4)**, 217-221.

CEN (1992) *ENV 1993-1-1 Eurocode 3, Design of Steel Structures, Part 1.1 - General Rules and Rules for Buildings*, European Committee for Standardization, Brussels.

Climenhaga, J.J. and Johnson, R.P. (1972a), "Moment-Rotation Curves for Locally Buckling Beams," *Journal of the Structural Division*, ASCE, 98(ST6), 1239-1254.

Climenhaga, J.J. and Johnson, R.P. (1972b), "Local Buckling in Continuous Composite Beams," *The Structural Engineer*, 50(9), 367-374.

Croce, A.D. (1970), *The Strength of Continuous Welded Girders with Unstiffened Webs*, CESRL Thesis No. 70-2, University of Texas at Austin, Austin, Texas, 78 pp.

Dishongh, B.E. and Galambos, T.V. (1992), "Residual Deformation Analysis for Inelastic Bridge Rating," *Journal of Structural Engineering*, ASCE, 118(6), 1494-1508.

Dutta, A. (1992), "Inelastic Stability Analysis of Plated Structures," Ph.D. dissertation, Purdue Univ., W. Lafayette, IN, 279 pp.

Dutta, A. and White, D.W. (1992), "Large Displacement Formulation of a Three-Dimensional Beam Element with Cross-Sectional Warping," *Computers and Structures*, 45(1), 9-24.

ECCS (1976), *Manual on Stability of Steel Structures*, 2nd Ed., ECCS - Committee 8 - Stability, European Convention for Constructional Steelwork, Publication No. 22, 328 pp.

ECCS(1984), *Ultimate Limit State Calculation of Sway Frames with Rigid Joints*, 1rst ed., ECCS - Committee 8 - Stability, Technical Working Group 8.2 - System, European Convention for Constructional Steelwork, Publication No. 33, 20 pp.

FHWA (1992), "Model Bridge Study, Volume II: Component Test Report," Publication No. FHWA-RD-90-066, Federal Highway Administration, Turner-Fairbank Highway Research Center, McLean, VA, 66 pp.

Galambos, T.V., Leon, R.T., French, C.W., Barker, M., and Dishongh, B. (1993), "Inelastic Rating Procedures for Steel Beam and Girder Bridges," National Cooperative Highway Research Program, Report 352, Transportation Research Board, National Academy Press, Washington, D.C., 111 pp.

Grubb, M.A. (1993), "Review of Alternate Load Factor (Autostress) Design," Transportation Research Record, No. 1380, Transportation Research Board, National Academy Press, Washington D.C., pp. 45-49.

Grubb, M.A. and Carskaddan, P.S. (1981), "Autostress Design of Highway Bridges, Phase 3: Moment-Rotation Requirements (AISI Project 188)," Technical Report 97-H-045(018-1), United States Steel Corporation Research Laboratory, 44 pp.

Grubb, M.A. and Carskaddan, P.S. (1979), "Autostress Design of Highway Bridges, Phase 3: Initial Moment-Rotation Tests (AISI Project 188)," Technical Report 97-H-045(019-4), United States Steel Corporation Research Laboratory, 37 pp.

Haaijer, G. (1957), "Plate Buckling in the Strain-Hardening Range," *Journal of the Engineering Mechanics Division,* ASCE, 83(EM2), 1212-1243.

Haaijer, G., Carskaddan, P.S., and Grubb, M.A. (1983), "Autostress Design of Steel Bridges," *Journal of Structural Engineering*, ASCE, 109(1), 188-199.

Holtz, N.M. and Kulak, G.L. (1973), "Web Slenderness Limits for Compact Beams," Structural Engineering Report No. 43, University of Alberta, Canada., 41 pp.

Huang, P.-C. (1994), "Finite Element Analysis of Inelastic Behavior of Structural Steel Beams and Bridge Girders," Ph.D. dissertation, Cornell Univ., Ithaca, NY, 295 pp.

Johnson, D.L. (1985), "An Investigation into the Interaction of Flanges and Webs in Wide Flange Shapes," Proceedings Annual Technical Session, Structural Stability Research Council, 395-405.

Kemp, A.R. (1986), "Factors Affecting the Rotation Capacity of Plastically Designed Members," *The Structural Engineer*, 64B(2), 28-35.

Kuhlmann, U. (1989), "Definition of Flange Slenderness Limits on the Basis of Rotation Capacity Values," *Journal of Constructional Steel Research*, 14, 21-40.

Kusuda, T., Sarubbi, R.G., and Thurlimann, B. (1960), "Lateral Bracing of Beams in Plastic Design," Report No. 205.E11, Fritz Engineering Laboratory, Lehigh Univ., Bethlehem, PA.

Lay, M.G. (1965), "Flange Local Buckling in Wide-Flange Shapes," *Journal of the Structural Division*, ASCE, 91(ST6), 95-116.

Lay, M.G. and Galambos, T.V. (1967), "Inelastic Beams under Moment Gradient," *Journal of the Structural Division*, ASCE, 93(ST1), 381-399.

Lukey, A.F. and Adams, P.F. (1969), "Rotation Capacity of Beams under Moment Gradient," *Journal of the Structural Division*, ASCE, 95(ST6), 1173-1188.

Nowak, A.S. (1995), "Calibration of LRFD Bridge Code," *Journal of Structural Engineering*, ASCE, 121(8).

Roeder, C.W. and Eltvik, L. (1985). "An Experimental Evaluation of Autostress Design," Transportation Research Record 1044, Transportation Research Board.

Schilling, C.G. (1997). "Simplified Inelastic Design of Steel Girder Bridges," submitted to *Journal of Bridge Engineering*, ASCE, 39 pp.

Schilling, C.G. (1993), "Unified Autostress Method," *Autostress Design of Highway Bridges*, Transportation Research Record, No. 1380, Transportation Research Board, National Academy Press, Washington D.C., pp. 28-34.

Schilling, C.G. (1988), "Moment-Rotation Tests of Steel Bridge Girders," *Journal of Structural Engineering*, 114(1), 134-149.

Schilling, C.G. (1986), "Exploratory Autostress Girder Designs," Project 188, Autostress Design of Highway Bridges, American Iron and Steel Institute, Washington, D.C., 81 pp.

Schilling, C.G. (1985), "Moment-Rotation Tests of Steel Bridge Girders," Project 188, Autostress Design of Highway Bridges, American Iron and Steel Institute, Washington, D.C., 52 pp.

Schilling, C.G., Barker, M.G. and Dishongh, B.E. (1996). "Simplified Inelastic Design of Steel Girder Bridges," Final Report, National Science Foundation Study on Development and Experimental Verification of Inelastic Design Procedures for Steel Bridges Comprising Noncompact Girder Sections, Univ. Missouri – Columbia, Columbia, MO, 107 pp.Schilling, C.G. and Morcos, S.S. (1988), "Moment-Rotation Tests of Steel Girders with Ultracompact Flanges," Project 188, Autostress Design of Highway Bridges, American Iron and Steel Institute, Washington, D.C., 62 pp.

Tansil, T.C. (1991), "Behavior of a Composite Plate Girder in Negative Bending," M.S. Thesis, University of Texas at Austin, Austin, Texas, 107 pp.

Vasseghi, A. and Frank, K.H. (1987), "Static Shear and Bending Strength of Composite Plate Girders," PMFSEL Report No. 87-4, Dept. of Civil Engrg., Univ. Texas, Austin, TX, 122 pp.

Wasserman, E.P. and Holloran, M.A. (1993), "Autostress: Tennessee's Experience," *Autostress Design of Highway Bridges*, Transportation Research Record, No. 1380, Transportation Research Board, National Academy Press, Washington D.C., pp. 35-44.

White, M.W. (1956), "The Lateral-Torsional Buckling of Yielded Structural Steel Members," Ph.D. dissertation, Lehigh Univ., Bethlehem, PA.

White, D.W. (1994), "Analysis of the Inelastic Moment-Rotation Behavior of Noncompact Steel Bridge Girders," Report No. CE-STR-94-1, School of Civil Engineering, Purdue Univ., W. Lafayette, IN, 151 pp.

White, D.W. and Abel, J.F. (1990), "Accurate and Efficient Nonlinear Formulation of a 9-Node Shell Element with Spurious Mode Control," *Computers and Structures*, 35(6), 621-642.

White, D.W. and Dutta, A. (1993), "Numerical Studies of Moment-Rotation Behavior in Steel and Composite Steel-Concrete Bridge Girders," Transportation Research Record, No. 1380, Transportation Research Board, National Academy Press, Washington D.C., pp. 19-27.

APPENDIX I

LIST OF NOTATION

C_b AISC LRFD coefficient that accounts for the effects of moment gradient on the lateral-torsional buckling capacity

D total web depth

D_c elastic depth of the web in compression

D_{cp} depth of the web in compression at the theoretical plastic moment capacity of the girder

E elastic modulus

E_{st} strain-hardening modulus at the onset of strain hardening in uniaxial tension or compression

F_{cr} elastic local buckling stress for the compression flange within the context of the AASHTO LRFD Q formula; critical compression flange stress, governed by yielding, inelastic buckling, or elastic buckling within the context of the AISC LRFD Appendix G.

F_y yield stress

F_{yc} yield stress of the compression flange

F_{yps} yield stress of post-tensioning tendons within the slab

F_{yrs} yield stress of the reinforcing steel within the slab

F_{yt} yield stress of the tension flange

F_{yw} yield stress of web

F_u ultimate tensile strength

L span length of prototype girder

L_b unsupported length between brace points

L_{b1} unsupported length of the critical unbraced segment adjacent to the pier section

L_{b2} unsupported length of non-critical unbraced segments not adjacent to the pier section

L_{hog} length of the simulated hogging moment region on each side of the pier, assumed equal to $0.2L$

M internal bending moment

M_e, M_{1e}, M_{2e} Pier moments under factored loading, obtained from elastic moment envelopes

M_{max} the larger of the moments at the ends of the unsupported length

M_{max}^- maximum section capacity assumed in pier $M\text{-}\theta_p$ model

M_{min} the smaller of the moments at the ends of the unsupported length

M_n nominal moment capacity

M_p cross-section plastic moment capacity

M_{pe} effective plastic moment

M_{pier} total pier moment obtained from inelastic shakedown analysis

M_r bending moment above which yielding effects are assumed to become significant in the calculation of the flexural capacity by the AISC LRFD Specification

M_{rd} pier-section redistribution moment

M_y yield moment

Q_{fl} for girders with noncompact flanges, estimated ratio of the elastic local buckling and yield strengths of the compression flange; for girders with compact flanges, estimated ratio of the elastic local buckling and yield strengths of the compression flange corresponding to the AASHTO flange compactness limit

Q_p value of Q_{fl} for which it is assumed that the cross-section is capable of developing the plastic moment M_p by the Q formula

R_{PG} plate girder bending strength reduction factor in the AISC LRFD Specification, which accounts for the effects of web bend buckling and post-buckling strength on the flexural capacity of plate girders

R_b plate girder bending strength reduction factor in the AASHTO LRFD Specifications, which accounts for the effects of web bend buckling and post-buckling strength on the flexural capacity of plate girders

R_{max} rotation capacity corresponding to the onset of instability due to lateral and/or local buckling

R_{sys} system deformation capacity

R_{ult} rotation capacity based on the rotation at which the moment falls below M_p on the descending portion of the moment-rotation curve

V internal shear force

$V_{n.ell}$ nominal web shear capacity based on the spacing of the ordinary transverse stiffeners closest to the pier section

V_n nominal web shear capacity

a_r ratio of the web area to the compression flange area in the AISC LRFD Specification; ratio of twice the elastic web area in compression to the compression flange area in the AASHTO LRFD Specifications

a_{rp} ratio of twice the web area in compression at the theoretical plastic moment capacity of the girder to the compression flange area

b_{fc} width of the compression flange

c_f width of plate effectively stressed at F_y in tension adjacent to a flame cut edge

c_{fw} final tension block width due to welding at web edges that are previously flame cut

c_w width of plate effectively stressed at F_y in tension on each side of the centerline of the weld in the flanges and at the edges of the web plate, due to welding between the web and flange plates, assuming a single pass weld

c_2 final tension block width in the flange plates on each side of the centerline of the web-flange juncture, based on the assumption that the web is fillet welded on each side to the flange plates

d least panel dimension

d_o transverse stiffener spacing

$d_{o.el}$ spacing of "ordinary" transverse stiffeners

$d_{o.in}$ spacing of any additional "inelastic restraint" transverse stiffeners adjacent to the pier section

f_c stress in the compression flange due to factored loading

f'_c concrete compressive strength

f_{rc} residual stress in compression

k flange buckling coefficient

m_{ipj} moment at pier i corresponding to a unit plastic rotation at pier j

n modular ratio

r_t radius of gyration of the compression flange plus one-third of the web in compression, about the vertical axis of the web

r_y radius of gyration of the compression flange plus one-half the total depth of the web about the minor axis of the cross-section

r_{yc} radius of gyration of the compression flange about the minor axis of the cross-section

t thickness of plate

t_{fc} thickness of the compression flange

t_s slab thickness

t_w thickness of the web

δ_{oL} initial sweep of the compression flange within each unsupported length

δ_{of} initial tilt of the compression flange within the length of each panel

δ_{ow} initial out-of-flatness within the web panels

ε_{st} strain at strain-hardening in uniaxial tension or compression

λ slenderness parameter for strength calculations in the AISC LRFD Specification, equal to $b_{fc}/2t_{fc}$ for flange local buckling, D/t_w for web local buckling, and L_b/r_y or L_b/r_{yc} for lateral-torsional buckling

λ_r generic term for slenderness limits beyond which elastic buckling would theoretically govern the design resistance for local flange, local web or lateral-torsional buckling in the AISC LRFD Specification

λ_p generic term for slenderness limits below which the plastic moment capacity M_p can be reached prior to the strength being affected by the corresponding inelastic buckling limit states for local flange, local web or lateral-torsional buckling in the AISC LRFD Specification

ϕ resistance factor

ϕ_v shear resistance factor

θ_{RL} plastic rotation at the onset of load-shedding in the proposed pier moment-rotation relations

θ_e theoretical rotation at which the plastic moment capacity is based on the elastic beam stiffness

θ_{max} rotation between the ends of test beams at the onset of instability due to lateral and/or local buckling

θ_p plastic rotation

θ_{pi} plastic rotation at pier i